Methods for studying the cell cycle in African Trypanosomes

Research Masters Thesis

Max Pendlebury BSc (Hons)

Lancaster University

September 2023

I, Max Pendlebury, confirm that the work presented in this thesis is my own and has not been submitted in substantially the same form for the award of a higher degree elsewhere. Where information has been derived from other sources, I confirm this has been indicated in the thesis.

Submitted in part fulfilment of the requirements for the degree of Masters by Research Biomedical Science.

Contents

(1) Abstract

African trypanosomes are a genus of unicellular parasitic organisms that cause both human and animal African trypanosomiasis. While HAT, caused by *Trypanosoma brucei rhodesiense or gambiense*, has shown record low cases in recent years, the elimination of AAT remains difficult due to many complicating factors. One of these factors is the comparatively poor understanding of the main causative agent of AAT, *Trypanosoma congolense*. Both *T. brucei* and *T. congolense* possess a single flagellum that originates from inside the cell and exits through a membrane invagination called the flagellar pocket. The flagellar pocket and its associated structures are not only critical for parasite survival and virulence but also for coordinating the cell cycle. Improving our understanding of cell cycle regulation in these species could lead to novel drug targets, which could be aided by utilisation of a suitable synchronisation method. This project aims to optimise protocols for both the synchronisation and enrichment of flagellar pocket associated cytoskeletal structures (F-PACS) in African trypanosomes to provide opportunities for greater analysis of the cell cycle. To synchronise *T. brucei*, centrifugal counter-flow elutriation (CCE) was used to separate cells based on their hydrodynamic volume. Enriched fractions were collected containing >97% of cells in G1 in PCF, and >98% in BSF. Once returned to culture, this population continued to grow in a synchronous fashion. A protocol for enrichment of F-PACS in PCF *T. brucei* was optimised. Synchronised samples were generated for analysis of changes in phosphosite abundance across the cell cycle. Attempts were made to optimize mechanical and chemical synchronisation techniques for use on *T. congolense*, achieving a ~76% enrichment in G1 by CCE. This project provides useful optimisations for continued study of the cell cycle in trypanosomes.

(2) Introduction

(2.1) African trypanosomiasis

(2.1.1) Prevalence and impact

African trypanosomiasis is a deadly, neglected tropical disease caused by protozoan parasites of the genus *Trypanosoma* affecting people and livestock. The disease is transmitted by Tsetse flies belonging to the genus *Glossina*, which are found in 38 countries throughout sub-Saharan Africa. Infections usually occur in discrete geographical foci within the tsetse belt, as not everywhere within the Tsetse fly range is suitable for trypanosomes. In these foci, environmental conditions are ideal for vector-host interactions – permitting transmission when parasites exit the flies' mouthparts during a blood meal (Wamwiri and Changasi, 2016). These conditions include moderate temperature, 75-90% humidity and shade, and where these conditions intersect with livestock farming, transmission between wild species, domesticates and people occurs (figure 2.1) (Kasozi et al., 2021). This is because the ~250 discrete foci occur primarily within poor, rural areas which usually corresponds with areas for farming, fishing, or hunting. Political turbulence, poverty, and war lead to increased transmission through the encroachment of people into these foci. Some Tsetse species have also adapted to urban environments and are found in high-density urban centres within West Africa (Malvy and Chappuis, 2011).

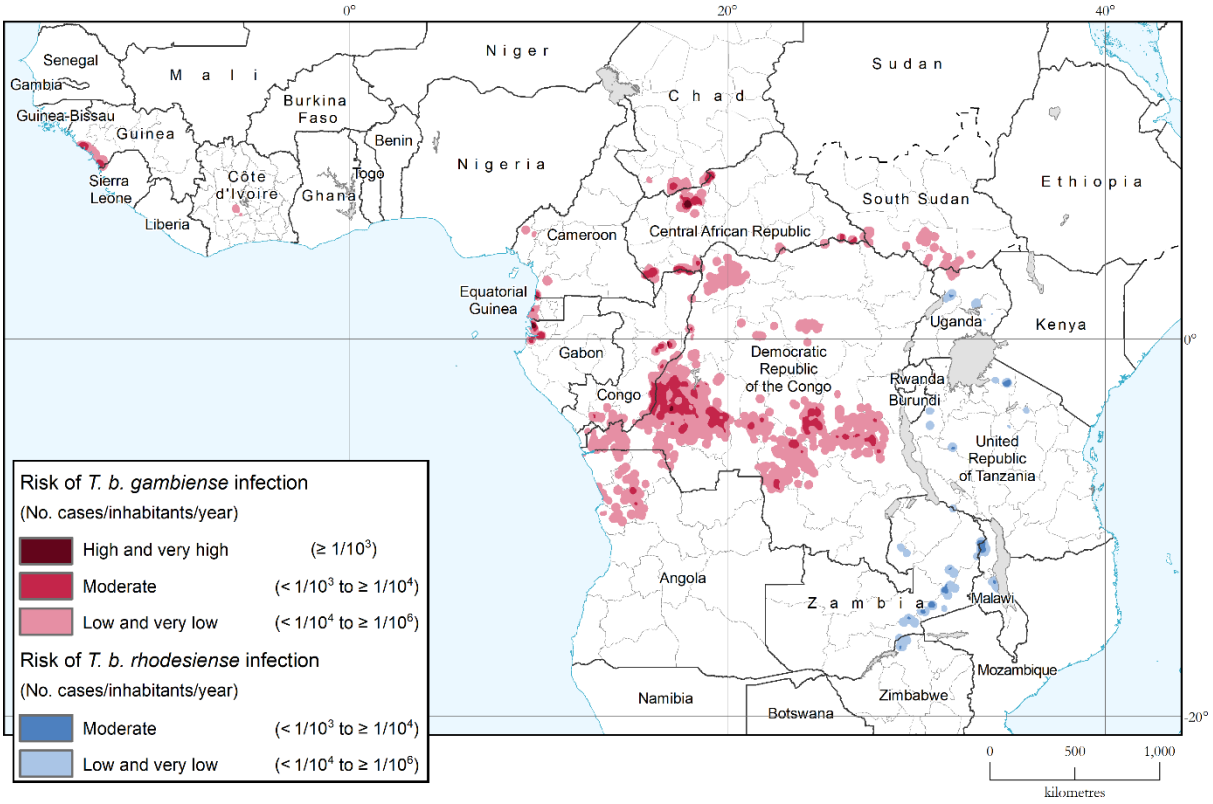

Figure 2.1 Map showing the geographical distribution of *T. b. gambiense* and *T. b. rhodesiense* infections (Franco et al., 2022).

(2.1.1.1) Human African Trypanosomiasis

Human African trypanosomiasis (HAT), also known as African sleeping sickness, is caused by infection with either *Trypanosoma brucei rhodesiense* or *gambiense*. Infection by *T. brucei rhodesiense* results in acute HAT while *T. brucei gambiense* infection causes chronic HAT and accounts for 90-95% of endemic cases. An estimated 70 million people are currently at risk of contracting HAT (Simarro et al., 2012). HAT infection is split into early and late stages, in the early stage the parasite colonises the vasculature, resulting in fever, anaemia and abnormal function of the liver, kidney and heart. The late stage of infection occurs when the parasites cross the blood-brain barrier, resulting in sleep disorders as well as various motor and

sensory symptoms (Kennedy and Rodgers, 2019). The World Health Organisation (WHO) aims to eliminate HAT by 2030 (WHO, 2022) and there has been major progress in reducing case numbers. At its most prevalent, HAT cases reached 30,000 annually during the 90s. However, cases have reduced drastically, there were 2,184 new recorded cases in 2016, 1,447 in 2017 and 977 in 2018, due to a combination of treatment and control methods (Ozioko et al., 2020).

(2.1.1.2) Animal African trypanosomiasis (AAT)

Trypanosomes can also parasitise a range of animal species resulting in animal African trypanosomiasis (AAT) or nagana. This impacts a wide range of wild mammals, as well as domesticated bovines, equines, dogs, camels, goats and sheep. Wildlife preserves act as reservoirs for trypanosomes, and as increasing pressure for population growth and climate change result in human encroachment into these areas, the probability of transmission increases (Kasozi et al., 2021). AAT is caused by multiple trypanosome species, *Trypanosoma vivax*, *Trypanosoma congolense* and *T. brucei brucei*, with *T. congolense* and *T. vivax* being the most relevant causative agents (Morrison et al., 2016). Infection with these species results in waves of parasitaemia, which leads to anaemia, pyrexia, lethargy, emaciation, and death (Katabazi et al., 2021). The complexity of the disease is increased not just by diversity in causative agents but also by mixed infections and diversity in hosts and their susceptibility to different disease-causing strains (Morrison et al., 2016). There are 3 *T. congolense* subgroups, savannah, forest, and Kilifi, with savannah showing the most severe symptoms (Bengaly et al., 2002). In ruminants, the disease causes

reduced milk and meat production, reduced fertility, and abortion (Morrison et al., 2022). This results in economic losses in sub-Saharan Africa, a region in which 309 million livestock farmers already earn less than USD 2 a day and where 32% of livestock are at risk of infection. The total economic losses of AAT are estimated to be US$ 4.75 billion annually, reducing occurrence of the disease would help to reduce instability, improve food security, and improve the standard of living (Abro et al., 2021).

(2.1.1) Treatment and control

(2.1.2.1) Treatment of gambiense HAT

Advancements in HAT control and treatment have resulted in historically low recorded cases and have enabled substantial progress towards the World Health Organisation's (WHO) elimination target. The current strategy for treatment of HAT depends on the health of the patient, the species, and the stage of infection (Figure 2.2). The early stage of infection is characterised by parasites present in the hemolymphatic system before progression to the meningoencephalitis stage where parasites invade the central nervous system (CNS) (Maxfield and Bermudez, 2023). Until recently, standard treatment of stage I of gambiense HAT was injections of pentamidine, but in 2018, the new orally administrated drug fexinidazole was authorised for use in treating HAT (Das et al., 2021). Fexinidazole belongs to the Nitroimidazole class of drugs, it is inactive until reduced by NADH-dependent nitroreductase I, a mitochondrial enzyme that is absent in absent in animals. The intermediate products of the reduction reaction react non-specifically with

biomolecules resulting in cell death (Bernhard et al., 2022). Though effective against stage I and early stage II, it is ineffective against late-stage II infections (Bernhard et al., 2022). Stage II of the infection is diagnosed by analysis of cerebrospinal fluid, a white blood cell count of >5 WBC/µl indicates stage II (Lutje et al., 2013). From 2009, the standard treatment for late-stage II infections became nifurtimox-eflornithine combination therapy (NECT). This has advantages over eflornithine monotherapy, requiring 14 intravenous infusions compared to 56 and resulting in fewer side effects with a comparable cure rate (Yun et al., 2010). Pentamidine remains as a second-choice treatment where fexinidazole is not appropriate, particularly in young children. Pentamidine is a DNA binding agent that results in loss of kDNA (Thomas et al., 2018). It is a generally well-tolerated drug, with the major disadvantage being that it must be administered through painful intramuscular injections (WHO, 2019).

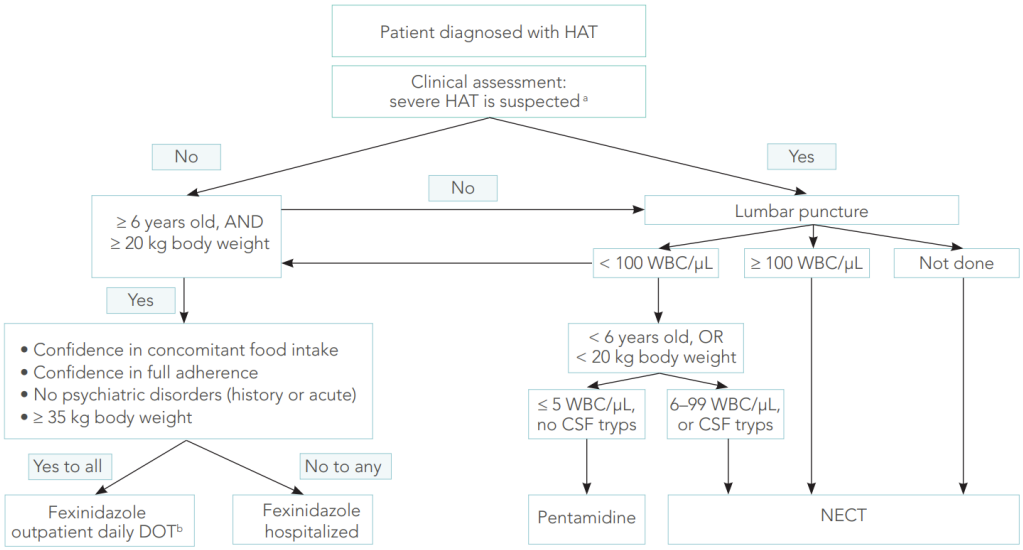

Figured 2.2 Treatment map for patients diagnosed with *T. b. gambiense* HAT (WHO, 2019).

(2.1.2.2) Treatment of rhodesiense HAT

Treatment of rhodesiense HAT differs from gambiense HAT, suramin used to be used as a treatment for stage I of both diseases but is now limited to the rhodesiense variety. It is taken up through the endocytic pathway and acts as a non-specific enzyme inhibitor, in *T. brucei* it inhibits cytokinesis (Venturelli et al., 2022). For stage II, melarsoprol is administered. Unfortunately, melarsoprol is extremely toxic and results in fatal reactive encephalopathy in 10% of patients (Baker et al., 2013). There is already widespread resistance to melarsoprol, with resistance resulting in a surge in cases during the 1990s. Resistance is likely the result of a mutation in the AQP2 transporter gene (Fairlamb and Horn, 2018).

(2.1.2.3) Tsetse control

As well as the use and development of trypanocidal drugs, control of the vector and more advanced diagnostic methods have also contributed to the reduction in HAT cases. In Zanzibar, the sterile insect technique was used to eliminate tsetse flies from the country entirely in 1997, 3 years later Zanzibar saw substantial increases in milk and meat production (Kabayo, 2002). However, the feasibility of applying this technique continent-wide is debated, owing to the high cost and amount of required infrastructure (Aksoy et al., 2017). There are cheaper methods, targets surrounded by netting, containing the chemoattractants octenol and para-cresol, were used to decrease tsetse density by 80% nn a control area in Guinea (Courtin et al., 2015). Sequencing of tsetse fly genomes has also provided opportunities to increase knowledge of the tsetse fly olfactory system to improve the efficacy of chemo

attractants for use in targets and traps (Aksoy et al., 2017). There have also been improvements in diagnostic methods, while antibody testing and microscopy have been crucial in combating HAT, new techniques such as loop-mediated isothermal amplification allow for rapid and robust detection of trypanosome DNA (Álvarez-Rodríguez et al., 2022).

(2.1.2.4) Treatment of AAT

Despite the success of controlling the transmission of HAT, AAT is still a major problem. Outside of the economic burden imposed by AAT, true HAT elimination will be impossible while large trypanosome reservoirs exist in wild and domesticated animals. There are currently 3 drugs used to treat *T. congolense* AAT, homidium bromide, isometamidium chloride (ISM) and diminazene aceturate (DA). Homidium bromide cannot cross the BBB, so is used to treat early infections. It acts by inhibiting replication of both nuclear and kinetoplast DNA (Venturelli et al., 2022). Diminazene is the most widely used trypanocide for AAT treatment, it interferes with DNA replication but cannot cross the BBB and resistance is widespread (Kasozi et al., 2022). Isometamidium chloride is used as a prophylactic, providing 3 months protection, though resistance has been reported in *T. congolense* (Mekonnen et al., 2018).

(2.1.2.5) Issues facing AAT treatment

Despite the availability of trypanocidal drugs, there are issues regarding their use. The biggest problem is the availability and cost of diagnosis. The haematocrit

centrifugation technique is cheap and applicable to field applications but lacks sensitivity. Immunological and molecular methods are more sensitive but require expertise and are generally expensive (Richards et al., 2021). This leads to many farmers practising visual diagnosis, with varying degrees of success. In one study in Kenya, 53% of treatments administered for AAT were used on non-infected cattle (Machila et al., 2003). In southwest Ethiopia, 87% of DA treatments, and 48% of ISM treatments, administered to calves were overdosed, with only 30.8% of all treatment being administered with veterinary assistance (Moti et al., 2015). Furthermore, a study of disease management in Mali and Burkina Faso showed that 25% of farmers failed to identify the correct injection site (Liebenehm et al., 2011). Even with the correct administration of trypanocidal drugs, counterfeit and poor-quality drugs remain a large problem. One study of non-compliant drugs (incorrect dose of active ingredients) showed that in some countries, 60% of trypanocidal drugs are non-compliant, regardless of whether they were purchased from an official source (Bengaly et al., 2018).

(2.1.2.5) Drug resistance

Resistance to trypanocidal drugs has been reportedly widespread for several decades, however, as previously established, there are many factors outside of drug resistance that can result in treatment failure. Widespread resistance has been reported in myriad studies based on a DPnII-PCR-RFLP, a test which identifies mutations in the TcoAT1 transporter gene (Chitanga et al., 2011; Tchamdja et al., 2017). However, closer analysis of TcoAT1 has revealed that it is not involved in

diminazene transport and likely does not contribute to DA resistance in *T. congolense* (Munday et al., 2013). Though there are more robust tests for resistance, such as trypanocidal drug ELISAs (Delespaux et al., 2002), currently little is known about the true prevalence of resistance in nature. Ultimately, this highlights the need for further study of the diverse causative agents of AAT.

(2.2) Overview of trypanosome biology

(2.2.1) Life cycle of *T. brucei* and *T. congolense*

(2.2.1.1) Life cycle of *T. brucei*

African trypanosomes are digenetic parasites that alternate between the tsetse fly and mammalian hosts, requiring changes in gene expression and morphology to adapt to disparate environments. If a tsetse fly ingests a blood meal from a host infected with *T. brucei*, the ingested parasites differentiate from bloodstream form characterised by a variable surface glycoprotein coat to procyclic form, and the variable surface glycoprotein (VSG) coat is replaced by a procyclin coat (Rose et al., 2020). This procyclin coat is composed of two related protein groups, extensive repeats of glutamic acid and proline (EP) and glycine, proline, glutamic acid, glutamic acid, threonine pentapeptide repeats (GPEET) (Utz et al., 2006). Procyclics colonise the midgut before migrating to the ectoperitrophic space between the peritrophic matrix (PM) and gut epithelium, possibly by penetrating the PM (Rose et al., 2020). Parasites progress to the salivary glands where they differentiate from procyclic trypomastigotes to epimastigotes through asymmetric division, they then further differentiate into the mammal infective metacyclic trypomastigote form (Sharma et

al., 2008). Once in the mammalian host, they differentiate into slender, rapidly proliferating bloodstream forms which switch their VSG coat to evade the mammalian immune system. Parasites colonies the blood, lymphatic system, and interstitial spaces of organs including the heart, kidney, and lungs, eventually colonising the brain (Trindade et al., 2016). At high density, they differentiate into shorter, non-proliferating stumpy forms which are preadapted for survival in the tsetse fly (Breidbach et al., 2002). This is a result of the quorum sensing pathway in response to presence of stumpy inducible factor (SIF), differentiation to stumpy form is also thought to be a form of self-regulation to increase host survival by reducing parasitaemia (Schuster et al., 2021). A blood meal restarts the cycle and bloodstream parasites differentiate into procyclic form.

(2.2.1.2) Life cycle of *T. congolense*

The life cycle of *T. congolense* is less well characterised when compared to *T. brucei*. Like in *T. brucei*, differentiation from bloodstream form to procyclic form occurs when a tsetse fly ingests a blood meal from an infected host resulting in a loss of the variable surface glycoproteins. However, in *T. congolense*, the main surface antigen is GARP, which contains no amino acid repeats in its primary sequence (Utz et al., 2006). Procyclic trypomastigote parasites then migrate to the mouthparts where they attach in the labrum of the proboscis and differentiate into proliferative epimastigotes. In the labrum they differentiate into metacyclics with a VSG coat, pre-adapting them for the mammalian host (Peacock et al., 2012). In the mammalian host, they differentiate into proliferative bloodstream form. Unlike *T. brucei*, they

mainly adhere to vasculature, but have also reportedly been found in lymph node tissue and connective tissue at the location of the tsetse bite (Periera et al., 2019). Unlike in *T. brucei*, *T. congolense* lack a morphological stumpy form, instead high parasitaemia results in cell cycle arrest and changes in gene expression (Silvester et al., 2018).

(2.2.1.3) Comparison of PCF and BSF *T. brucei*

Aside from the presence or absence of a VSG coat, there are many other differences between PCF and BSF stages that enable them to survive in disparate environments. One of these differences is a change in metabolism to meet their specific energy demands. BSF rely on substrate level phosphorylation of blood glucose which takes place within kinetoplastid specific glycosomes, whereas PCF utilise oxidative phosphorylation within the mitochondrion (Mayke et al., 2022). As a result of differences in energy metabolism between the BSF and PCF stages, there are clear morphological differences in the parasite's single large mitochondrion. PCF *T. brucei* have a more complex and branched mitochondrion with abundant cristae, while BSF have a simpler, unbranched mitochondrion which was once thought to be devoid of cristae (Mathews, 2005; Povelones et al., 2016). However, recent FIB-SEM imaging of the mitochondria in BSF *T. brucei* has indicated that although cristae volume and surface area is reduced, they are still present in some capacity, and cristae biogenesis does occur (Bílý et al., 2023). Additionally, (Bílý et al., 2023) discuss the possibility that cristae biogenesis and mitochondrial fusion are necessary for cell division in BSF.

The PCF mitochondrion has all the necessary components for the complete respiratory chain, contains Kreb cycle enzymes and has high expression of ATPsynthase. In comparison, ATPsynthase is less abundant in BSF and functions to maintain mitochondrial membrane potential by hydrolysing ATP rather than synthesising it (Brown et al., 2006).

There are other important differences that can be observed between the different lifecycle stages. Other changes result from the differing surface proteins, endocytosis occurs much more rapidly in BSF due to the need for parasites to uptake and recycle VSGs to avoid the host immune system – this enables current surface VSGs to be internalised in ~12 minutes (Engstler et al., 2004). The rate of endocytosis in PCF is an estimated 20-fold lower, though endocytosis in both stages is clathrin-mediated (Vincent et al., 2013). Life cycle stages also differ in motility, reflecting the greater viscosity of the mammalian blood that BSF *T. brucei* traverses. Although the flagellum of both functions through alternating left-handed and right-handed helical waves, BSF show greater overall velocity (Rodríguez et al., 2009). Many differences affect the cell cycle, such as the presence of a novel transmembrane junction (flagella connector) found in PCF *T. brucei* which functions to connect the old and new flagella during flagellum biogenesis (Briggs et al., 2003). This, and other differences between the cell cycle in different life cycle stages, will be discussed further in later chapters. Overall, this demonstrates that the study of one life cycle stage is insufficient for the understanding of the whole organism.

(2.2.2) Genetic organisation and regulation

(2.2.2.1) Genome organisation

The nuclear genome of *T. brucei* contains 11 megabase-sized housekeeping chromosomes, alongside ~5 intermediate chromosomes (200-900 kb) and ~100 minichromosomes (30-150 kb), with the haploid genome totalling ~35 Mb (Daniels et al., 2010). The megabase chromosomes encode approximately 8,800 protein-coding genes (Maree and Patterton, 2014). 55% of a minichromosome is made up of *Trypanosoma brucei* repeat (TBR) sequences, they form the central core of the minichromosomes and act as the origin of replication (Reet et al., 2021). Variety in VSGs is critical to the parasite's virulence, most of the >1000 VSG genes are located on the 11 large chromosomes, as either complete VSGs or VSG pseudogenes that can form full VSGs through DNA recombination. Alongside large chromosomal VSGs, some intermediate chromosomes possess VSG expression sites, and each minichromosome can have up to 2 VSG genes (Bessat and Ersfeld, 2009). *T. brucei* also possesses a unique mitochondrial genome organised as a catenated network of two distinct classes of circular DNA that forms a large disk-shaped structure. There are a few dozen ~23 kb maxicircles encoding for mitochondrial proteins, and 5000-10000 ~1 kb minicircles coding for guide RNAs (Cooper et al., 2019).

T. brucei protein coding genes are located within non-overlapping polycistronic transcription units (PTUs), with all genes in a PTU being transcribed continuously despite the genes being functionally unrelated. Adjacent PTUs on the same strand are arranged head to tail, while PTUs on opposite strands are transcribed in opposite directions, these are separated by strand switch regions (SSR) (Maree and Patterton,

2014). Transcription appears to begin within SSRs, however, RNA polymerase II promoters or transcription factors are elusive. Instead, histone variants H4K10ac, H2AZ and H2BV are enriched up to 300-fold at hypothesised RNA pol II start sites. This implies that chromatin density and nucleosome stability play an increased role in transcription initiation (Siegel et al., 2009). Due to this unusual gene arrangement, post-transcriptional regulation plays an increased role in controlling gene expression.

(2.2.2.2) Post-transcriptional regulation

After transcription of PTUs by RNA polymerase II, the polycistronic transcripts are processed into individual mRNAs by 2 trans-splicing reactions. One adds a 39bp capped spliced leader RNA, the other adds a 3' polyA tail (Clayton et al., 2019). The modification, localisation, and degradation of mature mRNAs is regulated by a diverse array of mRNA binding proteins (RBPs). mRNA turnover plays a large role in mRNA abundance, with the mRNA degradation mechanism being analogous to other eukaryotes. First, the polyA tail is removed by the CAF1/NOT complex, resulting in the loss of polyA binding protein, followed by removal of the cap, then degradation by the 5' exonuclease XRNA (Manful et al., 2011). The average mRNA half-life is 5-20 minutes, though some exceed 2 hours, this can be changed by binding of RBPs. PUF9 is a pumilio-domain protein that extends the half-life of a small number of mRNAs that are upregulated in late G1-phase (Clayton et al., 2013).

Genes within kDNA are also regulated through post-transcriptional methods. Each maxicircle encodes 18 proteins involved in the respiratory transport chain plus 2 ribosomal RNAs (Peña-Diaz et al., 2017). 12 of these transcripts require uridine

insertion to generate a functional mRNA, minicircles encode guide RNA (gRNA) that acts as a template for U-insertion/deletion in a process known as RNA editing. There are 300-400 classes of gRNAs in *T. brucei*, though many classes are seemingly redundant. Some proteins may require >30 different gRNAs to produce mature mRNAs (Read et al., 2015). Each gRNA has a 5' anchor that binds via Watson-Crick base pairing to the mRNA, the central region binds through wobble base pairing and directs U insertion/deletion by being complementary to the desired sequence (Cooper et al., 2022).

(2.2.3) *T. brucei* cell biology

(2.2.3.1) Overview

T. brucei has a single, near-spherical nucleus located roughly at the centre of the cell body (Sherwin and Gull, 1989). It possesses a single large, highly branched mitochondrion, though the exact morphology is dependent on the life cycle stage. The mitochondrion stretches to encompass an area both posterior and anterior to the nucleus (Povelones et al., 2013). The mitochondrion contains the disc-shaped kinetoplast, a specialised structure that contains the mitochondrial DNA (kDNA) within a catenated array of circular DNA (Gluenz et al., 2011). In BSF, the kinetoplast is located at the posterior end of the cell, while in PCF it is located between the posterior of the cell and the nucleus (Mathews, 2005). *T. brucei* has a single flagellum, which has a canonical 9 + 2 axoneme structure which is nucleated from the basal body. The basal body connects to the kinetoplast through a tripartite attachment complex (TAC) composed of exclusion zone filaments and unilateral

filaments (Hoffmann et al., 2018). The flagellum exits the cell posterior to the nucleus through the flagellar pocket (FP), the flagellum remains associated with the cell body until it extends beyond the cell and overhangs slightly (Langousis and Hill, 2014). The basal body has 2 sections, a 9 + 0 triplet arrangement of microtubules and a transition zone of 9 + 0 doublet microtubules. The pro-basal body is an immature basal body that lacks the transition zone (Vaughan and Gull, 2015). The flagellar pocket is the only site of endo/exocytosis, the flagellar pocket collar (FPC) is a cytoskeletal component located where the flagellum exits the celland forms a tight junction between the pellicular, flagellum and FP membranes (Perdomo et al., 2016). The Bilobe is a cytoskeletal structure located adjacent to the FPC that is composed partly of Centrin2 and Centrin4 – hinting at a role in microtubule organisation (Morriswood et al., 2009). In *T. brucei*, the Golgi apparatus is asymmetrically distributed towards the flagellum. The ER is highly dynamic, and its exact confirmation depends on the life cycle stage. Each cell also possesses one lysosome, and many glycosomes, lipid droplets, and RNA granules (Halliday et al., 2019).

(2.2.3.2) Cell shape and subpellicular array

BSF *T. brucei* cells have a long and slender shape that is determined by a helical array of microtubules. Though the exact dimensions of the cell vary greatly by lifecycle stage and laboratory strains, a BSF *T. brucei* cell body is approximately 25µm long and 3µm wide at its widest point (Alizadehrad et al., 2015). The microtubules follow a left-handed helical pattern which tapers at the anterior and posterior, with the posterior being broader and the anterior having a pointed shape (Sun et al., 2018;

Hemphill et al., 1991). This array, known as the subpellicular array, is a single layer of microtubules below the cell membrane consisting of >100 individuals microtubules cross-linked with each other, forming an inward facing cage-like structure (Sun et al., 2018). The distance between adjacent microtubules (18-22nm) is maintained across the entire length of the cell despite differing cell width, this is achieved through a greater number of microtubules at the widest point and stepwise termination of microtubules as the cell tapers (Sinclair and Graffenried, 2019). The helical and interconnected nature of the array enables flexibility, and changes in the spacing and orientation of the microtubules are tied to flagellum beating and enable the corkscrew-like movement of the parasite (Sun et al., 2018). The microtubules originate from microtubule organizing centres (MTOCs), most originating from the anterior of the cell but converging at the posterior, with biogenesis of new microtubules occurring from the anterior (Sheriff et al., 2014). Biogenesis of new microtubules during the cell cycle also occurs within other regions, with notably high levels of microtubule polymerisation occurring within proximity of the new flagellum attachment zone (Sheriff et al., 2014). The subpellicular array is divided into subdomains by microtubule associated proteins (MAPs) which bind, directly or indirectly, to tubulin dimers. Posterior microtubules are bound by PAVE1 which forms a complex with PAVE2, this complex functions to stabilise growing microtubules and PAVE1 depletion results in the loss of the characteristic tapered cell posterior (Sinclair et al., 2021). These MAPs may be regulated by TbAIR9, TbAIR9 RNAi results in the even distribution of PAVE1 rather than localisation to the posterior domain (Sinclair et al., 2021). The cytoskeleton of *T. brucei*, unlike its mammalian counterparts, is a stable structure that can be isolated by detergent

extraction (Hemphill et al., 1991). The subpellicular array is closely associated with a range of important flagellar pocket associated cytoskeletal structures (figure 2.3)

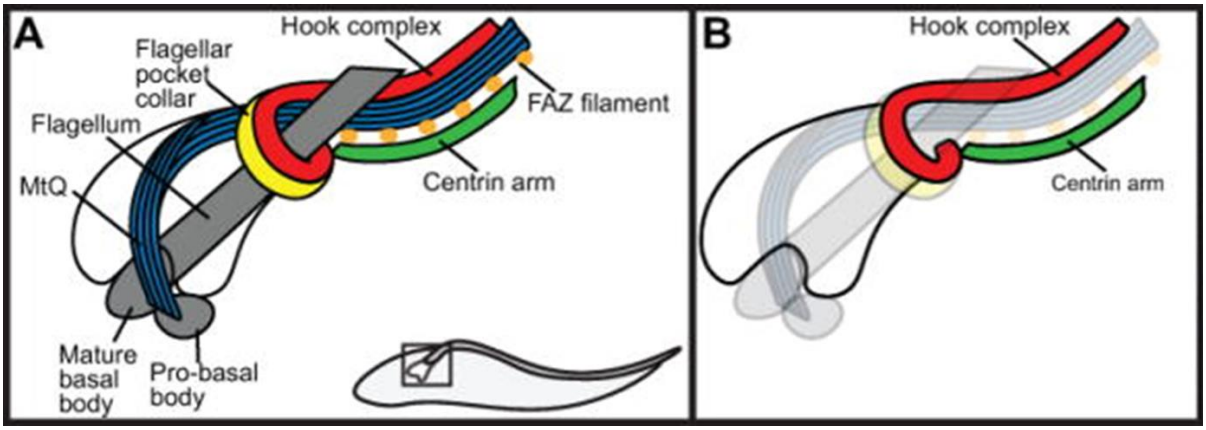

Figure 2.3 Representation of flagellar pocket associated cytoskeletal structures in *T. brucei*. (A) Schematic of cytoskeletal structures associated with the flagellar pocket. (B) Schematic focussing on the hook complex and centrin arm (Perry et al., 2018).

(2.2.3.3) Flagellar pocket – structure and function

The flagellar pocket is a highly critical structure for *T. brucei* survival and virulence. The flagellar pocket is a specialised membrane invagination, the membrane is continuous with the flagella membrane and cell membrane yet remains functionally and biochemically distinct from both (Gadelha et al., 2009). The largest component of the FP is a large balloon-shaped membrane that ends at the FPC. The membrane has an asymmetric bulge at one side where the intracellular portion of the flagellum is located with the golgi and pro-basal body located adjacent to this bulge (Lacomble et al., 2009). Between the 9 + 0 triplet microtubules and the transition zone of the basal body are transitional fibres that connect to the flagellar pocket membrane (Vaughan and Gull, 2015). Between the FPC and cell membrane is a transitional neck

region, only slightly wider than the flagellum. Specialised microtubules originating between the basal and pro-basal body, termed the microtubule quartet (MtQ), traverses the FPC, and then occupies the neck before rejoining the subpellicular array. The flagella attachment zone also begins at the neck, on the opposite side to the quartet (Lacomble et al., 2009).

The flagellar pocket has several key functions. (1) It is the sole site for endo/exocytosis and provides a platform for the binding of receptors without exposure to the host immune system (such as the transferrin receptor for uptake of Iron). (2) It is involved in trafficking and recycling of GPI-anchored surface proteins. (3) It is essential for evasion of the host immune system (Demmel et al., 2014).

(1) The flagellar pocket is a key site for the transport of essential molecules, the haem receptors for both BSF and PCF (TbHbR and TbHRG) are located in and around the pocket (Halliday et al., 2021). It is also the main route for iron uptake, with the transferrin receptor located in the FP for the uptake of Fe^{3+} from its environment (Kariuki et al., 2019).
(2) GPI anchored proteins include variable surface glycoproteins (BSF) and procyclins (PCF), with VSGs being important for defence against the mammalian host's active immune system. As the parasite moves through the viscous media, binding of an antibody to the VSG increases resistance and causes the VSG to be dragged towards the FP (Link et al., 2021). Removal of the VSG from the flagellar pocket is entirely dependent on clathrin-mediated endocytosis (Engstler et al., 2004).

(3) The FP also plays a role in innate immunity. Human serum has trypanolytic qualities that prevents infection by *T. brucei brucei* and *T. congolense* due to the presence of trypanosome lysis factor (TLF) (Pays and Vanhollebeke, 2009). Expression of serum resistance-associated protein (SRA) in *T. brucei rhodesiense* confers resistance to TLF, SRA must localise to the FP before rapid endocytosis. The role of the FP in resistance is debated, with one study showing 37% of cells show SRA localised to the FP (Stephens and Hajduk, 2011), and others showing 3.2% (Bart et al., 2015), indicating the TLF-SRA interaction occurs intracellularly rather than at FP membrane.

(2.2.3.4) The flagellar pocket collar

The flagellar pocket collar is a ring structure delineating the end of the flagellar pocket membrane. A key component of this structure is TbBILBO1, this protein has orthologues in every other trypanosome and no orthologues in any non-kinetoplastid species. BILBO1 synteny is maintained even within distantly related trypanosomatids such as those in the *Phytomonas* genus (Perdomo et al., 2016). TbBILBO1 has an N-terminal globular domain, 2 EF hand domains, a long coiled-coil domain, and a C-terminal leucine zipper. Coiled-coil domains form an antiparallel dimer and leucine zippers of adjacent dimers associate to form filamentous chains (Vidilaseris et al., 2015). BIBLO1 interacts with BILBO2 and FPC4, both BILBO1 and BILBO2 bind to FPC4 through their structurally similar N-terminal domain, while BILBO2 binds BILBO1-EF1 hand domain through its BILBO1-binding domain. BILBO2 binding modulates the shape of BILBO1 polymers, this may play a role in the cell cycle as BILBO2 is a cell

cycle regulated (CCR) protein (Isch et al., 2021). FPC4 binds to both BILBO1 and BILBO2 through its C-terminal domain, and the N-terminal domain binds microtubules (Albisetti et al., 2015). The MtQ associates with both the FPC, and the hook complex.

(2.2.3.5) The hook complex

The hook complex is a fish-hook shaped structure adjacent to the FPC neck and is defined by the presence of TbMORN1 (Perry et al., 2017). The exact function of the hook complex is unknown, but it is essential for viability in BSF *T. brucei*. In literature, the hook complex may be referred to as part of a larger complex termed the bilobe, which also includes the centrin arm, though the spatial and structural separation between the two has led to them being referred to separately (Morriswood and Schmidt, 2015). TbSmee1 is a component of the hook complex and a substrate of TbPLK – an important cell cycle regulator, depletion of TbSmee1 results in a hook complex with an aberrant morphology (Perry et al., 2017). FPC4 has been proposed to link the FPC and hook complex due to its ability to bind isolated microtubules (Albisetti et al., 2017), however, TbBHALIN has also been proposed (Broster Reix et al., 2021).

(2.2.3) Overview of *T. congolense* biology

(2.2.3.1) Genomic organisation and gene expression

T. congolense is a poorly studied organism compared to *T. brucei*, especially regarding study of the cell cycle. Like *T. brucei*, *T. congolense* genes are organised into PTUs which must undergo post-transcriptional processing via trans-splicing (Fervers et al., 2018). Though they are closely related organisms, there are many important differences. Like *T. brucei*, *T. congolense* encode VSGs for immune evasion, but the regulation of VSG transcription is different. *T. congolense* IL3000 strain possess 240-320 minichromosomes which are on average ~30 kb. These are composed primarily of a 369 bp repeat that total ~25 kb, this core region is flanked by telomeres (Abbas et al., 2018). These contain coding regions for VSG genes as well as conserved non-coding regions which may act as a promoter, in place of a VSG expression sites. *T. brucei* also have expression site associated genes (ESAG) closely associated with the telomeric region, which are not present in *T. congolense* (Abbas et al., 2018). The VSG repertoire is also different between species, with *T. congolense* VSGs evolving from several ancestral lineages, and *T. brucei* VSGs evolving more recently. ESAG6/7, which encode the transferrin receptor in *T. brucei*, is thought to have evolved from a *T. brucei* specific VSG which has gained additional function, while *T. congolense* also shows distinct VSG derived sequences such as Fam14 and Fam15 (Jackson et al., 2012).

Both BSF *T. brucei* and *T. congolense* show gene expression changes in response to increasing parasite density. As previously mentioned, *T. congolense* does not show a morphological stumpy form in response to increasing parasitaemia, instead changing

gene expression. Of the genes upregulated, many encode non-VSG cell surface proteins of a family that includes ESAG6/7 in *T. brucei* but is considerably expanded in *T. congolense* (Silvester et al., 2018).

(2.3.3.2) Cytoskeletal network

T. congolense show some differences in the cytoskeletal network and its associated structures when compared to *T. brucei*. Comparative studies of motility between *T. vivax*, *T. brucei*, *T. evansi* and *T. congolense* demonstrate that *T. congolense* are by far the weakest swimmers, being nearly unable to swim in a consistent direction. The author describes the non-directional movement as 'tumbling', *T. brucei* spent 21-25% of their time tumbling, compared to 94% in *T. congolense* (Bargul et al., 2016). (Bargul et al., 2016) Attributes this to their short and inflexible cell body, with the flagellum following a straighter path along the body making it unable to generate 180° turns like seen in *T. brucei* (Figure 2.4). The reduced swimming capacity is due to the flagellum of *T. congolense* having a divergent function, being used to adhere to the vasculature of a mammalian host (Hemphill and Ross, 1995), this enables it to adhere to culture flasks in vitro (Thonnus et al., 2017). In BSF *T. brucei*, a mobile transmembrane junction called the groove facilitates the growth of the new flagella parallel to the old. There is conservation of groove proteins in *T. brucei* and *T. congolense*, but *T. congolense* lacks the canonical groove structure and shows different spatial organisation of the growing flagellum (Smithson et al., 2022).

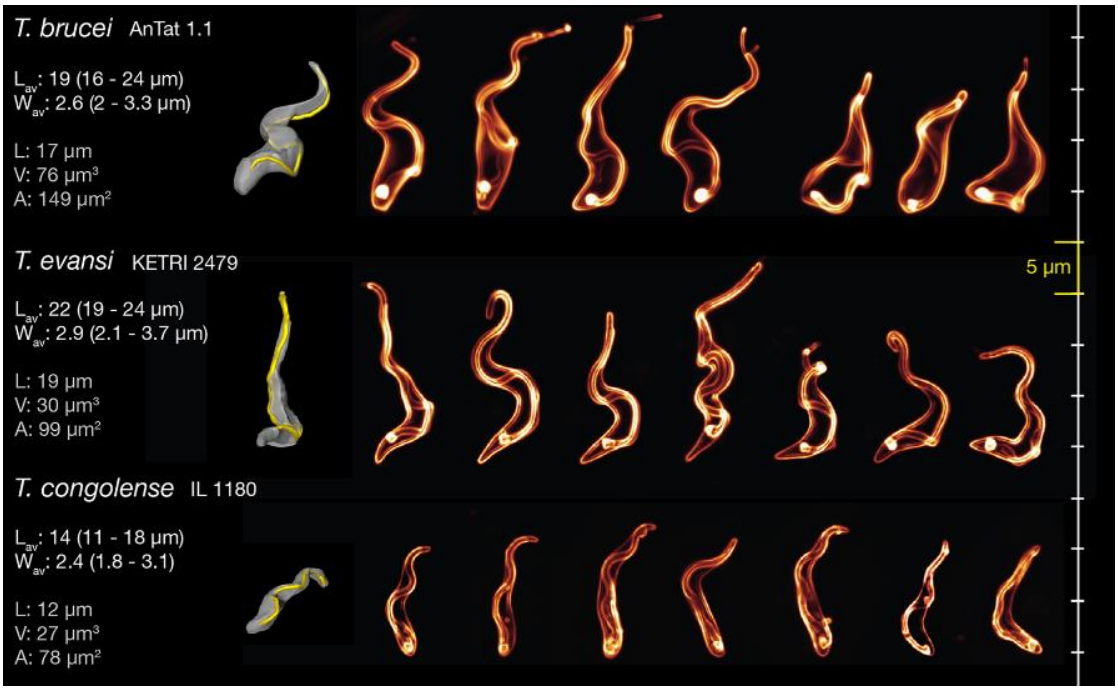

Figure 2.4 3D model of trypanosome species comparing cell shape and size. Adapted from (Bargul et al., 2016).

(2.3) *T. brucei* cell cycle

(2.3.1) Cell cycle events

Over the course of the cell cycle*, T. brucei* must duplicate and segregate its nuclear genome, mitochondrial genome, its single-copy organelles, and the complex set of cytoskeletal structures (Figure 2.5). The general order of cell cycle events has been understood for some time, but there are still many questions surrounding division and regulation that remain unanswered. First, the pro-basal body matures into a second basal body, growth of the second flagellum is initiated, two new pro-basal bodies are formed, the new flagellum exits the flagellar pocket, the kinetoplast divides, the basal body and kinetoplast are separated, mitosis occurs, and finally the cell undergoes cytokinesis (Sherwin and Gull, 1989). There are also slight differences

between BSF and PCF replication. The PCF cell cycle is ~8.5 hours while BSF is ~6 hours, and in PCF the daughter nucleus is repositioned between the two divided kinetoplasts (Hammarton et al., 2007).

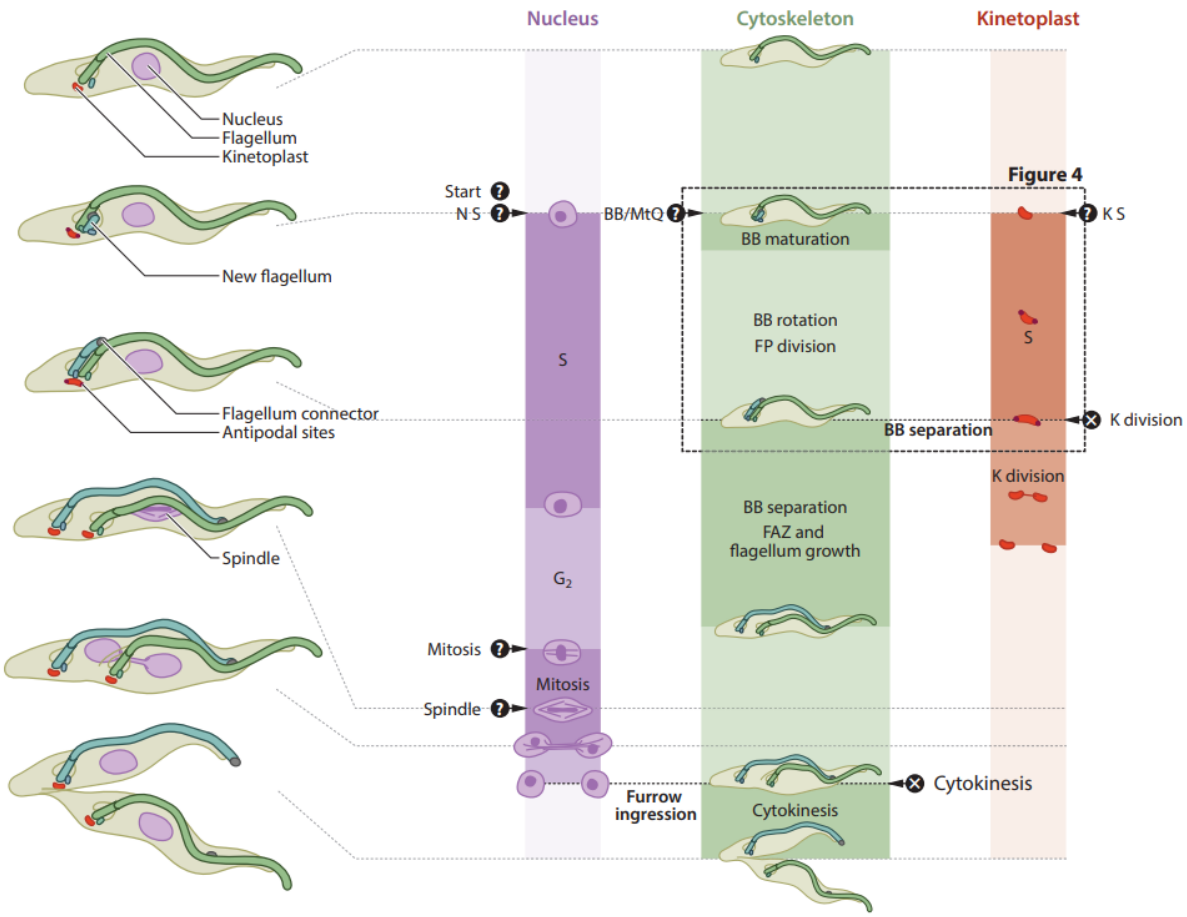

Figure 2.5 Overview of PCF *T. brucei* morphology and cell cycle events (Wheeler et al., 2019)

(2.3.1.1) Nuclear division

Nuclear DNA replication begins from several origins on each chromosome, these are bound by proteins related to the eukaryotic origin of recognition complex composed of ORC1-6 and modulated by CDC6 (Bleichert et al., 2015). Initially, only a homologue of ORC1/CDC6 could be identified, though other highly divergent ORC subunits have

now been found and the ORC1/CDC6 binding sites have been shown to colocalise to sites of replication initiation (da Silva et al., 2017). ORC1B localises to the nucleus during S-phase, then after the ORC complex assembles, the rest of the pre-initiation complex can form (Marques et al., 2016). The pre-initiation complex is composed of eukaryotic homologues though some proteins possess structural differences. For example, the ATPase and zinc finger domains of MCM1-7 are conserved, but CDC45 only shares 20-5% homology with its mammalian homologue (Dang and Li, 2011). After DNA replication, *T. brucei* nuclei undergo closed mitosis, meaning the nuclear envelope does not break down (Ogbadoyi et al., 2000). Unusually, *T. brucei* chromosomes do not appear to condense during interphase (Vickerman and Preston, 1970). Aside from this, mitosis progresses similarly to other eukaryotes but with a divergent kinetochore structure (Llauró et al., 2018).

(2.3.1.2) Kinetoplast division

kDNA replication occurs when topoisomerase II releases minicircles from the kDNA network, these are then replicated, transported to the poles of the kinetoplast and reattached to the network. Both minicircles and maxicircles are replicated unidirectionally via theta structures, however, maxicircles remain attached to the network during replication (Jensen and Englund, 2012). Segregation of the kinetoplast appears to begin during the kDNA division; it is tied to the separation of the cytoskeletal components. The kinetoplast is connected to the basal body and pro-basal body through the tripartite attachment complex (TAC), this acts as a substitute for the kinetochore in nuclear division (Ogbadoyi et al., 2003). The driver

of kinetoplast division is the separation of the basal bodies, discussed in the next section.

(2.3.1.3) Cytoskeletal division

The basal body acts as a master organiser for the surrounding cytoskeletal system. Each G1 cell has a basal and pro-basal body, at the G1/S transition, the pro-basal transition zone elongates and biogenesis of a new MtQ begins. The maturing basal body invades the flagellar pocket on the bulged side, and 2 new pro-basal bodies form perpendicular to the 2 mature basal bodies (Lacomble et al., 2010). As the new flagellum grows, a membranous ridge extends between the old and new flagella, beginning to form the new flagellar pocket (Lacomble et al., 2010).. The new basal body then rotates anticlockwise around the old basal body, the rotation drives the separation of the flagellar pocket into two and aligns with the formation of the new flagellar pocket collar (Lacomble et al., 2010). Separation of the two mature basal bodies also drives separation of the kDNA (Robinson and Gull, 1991). Though the basal body initiates growth of the new flagellum, interference with the basal body or associated components does not impact flagellum extension. Instead, the intraflagellar transport (IFT) system is necessary for continued extension of the new flagellum (Kohl et al., 2003). Duplication and separation of flagellar pocket associated structures is dependent on TbPLK, it localises to successive cytoskeletal components, and its arrival corresponds with the duplication of the basal body, FPC, bilobe and flagellum attachment zone (Ikeda and de Graffenried, 2012). It achieves this by associating with the growing MtQ which extends through all these structures in turn.

There is also a second TbPLK pool that is associated with the flagella connector (Ikeda and de Graffenried, 2012). From the beginning of the cell cycle, cells grow continuously in length until division (in PCF form), this requires the growth of new microtubules between already present and stable subpellicular array (Sheriff et al., 2014). During mitosis, new microtubules are intercalated into the existing subpellicular array to widen the centre of the cell, and inheritance of the subpellicular array is semi-conservative (Wheeler et al., 2013). After migration of the new basal body, the old and new FAZ are separated by the invasion of new microtubules, and the new FAZ grows from the posterior (Sunter and Gull, 2016). The new FAZ lies between the two flagella and defines the site of the cytokinesis furrow (Vaughan et al., 2008). The furrow progresses from anterior to posterior, dividing the cell on its longitudinal axis, separating the duplicated single-copy organelles between two slightly asymmetrical daughter cells (Wheeler et al., 2019).

(2.3.2) Cell cycle regulation

(2.3.2.1) Regulation of interphase

Cell cycle progression in *T. brucei* is regulated by a diverse array of protein kinases, including CDKs, MAPKs, aurora-like kinases, and polo-like kinases. Receptor-linked tyrosine kinases and G-protein coupled receptors are not found in trypanosomes, meaning the G1 checkpoint regulation must be divergent from mammalian cells (Torri et al., 2006). The *T. brucei* genome encodes 10 cyclins and 11 Cdc2-related kinases (CRK). RNAi studies have shown that CRK1 and CRK2 are necessary for the G1/S transition, both interact with CYC2, while CRK1 also interacts with CYC4, CYC5

and CYC7 (Gouguechon et al., 2007). Other G1 events must be regulated, TbCentrin1 and TbCentrin2 are necessary for both basal body and Golgi duplication, with TbCentrin2 expression being regulated by TbCentrin4 (He et al., 2005; Wang et al., 2012). The role of PLK in G1 will be discussed further in the next chapter. Regulation of nuclear DNA licensing during S-phase is not a completely understood process and is highly divergent from other eukaryotes, but TbORC1B plays a crucial role (Marques et al., 2016). kDNA licensing is regulated by HslVU protease, which controls the abundance of the mitochondrial helicase TbPIF2 (Liu et al., 2009). Regulation of the G2/M transition is controlled by the CRK3-CYC6 pair, however, CYC6 also forms a complex with CRK9, while CRK3 also forms a complex with CYC2. CYC8 RNAi also delays the G2/M transition but its binding partner is not currently known (Li, 2012).

(2.3.2.2) Regulation of mitosis and cytokinesis

The Aurora B kinase homologue TbAUK1 forms a chromosomal passenger complex (CPC) with CPC1 and CPC2, this complex localises at the chromosomes, then moves to the central spindle during the metaphase-anaphase transition. After this, it migrates to the growing FAZ and can then be found at the cleavage ingression during cytokinesis (Li et al., 2008). TbTLK1 is a substrate of TbAUK1 that is necessary for spindle assembly and chromosome segregation (Li et al., 2007). Homologues for the anaphase promoting complex have been identified which form a ubiquitin-ligase complex necessary for the transition to anaphase (Bessat et al., 2013). Both TbAUK1 and TbPLK are implicated in cytokinesis, inhibition of TbPLK results in major cytokinesis defects that cause total growth arrest. However, studies on populations

synchronised to early G1 have shown that inhibiting TbPLK 3.5 hours into the cell cycle results in 50% decline in growth, and at 5.5 hours no reduction in growth. This shows that TbPLK phosphorylates its target early in the cell cycle and that this is required for cytokinesis to occur (Lozano-Núñez et al., 2013). Despite having some knowledge of proteins involved in the regulation of the cell cycle, there are large gaps in our understanding, with many homologous proteins, such as PLK, having divergent functions in trypanosomes. Further study of CCR proteins will be necessary to further our understanding of these processes, this necessitates evaluating what methods should be used to accurately study the cell cycle.

Table 2.1 Cell cycle regulators in *T. brucei* and *T. congolense*. Key cell cycle regulators were identified in *T. brucei*, and homologues were found in *T. congolense* using TryTrypDB (Aslett et al., 2010).

Cell cycle phase	Protein name	*T. Brucei* protein ID	*T. Congolense* orthologue protein ID
G1	CY2C	Tb927.11.14080	TcIL3000_0_08150
	CRK1	Tb927.10.1070	TcIL3000_10_880
	CRK2	Tb927.7.7360	TcIL3000_7_5980
S	ORC1b	Tb927.9.2030	TcIL3000_9_510
G2M	CRK3	Tb927.10.4990	TcIL3000_10_4170
	CYC6	Tb927.11.16720	TcIL3000_11_16610
	CYC8	Tb927.7.1590	TcIL3000_7_1110
	CRK9	Tb927.2.4510	TcIL3000_2_850
Mitosis	TLK1	Tb927.4.5180	TcIL3000_0_18290
	AUK1	Tb927.11.8220	TcIL3000.11.8760
	CPC1	Tb927.6.4820	TcIL3000_6_4300
	CPC2	Tb927.11.14840	TcIL3000.11.15130
Cytokinesis	PLK	Tb927.7.6310	TcIL3000_7_5220

(2.3.3) Study of the cell cycle

There are many questions currently unanswered regarding how *the T. brucei* cell cycle is regulated. The biogenesis, movement and separation of the cytoskeletal components, including those associated with the flagellar pocket, is a key driver of the cell cycle. Cells in culture where mitosis has been artificially inhibited still can undergo cytokinesis, producing cells that lack a nucleus termed 'zoids' (Robinson et al., 1995). Though the duplication and movement of flagellar pocket associated cytoskeletal structures (F-PACS) is necessary for faithful completion of the cell, the pathways that regulate these processes have not been fully characterised. The methods used for studying both the cell cycle and F-PACS, should therefore be explored and scrutinised.

(2.3.3.1) Cell cycle study in asynchronous populations

Much of the work to elucidate the role of key cell cycle regulators in *T. brucei* has been done in asynchronous cultures using a reductionist approach, which typically involves monitoring a modified protein. Changes in localisation and abundance can be monitored by expression of a fluorescent tag. Cell lines that enable depletion (through RNAi, degradation, or inhibition) or overexpression of the target protein allow for analysis of the generated phenotype which may elucidate the proteins' function (Morriswood and Engstler, 2016). Following observation of a phenotype, the point in the cell cycle that the phenotype is seen and the point at which inhibition results in a defect must be determined, this is commonly done by nuclear and kinetoplast counts or flow cytometry. However, the resolution of these techniques is

poor as ~70% of asynchronous *T. brucei* cells are 1N1K, and flow cytometry cannot distinguish G2 from M phase cells. One approach to improve resolution is to use both techniques, as shown in one study examining the role of PUF9 (Archer et al., 2009). Further characterisation can be achieved using more specific markers against structures or organelles to give a more accurate estimate of cell cycle progression. Utilising a non-disruptive synchronisation technique would make this process more efficient while enabling large-scale, global transcriptomic and proteomic studies of the cell cycle.

(2.3.3.2) Cell cycle synchronisation methods

There are many methods that have been employed to synchronise cell populations, these fall into two main categories, treatment of an asynchronous population resulting in reversible cell cycle arrest or mechanical isolation of cells in a specific cell cycle phase. The most common synchronisation treatment for *T. brucei* is hydroxyurea (HU). HU inhibits ribonucleotide reductase by a reduction reaction of the radical centre of the R2 subunit, inhibiting the production of dNTPs and therefore DNA synthesis (Ligasová and Koberna, 2021). One study on *T. brucei* shows that a 6-hour induction with HU results in a heavily enriched S phase population – however, this synchronisation is not recognisably maintained through to the next cell cycle (Forsythe et al., 2009). Aside from duration, there are other problems with HU synchronisation, mainly that it induces replication stress. HU treatment results in depleted dNTPs, generation of reactive oxygen species and inhibition of active replication forks, leading to the accumulation of ssDNA, increased chromosome

fragility, replication fork collapse, deregulated chromatin remodelling, errors during cell cycle progression and cell death (Musiałek and Rybaczek, 2021). In PCF *T. brucei*, starvation methods can be used to achieve semi-synchronous populations. Cells are seeded at a high density (10^7 cells/ml) and left without additional nutrients, after 2 days cells are diluted into fresh media, resulting in a population initially enriched to G0/G1. However, even immediately after addition to fresh media there is a notable G2/M population, the cells stall for ~3 hours, and all synchronicity is lost after ~12 hours or one complete division (Gale et al., 1994). These factors alone make it undesirable as a synchronisation method, but serum starvation has also been shown to result in DNA fragmentation in mammalian cells (Kues et al., 2000). Regardless of whether the mechanism underpinning starvation-induced stress is the same between mammals and trypanosomes, the 3-hour delay in rejoining the cell cycle is undoubtedly a result of stress.

One method of mechanical isolation is flow cytometry-based cell sorting. These protocols utilise commercial dyes combined with flow cytometry to sort cells based on DNA content. This has been used to enrich populations to G0/G1 and G2/M in PCF and BSF *T. brucei* (Siegel et al., 2008; Kabani et al., 2010). Despite the advantage of being a simple process, it suffers from low yield and low specificity as G0 cells cannot be differentiated from late G1 cells undergoing kinetoplast replication (Morriswood and Engstler, 2016). However, the main issue is the progression of cells post-enrichment. Cells do not progress synchronously through the cell cycle, instead, the initial enrichment is maintained for up to 7 hours before cells return to pre-enrichment ratios (Kabani et al., 2010). Overall makes it a poor choice for studying post-sort changes in the cell cycle. An alternative method is centrifugal counter-flow

elutriation, which physically separates cells based on hydrodynamic volume. A specialised centrifuge is combined with a buffer pumped in the opposite direction to the centrifugal force (counter-flow) which keeps cells in suspension, incremental increases in counter-flow speed results in the elution of cells based on size (Benz et al., 2017). This has been used to generate fractions containing 97% G1 PCF cells, with some synchronicity lasting up to 3 cell cycles. In PCF, early G1 cells can be separated from mid and late G1 populations. In BSF, some cells appear to become stalled in G1, indicating it may cause stress to some cells (Benz et al., 2017).

Centrifugal counter-flow elutriation represents the best option for studying changes in the cell cycle, and it has been applied to study key cell cycle regulators such as TbPLK (Ana Lozano-Núñez et al., 2013). It has also been applied to global studies of the cell cycle, being utilised to identify changes in protein abundance and phosphorylation throughout the cell cycle (Benz and Urbaniak, 2019). Though the method has been optimised for use in *T. brucei*, optimisation for use on understudied trypanosomes such as *T. congolense* would present an opportunity to increase our understanding of the causative agents of AAT.

(2.4) Aims and background

(2.4.1) Background to the project

Faithful replication of organelles is essential for cell division amongst all eukaryotes. in *T. brucei* and *T. congolense*, many unique, single-copy organelles must be duplicated and positioned correctly to maintain parasite viability and virulence

(Gadelha et al., 2009). *T. brucei* cells possess one permanent membrane invagination, known as the flagellar pocket, which contains the intracellular portion of the single flagellum, and is the sole site of endo/exocytosis (Engstler et al., 2004). The flagellar pocket is associated with the basal body and range of cytoskeletal structures (F-PACS), including the flagellar pocket collar and hook complex (Perry et al., 2017). The biogenesis and movement of the F-PACS is necessary for the repositioning of the daughter flagellum, the formation of the new flagellum attachment zone and cytokinesis (Lacomble et al., 2010). Many of the F-PACS components are unique to trypanosomes, thus proteins involved in the regulating biogenesis and positioning of these structures may act as suitable candidates for drug discovery.

TbPLK is one protein known to regulate biogenesis and positioning of these structures. Early in the cell cycle, TbPLK localises successively to the basal body, flagellar pocket collar, hook complex and flagellum attachment zone, the timing of this corresponds to the duplication of these structures (Ikeda and de Graffenried, 2012). Previous studies have shown that inhibition of PLK using a small molecule inhibitor leads to cytokinesis defects (Lozano-Núñez et al., 2013). The timing of inhibition also plays a role (figure 2.6), inhibition of PLK at the start of the cell cycle results in a 100% growth reduction, inhibition at 3.5 hours results in a 50% growth reduction and inhibition at 5.5 hours does not impact growth. This suggests that TbPLK mediates an event necessary for cell cycle progression early in the cell cycle (Lozano-Núñez et al., 2013). Isolation of the F-PACS combined with phosphoproteomic analysis may elucidate further TbPLK targets and contribute to a greater understanding of the *T. brucei* cell cycle.

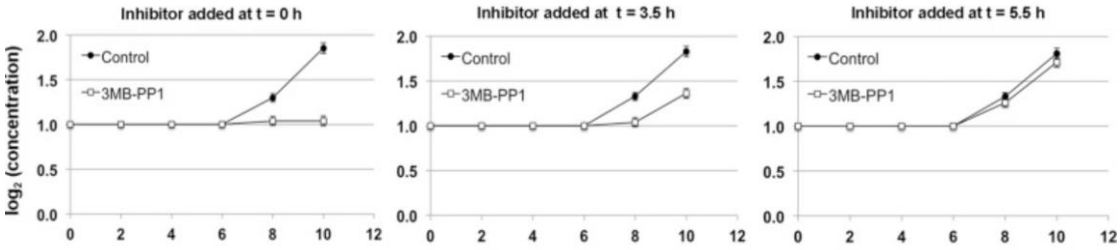

Figure 2.6 Growth of synchronised, analogue sensitive *T. brucei* after addition of small molecule inhibitor 0, 3.5 and 5.5 hours into the cell cycle. Addition of the inhibitor at T=0 h completely blocks cell cycle progression, reduces growth by 50% when added at T=3.5 h, and has minimal impact when added at T=5.5 h. Figure adapted from (Lozano-Núñez et al., 2013).

(2.4.2) Aims of the project

Centrifugal counter-flow elutriation (CCE) is a technique that separates cells based on sedimentation velocity and has previously been used to enrich *T. brucei* cells at G1 (Benz et al., 2017). This project aims to optimise the methodology for enrichment of the flagellar pocket associated structures in synchronised populations. These methods could then be used to generate phosphoproteomic samples of synchronised cells to monitor changes in phosphosites and elucidate further TbPLK substrates.

- **Objective 1:** The CCE will be validated by generating G1 enriched samples in both bloodstream and procyclic *T. brucei*. Fractions will be grown in culture,

with samples taken for flow cytometry every hour to ensure synchronised progression through the cell cycle.

- **Objective 2:** Conditions for the enrichment of F-PACS will be optimised using different salt buffers. Differences in protein retention between the salt conditions will be assessed by measuring total protein abundance. Presence of key F-PACS will be determined by immunofluorescence microscopy and western blot.
- **Objective 3:** Cell cycle regulation in *T. congolense* will be explored by generating tagged cell lines of cell cycle regulated proteins, including PLK, and by optimising cell cycle synchronisation methods.

(3) Methods

(3.1) Cell culture

(3.1.1) BSF *T. brucei* cell culture

BSF *T. brucei brucei* 2T1 Lister 427 strain were grown in HMI-11 (Hirumi and Hirumi, 1989) with 10% foetal bovine serum at 37 °C, 5% CO_2. Cells were grown in 5-10 ml of media and maintained at a density below 1×10^6 cells/ml. HMI-11 was made using 1 pack of Invitrogen HMI-9 powder, 10 g sodium bicarbonate, 500 ml Foetal bovine serum before ddH_2O was added to a final volume of 4.9 L. The pH was then adjusted to 7.3. 490 ml was filtered through a 0.2 µm sterile filter into sterile glass bottles and stored at 4°C until use. Before use, 5 ml L-glutamine (100x) and 5 ml pen-strep (100x) were added to a bottle.

(3.1.2) PCF *T. brucei* cell culture

PCF *T. brucei brucei* Lister strain was grown in SDM79 (Cunningham, 1977) with 10% foetal bovine serum, at 28 °C. Cells were grown in 5-10 ml of media and maintained below a density of 1×10^7 cells/ml. mNeonGreen::PFR1 protein (generated using v7 pPOT with blast resistance cassette) cell line was a kind gift from Professor McKean. SDM79 was made with 1 pack of Invitrogen SDM-79 powder, 10 g sodium bicarbonate, 750 ml heat inactivated Foetal bovine serum, 3.75 ml of 10 mg/ml hemin stock before ddH2O was added to a final volume of 4.9 L. The pH was then adjusted to 7.3. 490 ml was filtered through a 0.2 µm sterile filter into sterile glass

bottles and stored at 4 °C until use. Before use, 5 ml L-glutamine (100x) and 5 ml pen-strep (100x) were added to a bottle.

(3.1.3) BSF *T. congolense* culture

BSF *T. congolense* IL3000 strain were grown in TcoBSF-1 (MEM based media) (Coustou et al., 2010) with 15% goat sera at 34 °C, 5% CO^2. Cells were maintained below a density of 5×10^6 cells/ml. TcoBSF-1 was made using components in table 3.1 and ddH2O was added to a final volume of 425 ml. The pH was then adjusted to 7.3. 425 ml was filtered through a 0.2 µm sterile filter into sterile glass bottles and stored at 4 °C until use. Before use, 5 ml L-glutamine (100×) and 2.5 ml pen-strep (100x) were added to a bottle. Goat sera is never added to the media, instead, 50 ml aliquots of complete media plus goat sera (Gibco) were made. Aliquots of complete media were made by combining 42.5 ml of bottled media with 7.5 ml of goat sera, before pH adjustment, for use in routine culture.

Table 3.1 Components required for 500ml media before pH adjustment.

Component	**Quantity for 500 ml media**
MEM Powder (sigma)	4.8 g
Sodium bicarbonate	1.1 g
HEPES	2.98 g
Glucose	0.55 g

Sodium pyruvate	55 mg
Adenosine	5.3 mg
Hypoxanthine stock (0.1M)	0.5 ml
Thymidine	2.42 mg
Bathocuproinedisulphonic acid	5.65 mg
2-Mercaptoethanol	7 µl

(3.1.4) PCF *T. brucei* SILAC culture

1 L of SILAC media was made using 1 pack of Invitrogen SDM-79 SILAC powder, 2 g sodium bicarbonate, 0.75 g of 10 mg/ml hemin stock and ddH_2O up to a final volume of 880 ml. The pH was adjusted to 7.3 and 440 ml was filtered through a 0.2 µm sterile filter into sterile glass bottles which are stored at 4 °C. 10 ml of 100× L-glutamine and 10 ml of 100× Pen-strep are added to each bottle. To make complete media, 45 ml of the bottled media is combined with 5 ml Dialyzed, heat inactivated, foetal bovine serum. Labelled arginine and lysine were added to complete media at concentrations outlined in table 3.2 to make light, medium and heavy SILAC SDM79. Cells were allowed to acclimatise in light SILAC media, before being grown in light, medium and heavy SILAC for at least 3 days before use.

Table 3.2 Concentration of labelled amino acids added to SILAC media.

Label	**Concentration (mg/L)**
L-Arg.HCl (R0)	64.5

L-Arg.HCl (R6-$^{13}C6$)	66.3
L-Arg.HCl (R10-$^{13}C_6$,$^{15}N_4$)	67.5
L-Lys.HCl (K0)	21.6
L-Lys.2HCl (K4-$^{2}H_4$)	26.7
L-Lys.2HCl (K8-$^{13}C_4$,$^{15}N_4$)	27.3

(3.2) Synchronisation and analysis

(3.2.1) Centrifugal counter-flow elutriation of *T. brucei*

Elutriation was carried using a Beckman Coulter JE-5 elutriator. Intake tubes were placed into 70% ethanol and the pump was set to a moderate speed (~25 ml/min) for ~5 minutes. The ethanol was flushed from the system with 100 ml ddH2O, then 100 ml 1 × PBS, then 100 ml elutriation buffer, moving only the intake tube that is not active. Bubbles are removed from the tubing by gentle tapping on the instruments and visual inspection of the tubing. Flow speed was decreased to 8 ml/min (BSF) or 10 ml/min (PCF). The centrifuge speed was set to 1000 rpm for 1 minute, then back to 0 rpm, enabling all bubbles to be removed from the chamber. The centrifuge speed was steadily increased in increments of 1000 rpm to a final speed of 5000 rpm. Between 5×10^8 and 1×10^9 cells were harvested by centrifugation for 10 minutes at either 1000 × g (PCF) or 800 × g (BSF). The supernatant was removed, and the pellets were combined in an appropriate amount of elution buffer (5-20 ml). Cells were loaded into the elutriator at 5000 rpm at a flow speed of 8 ml/minute (BSF) or 10

ml/min (PCF). Formation of the boundary was monitored for ~10 minutes, flow rate was then increased to collect 150 ml (PCF) or 100 ml (BSF) fractions. Once the desired fractions were collected the flow speed was increased to 35 ml/min to remove remaining cells. To clean the rotor, the intake tube was switched from elutriation buffer, to ddH_2O, 1 × PBS then 100% ethanol in successive washes lasting ~5 minutes, before storing in ethanol. Cells were harvested by spinning at 1000 × g (PCF) or 800 × g (BSF) for 10 minutes, before being combined fractions collected at the same pump speed were combined. Samples were then prepared for analysis by desired methods, eluted cells were kept at 28 °C (PCF) or 37 °C (BSF).

(3.2.2) Hydroxyurea synchronisation

10 µg/ml of freshly prepared HU stock solution was added to media containing logarithmically growing *T. brucei* or *T. congolense* cells, flasks were left at 37 °C/34 °C for 6 hours. Cells were then spun at 1000 × g for 10 minutes and the supernatant removed. The pellet was resuspended in fresh media and spun at 2500 × g for 3 minutes, this was repeated once more. Cells were then returned to fresh media and allowed to propagate.

(3.2.3) Flow cytometry sample preparation: *T. brucei*

$1 \times 10^6 – 2 \times 10^6$ cells were collected in a microcentrifuge tube and centrifuged at 2500 × g for 3 minutes, the supernatant was removed, and the pellets were thoroughly resuspended cells in 1 ×PBS before addition of methanol to a final

concentration of 70%. Samples were stored at 4 °C overnight or until required. Once ready for analysis, samples were spun at 2500 × g for 3 minutes and the supernatant was removed. Pellets were resuspended in 1 × PBS, before spinning at 2500 × g for 3 minutes. The supernatant was removed, and the pellet resuspended in 1 ml PBS, 10 µg/ml propidium iodine and 10 µg/ml RNAseA. Samples were incubated at 37 °C for 45-60 minutes prior to analysis.

(3.2.4) Flow cytometry sample preparation: *T. congolense*

1×10^6 - 2×10^6 cells were collected in a microcentrifuge tube and centrifuged at 2500 × g for 3 minutes, the supernatant was removed, and the pellets were thoroughly resuspended cells in 1XPBS before addition of methanol to a final concentration of 50%. Samples were stored at 4 °C for 1 hour before addition of methanol to a final concentration of 70%. Samples were stored at 4 °C overnight or until required. Once ready for analysis, samples were spun at 2500 × g for 3 minutes and the supernatant was removed. Pellets were resuspended in 1 × PBS, before spinning at 2500 × g for 3 minutes. The supernatant was removed, and the pellet resuspended in 1 ml PBS, 10 µg/ml propidium iodine and 10 µg/ml RNAseA. Samples were incubated at 37 °C for 45-60 minutes in a shaking incubator prior to analysis.

(3.6) Flow cytometry data acquisition and processing

Beckman Coulter CytoFLEX and CytExpert software were used for analysis of samples. 10,000 events per sample were measured, events were gated first by forward/side scatter, then by PE-height and PE-width to remove doublets.

(3.3) F-PACS enrichment and analysis

(3.3.1) F-PACS enrichment

4×10^8 PCF *T. brucei* cells were centrifuged at 800 × g for 10 minutes, the supernatant was removed, and cells were resuspended in lysis buffer (ddH_20, 1% protease inhibitor mix). Lysed cells were pelleted at 800 × g for 10 minutes and resuspended in PEME (100 mM PIPES pH 6.9, 1 mM $MgSO_4$, 2 mM EGTA, 0.1 mM EDTA), 1% Igepal CA-63 and protease inhibitors (Tosyl-L-lysine chloromethyl ketone hydrochloride, leupeptin, phenylmethylsulfonyl fluoride, benzamidine). Samples were incubated at RT for 5 minutes before centrifugation at 1,800 × g for 10 minutes at 4 °C. The pellet was then resuspended in ice cold PEME (100 mM PIPES pH 6.9, 1 mM MgSO4, 2 mM EGTA, 0.1 mM EDTA), 1% Igepal CA-63, protease inhibitors and either 1M KCl or 1M NaCl. Alternatively, PEME, protease inhibitors and 65 mM $CaCl_2$ were used. Samples were incubated for 20 minutes on ice before centrifugation at 5100 × g for 20 minutes at 6°C and the supernatants discarded.

(3.3.2) Bradford Assay

A serial dilution of bovine albumin was performed to create samples with protein concentrations of 2000, 1500, 1000, 750, 500, 250, 125 and 25 µg/ml. 20 µl of each known sample and each test sample were added to an Eppendorf before addition of 1ml InstantBlue Coomassie protein stain (Abcam). The samples were mixed well, before being transferred to a 2 ml cuvette. A spectrophotometer set to measure 595 nm absorbance was calibrated using just InstantBlue with no protein. The known sample absorption was measured to create a standard curve before the test samples were measured. Test sample pellets were resuspended in lysis buffer (ddH_20, 1% protease inhibitor mix) of equal volume to the supernatants, immediately after sample generation.

(3.3.3) Immunofluorescence microscopy

~2×10^6 - 4.5×10^6 mid log PCF *T. brucei* cells were collected and centrifuged at 2500 × g for 3 minutes while glass slides were marked with a hydrophobic marker. The supernatant was removed, and cells resuspended in 1ml 1 × PBS before spinning at 2500 × g for 3 minutes. The supernatant was removed, and the pellet resuspended in an appropriate amount of 1 × PBS. Cells were pipetted onto the slide and allowed to settle but not dry out, slides were then fixed in 100% - 20 °C methanol for 5 minutes to overnight. Cells were then rehydrated with 1 × PBS before addition of DAPI covershield, the coverslip was placed and sealed with nail varnish.

(3.3.4) SDS-page – Coomassie stain

Protein samples were denatured by addition 5 x SDS samples and heating at 95 °C for 10 minutes. No more than 15 µl of sample was loaded onto a Biorad TGX mini precast gel in 1 × SDS running buffer. Samples were run at 180 V for 40 minutes or until the sample reached the end of the gel. Once run, the gel was removed and incubated in a container with Coomassie InstantBlue for 30 minutes on a rocking shaker. Before imaging the gel was rinsed with ddH20 and left to wash on the rocking shaker for 5 minutes before imaging.

(3.3.5) Western Blot

SDS-page gels were transferred to PVDF membrane using a Bio-rad Trans-Blot Turbo RTA Transfer Kit, the membrane was then transferred to a container of up to 25 ml 2.5% milk blocking solution and left on the rocking shaker for 20 minutes. The primary antibody was added at the desired concentration and left on the rocker overnight at 4 °C wrapped in tinfoil. The following day, the primary antibody was removed, and the membrane was rinsed 3 times then washed for 5 minutes. The membrane is then incubated in 2.5% milk solution containing the secondary antibody for >1 hour before imaging. EF1 was then used as a load control, with the membrane being incubated overnight with EF1 in 2.5% milk solution before being washed and incubated with the secondary antibody for >1 hour. αMORN1 and αBILBO1 were diluted 1/500. αEF1 was diluted 1/10,000. Antibodies were a kind gift from the Morriswood laboratory.

(3.3.6) Ethanol-chloroform extraction

Protein sample was resuspended in 50-200 µl of lysis buffer (ddH_20, 1% protease inhibitor mix) (1 volume). 4 volumes of 100% methanol were added, followed by 1 volume of chloroform. The solution was vortexed until there were no separate phases. 3 volumes of ddH_2O were added and vortexed thoroughly. The sample was centrifuged in a microcentrifuge at full speed, RT, for 1 minute. The upper phase was removed by pipetting without disturbing the protein. 3 volumes of methanol were added before vortexing. The sample was centrifuged at full speed, RT, for 5 minutes. The supernatant was removed without disturbing the protein pellet, which was left to air dry. The pellet was then resuspended in a suitable volume for its application.

(3.4) Cloning

(3.4.1) PCR

Primers were ordered from Sigma; full details are disclosed in the appendix. PCR reactions used 100 µl OneTaq 2 × Mastermix (Biolabs), 88µl ddH_2O and 8µl of primer mix. The primer mix was composed of 10 µl of forward primer, 10 µl of reverse primer and 80 µl H_2O. 50 µl of this solution were aliquoted into 4 PCR tubes, and 1 µl of *T. brucei*/*T. congo*lense gDNA were added to 3 tubes. Thermocycler reactions were programmed to denature samples at 94 °C for 30 s, anneal for 60 s at variable temperature (see appendix), and extend at 68 °C for 40 seconds for 35 cycles.

(3.4.2) Agarose Gel electrophoresis

1% agarose gel was prepared with 4 µl SYBR safe (Invitrogen) in 1 × TAE buffer. Samples were run adjacent to 5 µl 100 bp (Biolabs) or 1 kb ladder (Promega). 2 µl purple loading dye (Biolabs) was added to each sample. Samples were run at 115 V for 25-35 minutes. Gels were imaged on the BioRad Gel Doc EZ imager or the BioRad ChemiDoc MP imaging system running Image Lab software.

(3.4.3) Gel purification

The agarose gel was placed on a UV transilluminator, and the desired bands were excised with a scalpel. DNA was extracted using a Thermo Fisher GeneJET Gel extraction kit by following the manufacturer's protocol.

(3.4.4) Restriction enzyme digestions (diagnostic and prep)

Restriction digest reactions were composed of 16 µl DNA, 2 µl 10 x CutSmart buffer (NEB) and 1 µl of each of the 2 restriction enzymes. Samples were incubated at 37 °C for a minimum of 1 hour. Diagnostic digests were composed of 7 µl DNA sample, 1 µl 10 × CutSmart buffer and 1 µl of each restriction enzyme, before incubation at 37 °C for a minimum of 1 hour.

(3.4.5) Ligation

The ligation reaction was composed of insert DNA, backbone DNA, T4 DNA ligase and rapid ligation buffer in a ratio of 6:3:1:1. The amount of insert DNA necessary for a ligation reaction was calculated using the formula $\frac{\text{Backbone DNA (ng)} \times \text{insert length (kb)} \times 5\ \text{(ratio of insets to backbone)}}{\text{Length of backbone (kb)}}$. Ligation reactions were left overnight at room temperature.

(3.4.6) Transformation

5 µl of ligation reaction were added to thawed 25 µl aliquots of NEB High efficiency *E. coli* competent cells and left on ice for 10 minutes. Samples were placed in a 42 °C hot block for 45 seconds before being placed back on ice for 2 minutes. 200 µl of SOC solution was added to each sample, before being incubated for 45 minutes at 37 °C in a shaking incubator. 200 µl of solution was then pipetted and spread onto LB plates containing 100 µg/ml carbenicillin. LB plates were placed in a 37 °C incubator overnight before being transferred to 4 °C. For Blue-white screening, 30 µl of X-gal followed by 30 µl of IPTG is spread onto the plate ahead of the transformed bacteria.

(3.4.7) Plasmid purification using a miniprep kit

Suitable colonies were picked and added to 15 ml Eppendorf containing 3 ml of LB broth with 100 µg/ml carbenicillin. The Eppendorfs were left in a shaking incubator overnight at 37°C with the lids loose. These were then spun at 2500 × g for 10

minutes and the supernatant was discarded. The miniprep was conducted using the Thermo Fisher Genejet miniprep kit according to the manufacturer's protocol.

(4) Results

(4.1) Elutriation of PCF and BSF *T. brucei*

(4.1.1) Aims

Current literature has shown that both PCF and BSF *T. brucei* can be synchronised by centrifugal counter-flow elutriation (Benz et al., 2017). This results in greater than 95% synchronisation to early G1 in both, with fractions continuing to grow in a synchronised fashion when returned to culture (Benz et al., 2017). Samples are loaded into the elutriator (figure 4.1) when the counter-flow pump speed is low, and the centrifuge is spinning at its maximum of 5000 rpm. Cells are distributed in the chamber based on their sedimentation velocity or hydrodynamic volume, with smaller cells settling closer to the elution boundary and larger cells settling further away. Cells form a visible cell boundary layer within the chamber, where the cells are dense enough to be seen. The elution boundary is the widest point of the chamber, meaning the fluid velocity is lowest, when cells cross the elution boundary the

narrowing of the chamber increases fluid velocity and results in rapid elution. Increasing the pump speed results in the cells closest to the elution boundary being eluted, and cells further away move closer to it. Incremental increases in pump speed can therefore be used to generate fractions of increasing cell size, this should correspond to cell cycle progression. As pump speed increases, the cell boundary visibly shifts up the chamber. This chapter aims to validate the technique for use on both PCF and BSF *T. brucei*, as generating populations enriched in a specific cell-cycle stage is important for global studies of the cell cycle. It also briefly looks at alternative chambers with different properties, to compare to the standard chamber.

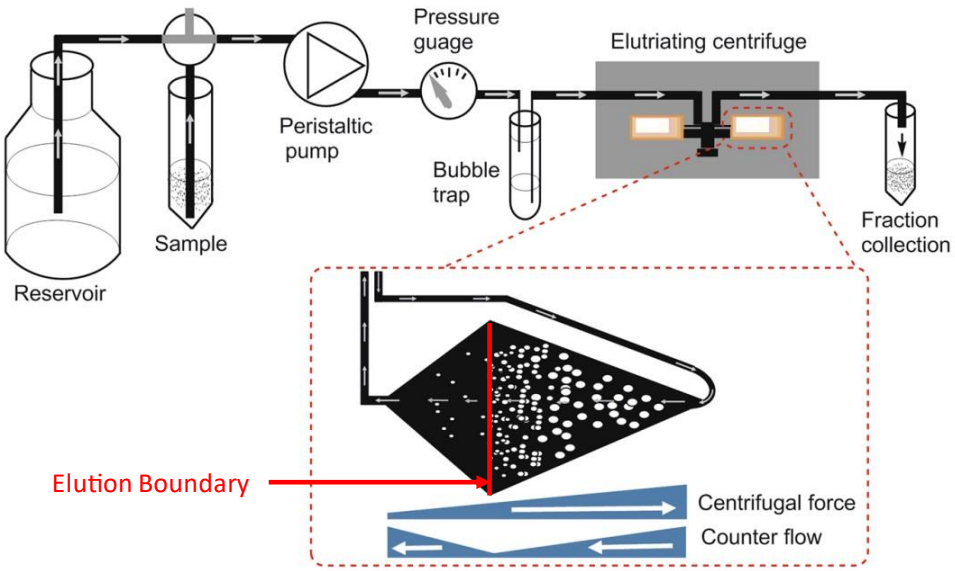

Figure 4.1 The layout and components of a centrifugal counter-flow elutriation system. The reservoir holds elution buffer, which is continuously pumped through the system, except for when the sample is loaded. One chamber is loaded, while the other chamber acts as a counterbalance. The kite shape of the chamber enables sorting based on sedimentation velocity, composed of density and volume. Cells that cross the elution boundary due to increasing counter-flow are rapidly eluted and collected.

(4.1.1) Synchronisation of PCF *T. brucei*

To validate the reproducibility of the CCE protocol, PCF *T. brucei* cells were elutriated and the contents of the collected fractions were analysed by flow cytometry, alongside an asynchronous sample. Flow cytometry enables the determination of cell cycle stage by using propidium iodide (PI) to stain DNA, cells are then excited at a wavelength corresponding to the excitation frequency of PI. The emission area therefore corresponds to the amount of DNA, the emission area (or DNA content) is then plotted against cell count in a histogram. An asynchronous sample is then used to determine the boundaries between G1 cells (which have 1 set of diploid chromosomes), G2 cells (2 sets of diploid chromosomes) and S phase (Between 1 and 2). These boundaries are then applied to the synchronised sample.

Initially, 150 ml fractions corresponding to flow speeds of 15 ml/min (F15), F18, F20, F22, F28 and F35 were collected and analysed by flow cytometry (figure 4.1). The sum of these fractions contained ~67% of the cells loaded into the system, and as the pump speed was increased, the percentage of cells in G1 was expected to decrease.

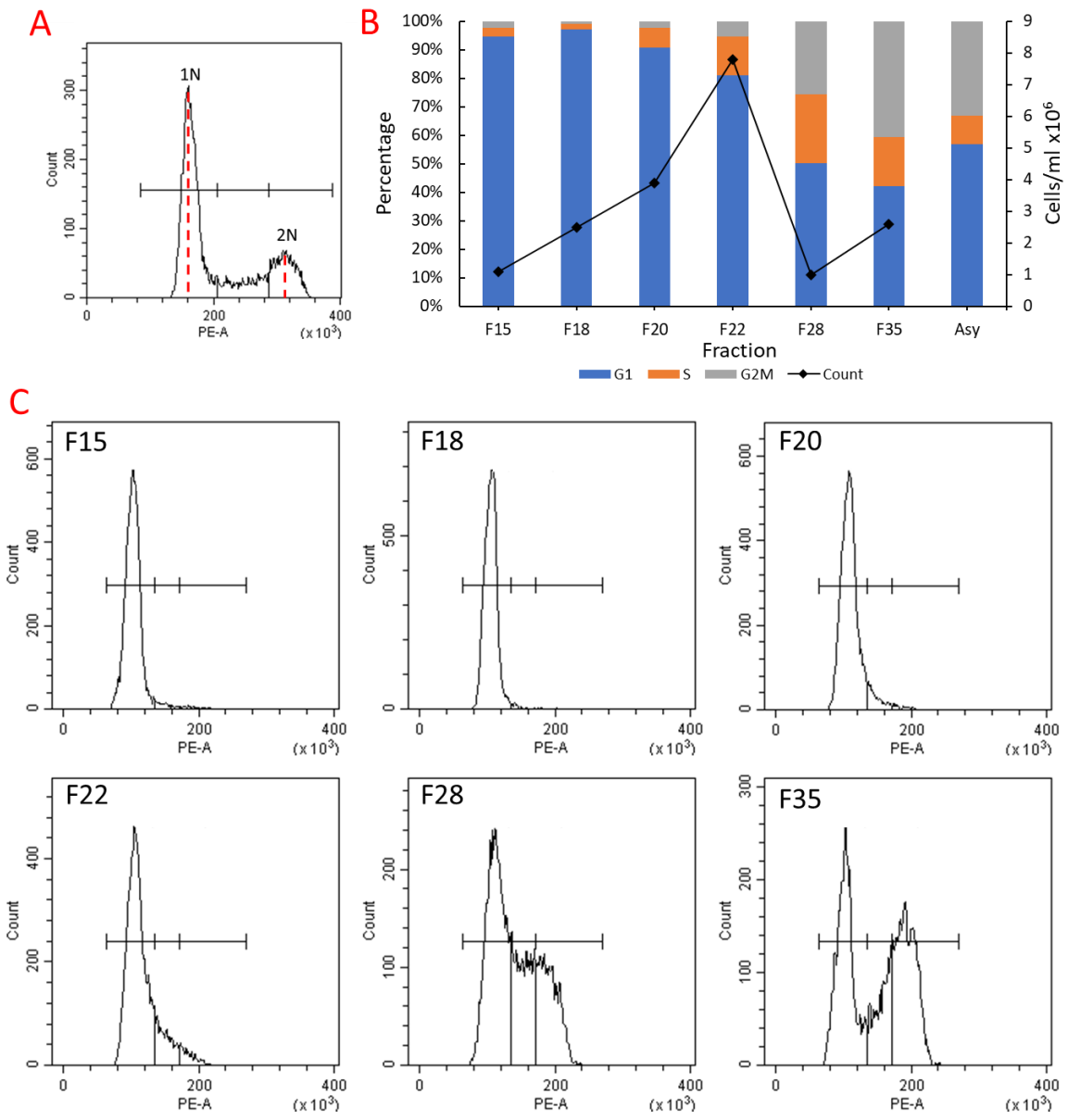

Figure 4.2 Characterisation of elutriation fractions collected at a variety of flow speeds. 1x10^9 PCF *T. brucei* were loaded into an elutriating centrifuge, 150 ml fractions were collected at 15, 18, 20, 22, 28 and 35 ml/min. (A) Flow cytometry histogram of asynchronous sample with 1N and 2N peaks highlighted, example boundaries have been set showing G1, S and G2M. (B) A bar chart showing the proportion of cells in each cell cycle stage and the cell count in each fraction. (C) Flow cytometry histograms of collected fractions, both F15 and F18 appear highly enriched in G1, as the flow rate increases the proportion of cells in G1 decreases. Asy represents asynchronous.

PCF *T. brucei* can be highly enriched in G1 using CCE as shown in figure 4.2. F15 is enriched in G1, with 94.5% of cells being present in G1. However, this is lower than F18 which contains 97% G1 cells even though smaller cells should be eluted at lower flow rates. This marginal difference is likely just a result of the relatively small overall population of the F15 fraction compared to the others collected. For this reason, in the following experiments, the F18 fraction was selected to represent the first true G1 enriched fraction. F18, F20 and F22 all appear to be heavily enriched in G1, with F20 and F22 likely representing cells further through G1, with F22 representing cells closest to entering S-phase. This assumption relies on there being a constant increase in cell sedimentation velocity throughout G1, as the physical separation of cells is based mainly on volume and density. This is supported by literature which shows that PCF *T. brucei* cells increase uniformly in volume throughout G1 which would in theory enable separation of early, mid, and late G1 cells (Benz et al., 2017). F28 contains the highest proportion of S-phase cells at 24% compared to 10% in the asynchronous population. This represents an enrichment of 2.4x, which is greater than the G1 enrichment seen in F18 (1.7x increase from the asynchronous). Though this is a large relative enrichment, it still leaves >75% of cells in G1 or G2M, making it subpar for proteomic studies of S phase. F35 contains the most G2M cells, but it still only represents 42% of the population, which is a 1.27x increase compared to the asynchronous population.

Though this data shows that CCE can be used to generate highly enriched G1 fractions, its suitability as a synchronisation method requires further experimentation by characterising fractions that have been returned to culture. PCF cells were synchronised and analysed over time to determine if fractions grow

synchronously when returned to culture; if there is a functional difference between F18, F20 and F22 fractions; and if fractions returned to culture can be used to generate enriched S and G2M populations. Elutriation of PCF cells was repeated using an identical method, however, only the F18, F20, and F22 fractions were collected. Importantly, F18 was not the first fraction collected, F15 was collected and then discarded, this was to prevent the cells that would have eluted at 15 ml/min from being combined with cells that elute at 18 ml/min. Fractions were then returned to culture and allowed to propagate for 8 hours, with samples for flow cytometry being taken every hour (figure 4.3). Populations were monitored for 8 hours as this is roughly the length of the PCF form cell cycle.

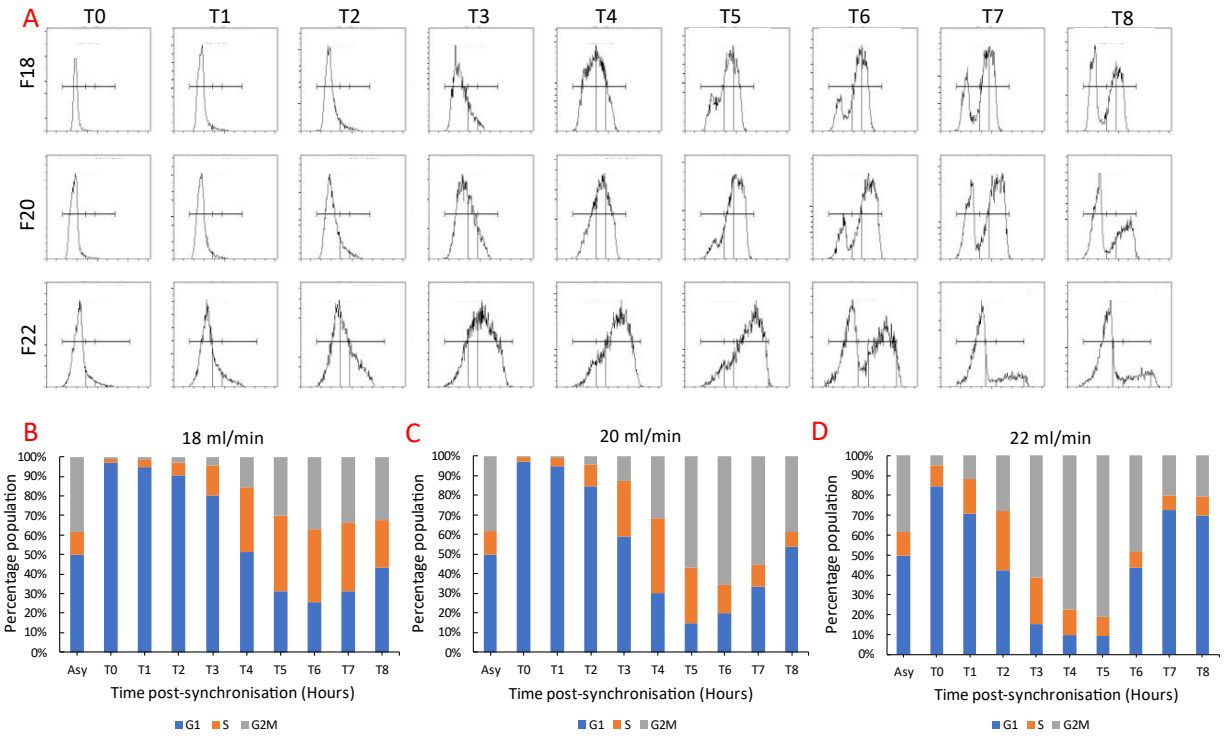

Figure 4.3 Culture and recovery of G1 enriched CCE fractions. 1x10^9 PCF *T. brucei* were loaded into an elutriating centrifuge, 150 ml fractions were collected at 18, 20, and 22 ml/min. Collected fractions were returned to culture and allowed to propagate, samples were collected for flow cytometry analysis every hour for 8 hours. (A) Flow cytometry histograms of collected fractions, rows represent the flow rate used to elute the fraction while the columns represent the hours post-collection. Each fraction appears to progress through the cell cycle synchronously. (B) Bar chart showing the percentage of the 18 ml/min fraction in each cell cycle stage at each timepoint. (C) Bar chart showing the percentage of the 20 ml/min fraction in each cell cycle stage at each timepoint. (D) Bar chart showing the percentage of the 22 ml/min fraction in each cell cycle stage at each timepoint. Histograms show cell count (Y) against propidium iodide emission area (X).

Once returned to culture, cells begin to grow without any obvious delay as seen in figure 4.3. At T0, the collected F18, F20 and F22 fractions appear nearly identical to those in figure 4.2 A, highlighting the reliability of the technique. At T0, 97% of F18 cells are in G1, the population then progresses synchronously through the cell cycle. The G1 population decreases every hour, reaching a minimum at T6, the G1

population then begins to increase, suggesting that some cells have divided and begun to re-enter the cell cycle. The results for T20 and T22 follow the same trend but seem to progress to the next cell cycle stage sooner. F20 G1 population is lowest at T5, and though the same is true for F22, the difference in G1 population between T4 and T5 is ~0.5%. This indicates that F18 represents early G1, with F20 and F22 G1 cells being closer to the G1/S transition. This explains why progression appears to be 'faster' in later fractions as cells are starting to progress from further into the cell cycle. This shows that CCE can be used to separate early from late G1 cells. Figure 4.3 also shows that CCE can be used to enrich all cell cycle stages, if indirectly. The fraction containing the highest S-phase population is F20 at T4, with 37% of cells in S-phase. This represents an enrichment of 3.1x, which is greater than can be achieved by directly collecting a higher flow rate fraction. F22 T5 represents the greatest enrichment of G2/M cells at 80%, a 2.35x increase from the asynchronous. Overall, this highlights that CCE can be used to isolate highly enriched G1 populations that remain viable. Growth of these populations can be used to obtain populations enriched in S-phase and G2M. This makes it ideal for global studies comparing different cell cycle stages.

(4.1.2) Synchronisation of BSF *T. brucei*

To validate that the conclusions drawn regarding CCE synchronisation of PCF *T. brucei* are applicable to BSF *T. brucei*, the experiments were repeated. 100 ml fractions corresponding to flow speeds of 15 ml/min (F15), F17, F19, F21, F23, F25,

F27, and F35 were collected and analysed by flow cytometry (figure 4.4). Higher flow rates should correspond to larger cells that are later in the cell cycle.

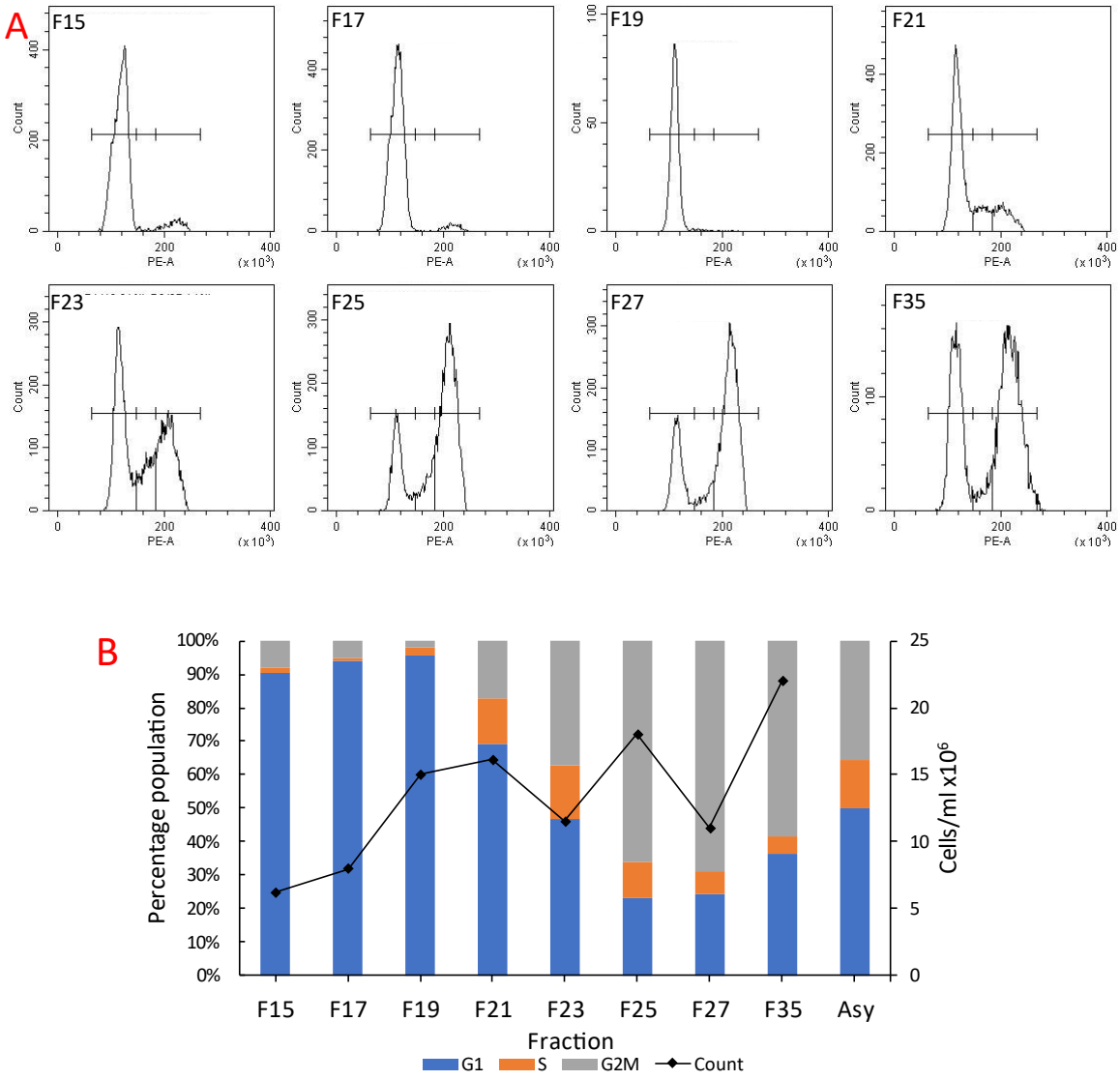

Figure 4.4 Characterisation of elutriation fractions collected at a variety of flow speeds. 1x10^9 BSF *T. brucei* were loaded into an elutriating centrifuge, 100 ml fractions were collected at 15, 17, 19, 21, 23, F25. F27 and 35 ml/min. (A) Flow cytometry histograms of collected fractions, F15, F17 and F19 appear highly enriched in G1, as the flow rate increases the proportion of cells in G1 decreases, excluding F35. (B) A bar chart showing the proportion of cells in each cell cycle stage and the cell count in each fraction. Asy represents asynchronous.

Figure 4.4 shows that, like with PCF, BSF *T. brucei* can be enriched in G1 using CCE. The F19 fraction contains the highest proportion of G1 cells at 95.5%, though F15 and F17 also contain >90% G1 cells. As flow rate increases, the proportion of G1 cells decreases until F35. F35 contains more G1 than F27, but this is likely due to 35 ml/min is a strong enough counter-flow to remove any cells left in the elutriator – including doublets. The highest proportion of G2M that can be directly obtained by CCE is in F27, containing >68% G2M cells or a 1.85x enrichment, which is greater than in PCF. However, there are no S-phase enriched fractions, the highest is seen in F23 at 16%, compared to 14% in the asynchronous sample.

To see if greater enrichment of other cell cycle phases could be achieved using CCE, elutriation of BSF cells was repeated. F15, F17 and F19 were collected and immediately returned to culture. Cells were allowed to propagate for 8 hours with samples for flow cytometry being taken every hour (figure 4.5).

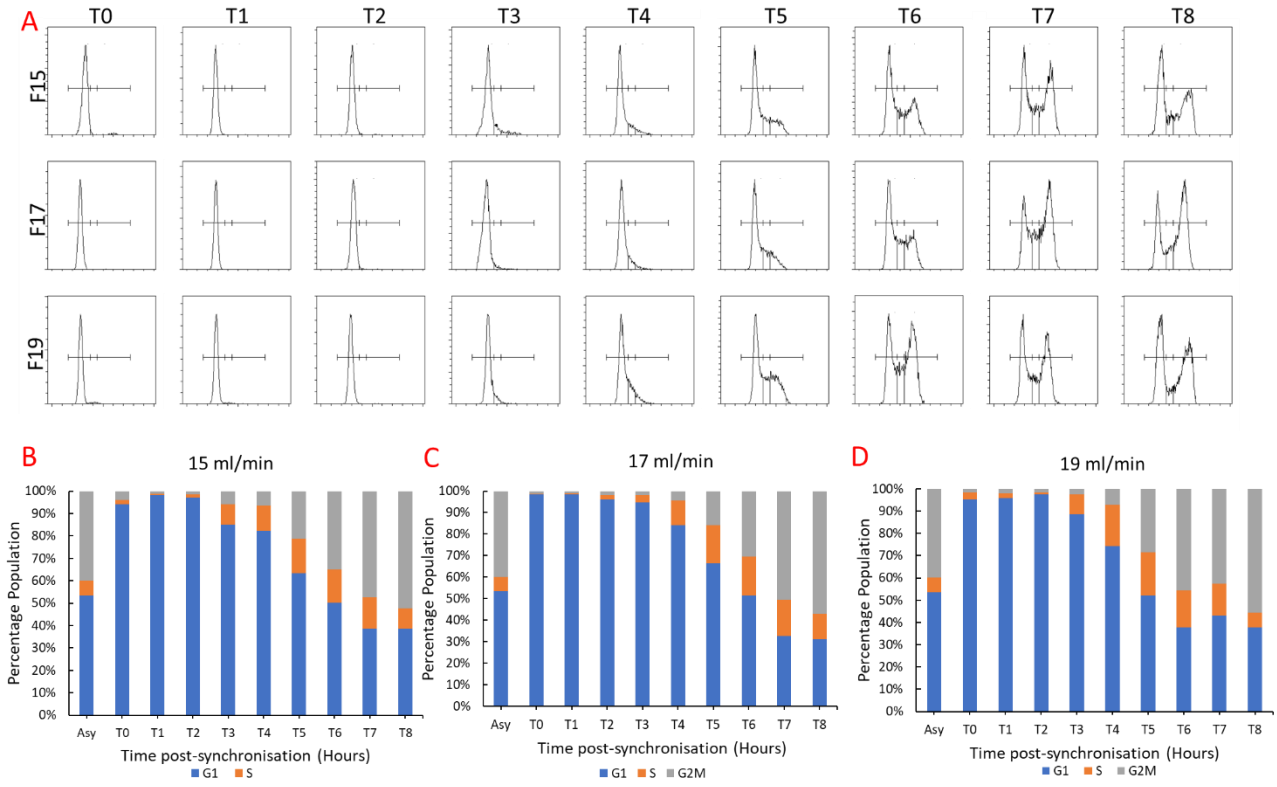

Figure 4.5 Culture and recovery of G1 enriched CCE fractions. 1x10^9 BSF *T. brucei* were loaded into an elutriating centrifuge, 100 ml fractions were collected at 15, 17, and 19 ml/min. Collected fractions were returned to culture and allowed to propagate, samples were collected for flow cytometry analysis every hour for 8 hours. (A) Flow cytometry histograms of collected fractions, rows represent the flow rate used to elute the fraction while the columns represent the hours post-collection. Each fraction appears to progress through the cell cycle synchronously, with the fractions progressing faster than early fractions. (B) Bar chart showing the percentage of the 15 ml/min fraction in each cell cycle stage at each timepoint. (C) Bar chart showing the percentage of the 17 ml/min fraction in each cell cycle stage at each timepoint. (D) Bar chart showing the percentage of the 19 ml/min fraction in each cell cycle stage at each timepoint. Histograms show count (Y) against propidium iodide emission area (X).

As shown in figure 4.5 C, immediately after synchronisation the populations were highly enriched in G1, up to a maximum of 98% in F15 and F17. Cells appear to grow and move through the cell cycle while maintaining some level of synchronicity.

However, it appears from the traces in 4.5 A that some cells may not be growing and instead remain in G1. The G1 population drops to lows of 38%, 31% and 37% in F15, F17 and F19 respectively. This is higher than the lowest G1 levels seen in PCF, at 25.5%, 19.9% and 9.3% in F18, F20 and F22 respectively. This stuck population is clear when looking at 4.5 A T5, as more cells begin to re-enter G2M there is still a clear G1 peak which does not diminish. It is also unclear whether cells are entering the cell cycle, the only timepoint at which the G1 population increases is F19 at T7, though it decreases again at T8. From this data alone it is difficult to ascertain whether cells are not able to renter the cell cycle, or if the previously 'stuck' G1 cells are re-entering the cell cycle and repopulating G2M at the same rate. The highest percentage of S-phase cells is found at F19 T5, S-phase cells make up 19.5% of the population, which is marginally higher than in the previous experiment but much lower than in PCF. The 3 BSF fractions also appear more similar than the 3 PCF form fractions. In figure 4.3 A there are clear differences between the histograms at each timepoint, whereas in figure 4.5 A there are only clear differences from T5 onwards, implying that the F15, F17 and F19 are similar in terms of composition.

From these results, CCE can be used to synchronise PCF cells effectively to G1, S and G2M, with separation of early, middle, and late G1 cells also being possible. These populations remain viable and grow synchronously when returned to culture. CCE can also be used to synchronise BSF cells and generate highly enriched G1 fractions, these populations are viable, but a subset of the population may show stalled/reduced growth.

(4.1.3) Synchronisation of PCF *T. brucei* using a Sanderson chamber

Previous literature has utilised the standard, kite-shaped chamber described at the start of the chapter to synchronise *T. brucei*. An alternative to the standard chamber is the Sanderson chamber, which is the same volume as the standard chamber but with a different shape and therefore different properties (figure 4.6).

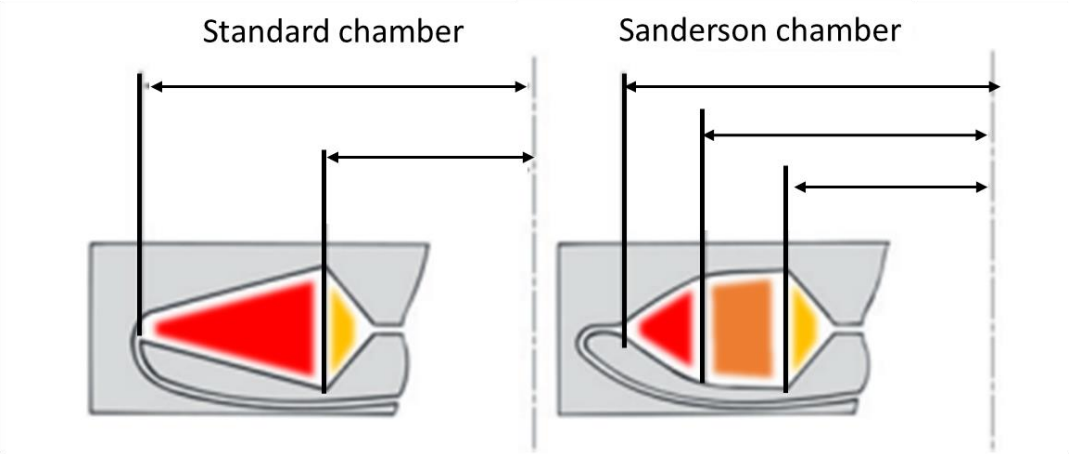

Figure 4.6 Cross section of the standard and Sanderson chambers with functionally distinct areas highlighted. Red represents the area where primary sorting occurs, orange represents where secondary sorting occurs and yellow is where elution occurs. Adapted from (Beckman Coulter, 2020).

The Sanderson chamber has a smaller area for primary sorting, meaning at low flow speeds the cells are concentrated further away from the elution boundary, closer to the chamber entrance. Theoretically, the second sorting chamber aids in the separation of smaller cells or more similarly sized cells. To test the Sanderson chamber, PCF cells were elutriated and 150 ml fractions corresponding to flow speeds of 13 ml/min (F13), F15, F17, F19 and F21 were collected and analysed by flow cytometry (figure 4.7).

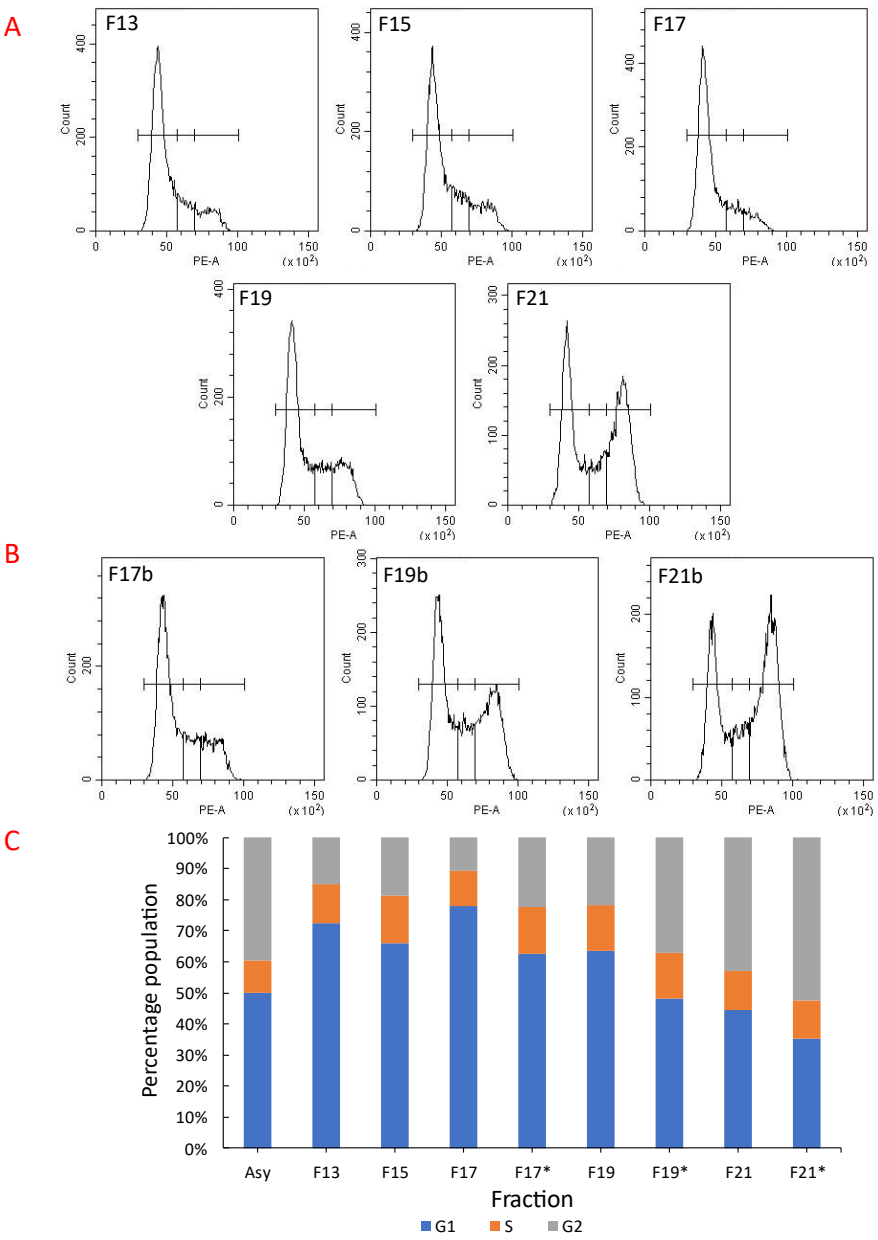

Figure 4.7 Characterisation of elutriation fractions collected at a variety of flow speeds using and Sanderson chamber. 1x10^9 PCF *T. brucei* were loaded into an elutriating centrifuge, 150 ml fractions were collected at 13, 15, 17, 19 and 21 ml/min. (A) Flow cytometry histograms of collected fractions (B) Flow cytometry histograms of fractions collected after observation of the breakdown of the cell boundary (C) A bar chart showing the proportion of cells in each cell cycle stage, * represents fractions where the visible cell boundary broke down. Asy represents asynchronous.

Figure 4.7 suggests that the Sanderson chamber is a poor choice for enriching PCF *T. brucei* populations to G1. Figure 4.7 A immediately shows that the Sanderson

chamber is worse for synchronising PCF *T. brucei* than the standard chamber, with the highest G1 enrichment being 77.9% compared to 97% using the standard chamber. There does not appear to be any S-phase or G2M enriched fractions, though full characterisation was stopped due to emerging technical difficulties. The main difficulty was the breakdown of the visible cell boundary layer, the area in the chamber in which the cells are dense enough to see. At several points, the cell boundary layer disappeared – indicating the removal or dispersion of cells within the chamber – the boundary layer soon reformed as cells returned to their equilibrium. As the 150ml fractions were collected in 3 50 ml falcon tubes, when the boundary broke down the current collection tube was marked and analysed separately, as seen in figure 4.7 B-C. These disturbed fractions show much greater proportions of G2M cells at the same flow rate, indicating that the breakdown of the boundary resulted in cells being eluted randomly rather than based on size. This may be due to changes in pressure, or a breakdown of the centrifugal force/ fluid velocity equilibrium due to the dynamics of the chamber. Regardless, the Sanderson chamber does not appear to be a suitable choice for the size-based separation of *T. brucei* cells.

(4.2) F-PACS enrichment of PCF *T. brucei* for proteomic study

(4.2.1) Aims

The flagellum and flagellar pocket can be isolated using detergent and high salt conditions (Perdomo et al., 2016). This process utilises a non-ionic detergent to solubilise the membrane and enable removal of cytosolic organelles. This is followed by incubation in high salt conditions, as certain salt conditions result in

depolymerization of the subpellicular array (Dolan et al., 1986), leaving the F-PACS (Figure 4.8). This is necessary as mass spectrometry techniques often lack the dynamic range to detect regulatory F-PACS proteins which often occur at low abundance compared to some cytoplasmic proteins. Though a common feature of flagella preparation protocols, the exact composition of the salt buffer can vary, with KCl (Koyfman et al., 2011), NaCl (Choi et al., 2014) or $CaCl_2$ (Sunter et al., 2015) commonly being used. The effect that different salt buffer conditions have on the enrichment of F-PACS is not known.

This chapter aims to optimise an F-PACS enrichment protocol for the purpose of analysing relevant cell cycle regulated proteins, particularly those targeted by PLK. TbPLK is an important protein for the regulation of cytokinesis and duplication of F-PACS components, with TbPLK inhibition resulting in severe cytokinesis defects. However, (Lozano-Núñez et al., 2013) have shown that inhibition of TbPLK 5.5 hours into the cell cycle does not result in cytokinesis defects until the following cycle. This suggests that TbPLK phosphorylates F-PACS targets early in the cell cycle – F-PACS enrichment and phosphoproteomic analysis may help reveal these targets. To do this comparative samples were generated to look for differences in protein composition/abundance utilising KCL, NaCl or $CaCl_2$ salt buffers. This was then combined with SILAC labelling and CCE to generate samples for proteomic analysis.

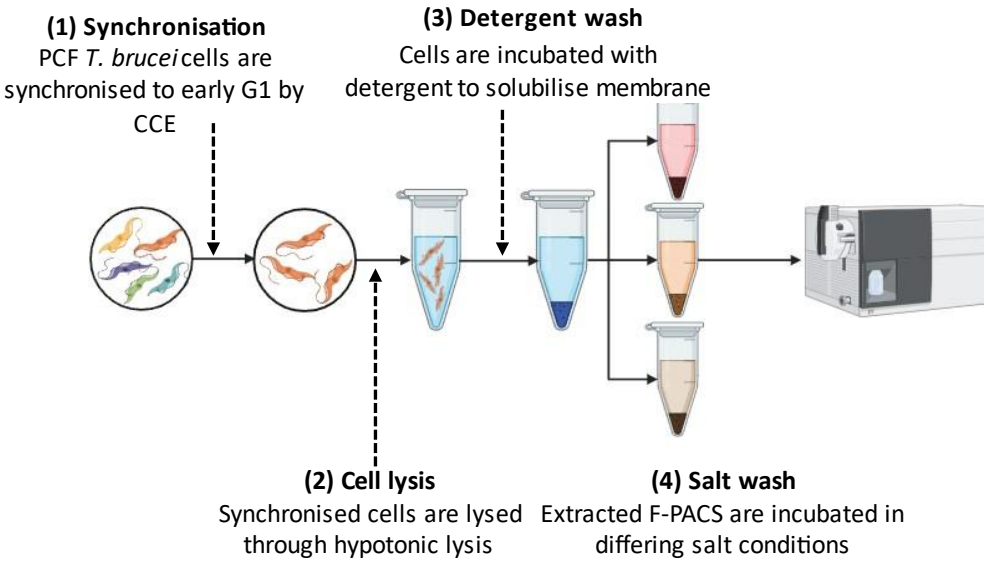

Figure 4.8 A schematic overview of the F-PACS enrichment protocol. After the generation of enriched F-PACS samples, the samples are sent for proteomic analysis. Cells are synchronised using CCE, before fractions are lysed. The whole cell lysates (WCL) are centrifuged, and the pellet is resuspended and incubated in NP-40 detergent. The samples are spun then resuspended and incubated in a salt buffer; the pellet is further treated before proteomic analysis.

(4.2.2) Verification of protocol

To verify that the F-PACS enrichment protocol was working as expected, an endogenously tagged mNeonGreen PFR1 cell line was used to generate 4 samples at different stages of extraction. The first sample contained whole cells, then lysed cells, then samples washed with a detergent buffer and finally samples washed with the salt buffer – in this case KCl (Figure 4.9). Samples were also stained with DAPI. This was carried out using asynchronous samples.

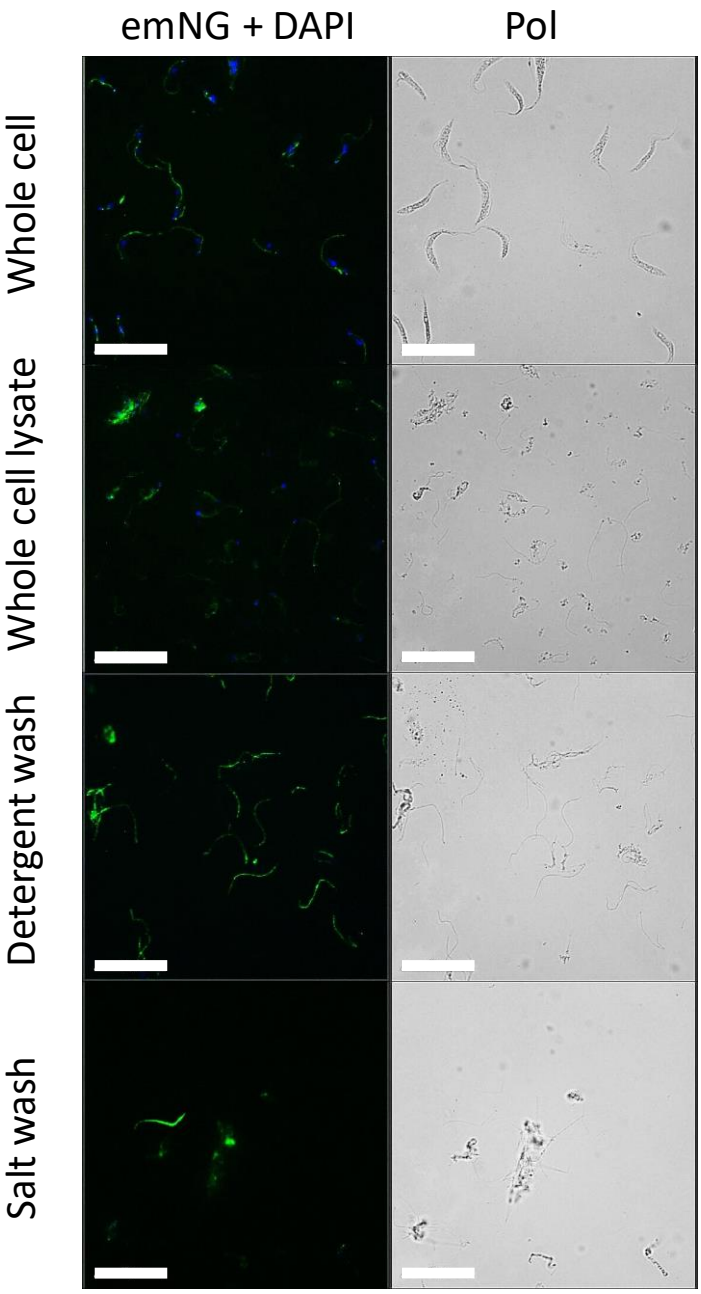

Figure 4.9 Fluorescent microscopy images of PCF *T. brucei* at different stages of F-PACS enrichment.

(Left) mNeonGreen signal from endogenously tagged PFR1 cell line (green) merged with DAPI stained DNA (blue). (Right) Polarised light images. Scale bar is 25µm.

F-PACS enrichment results in a reduction in the levels of DNA in the sample, as seen in figure 4.9. DAPI staining of whole cells and whole cell lysates reveals the clear presence of DNA. In the whole cells, the DNA localisation is consistent, with a smaller

signal localised at the posterior of the cell near the end of the flagellum corresponding to the kDNA network, and a larger signal located adjacent to the flagellum corresponding to the nuclear DNA. In the whole cell lysate sample, the DAPI signal seems to be reduced overall and less spatially consistent. Small DAPI signals can be seen adjacent to some isolated flagella, indicating that the kinetoplast still remains indirectly associated with the flagellum, whereas large DAPI signals are less visible, potentially indicating lysis of the nuclear membrane. There are also regions of this sample where cell material appears to clump together. The detergent wash samples show a large reduction in DAPI signal, though close analysis of the image does show the presence of some DNA. Though there are clumps of entangled flagella, many appear isolated. In the salt wash samples there is minimal detectable DAPI signal, but there is also a reduction in mNeonGreen signal. The polarised image shows most flagella appear within clumps, though some remain isolated – of the isolated flagella most show no mNG signal. The clumps also show a faint, dispersed mNG signal that doesn't appear to directly correspond to the positioning of the flagella.

(4.2.3) Characterisation of different enrichment conditions

After verification of the technique, optimisation began on the different salt buffer conditions. Samples were generated which corresponded to each stage in the protocol, whole cell lysates, detergent wash, and salt wash. At each stage, both the pellet (which would be carried forward for further processing) and the supernatant were kept to show the amount of protein being lost at each stage. For the salt buffer,

3 samples were generated corresponding to NaCl, KCl and $CaCl_2$. A Bradford assay was then carried out to estimate the protein concentration in each sample (figure 4.10).

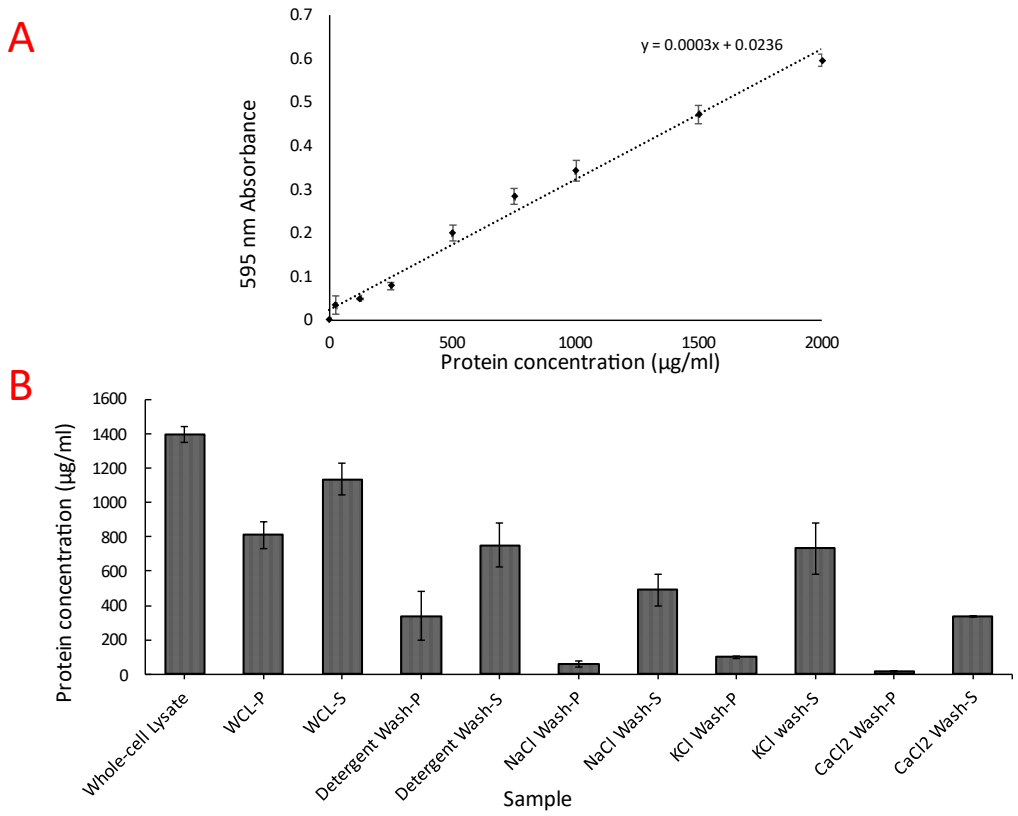

Figure 4.10 Bradford assay showing standard curve and protein concentration of known samples.

Cells were lysed with H_2O and protease inhibitors to prevent degradation of proteins. Samples were generated using an equal number of starting cells, each containing $4.9x10^7$ cells. Absorbance of samples was measured at 595 nm. (A) A standard curve of protein concentration was generated using serial dilution of bovine albumin and used to generate a line of best fit. (B) Bar chart of protein concentration per sample, the measured absorbance was used to estimate protein concentration using the equation of the standard curve line. Both known protein and unknown samples were generated in triplicate, error bars represent the standard curve. P and S suffix denotes pellet or supernatant, WCL denotes whole cell lysate.

The Bradford assay results (figure 4.10) show that each step in the F-PACS enrichment protocol results in a reduction in overall protein. It also shows that at each stage, more protein is discarded in the supernatant than is carried forward to the next step. The results indicate that out of the 3 salt buffers, KCl retains the most protein and $CaCl_2$ retains the least. The standard curve (A) appears to show a linear correlation between absorption and protein concentration, with most points fitting well with the trendline and relatively small variation within the replicates, indicated by the error bars. However, analysis of the bar chart immediately shows flaws – the protein concentration of the pellet and supernatant in one sample should total the protein concentration of the pellet in the previous sample. However, this is not seen, instead the pellet + supernatant always total more than the previous pellet - indicating error in the recorded values. Other possible explanations, as well as other considerations with this assay, are discussed further in later chapters. The Bradford assay was used to give a rough estimate of protein concentration at each stage to estimate cell load for samples that are equivalent in protein.

The next step was to identify general differences in the protein composition of samples generated using the 3 different buffers. To do this, 2 sets of samples were generated to run on an SDS-PAGE. The first set contained samples from every step of the procedure loaded by cell equivalence. The second set only contained the pellet and supernatants of the final products (not the intermediate steps), this sample was generated using a greater number of cells to make up for the loss in protein (Figure 4.11).

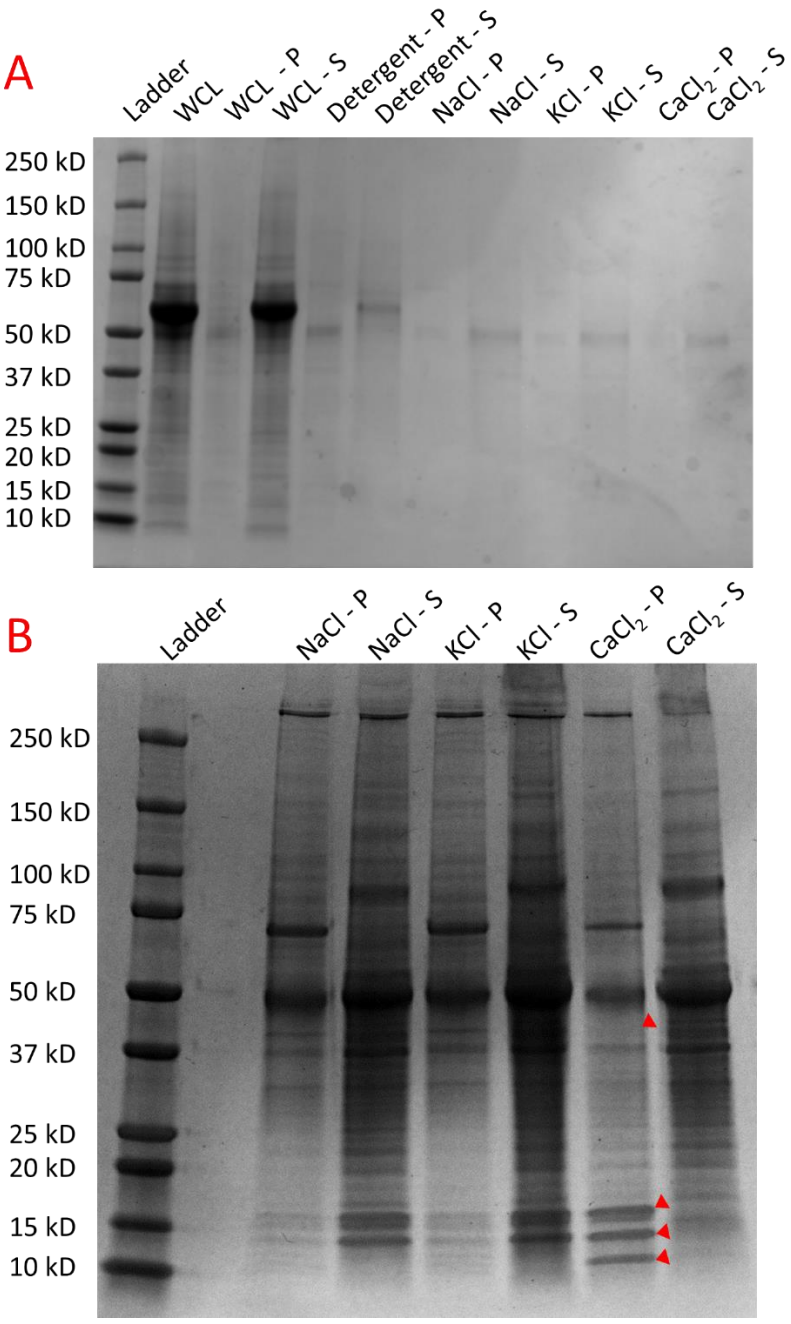

Figure 4.11 Coomassie stain of SDS-PAGE showing differences in the protein composition of enriched F-PACS samples. Cells were lysed with H_2O and protease inhibitors to prevent degradation of proteins. (A) $7.2x10^6$ cell equivalents were loaded per lane on an SDS-PAGE, the gel was incubated overnight in InstantBlue to stain protein. (B) $1x10^8$ cell equivalents were loaded per lane on an SDS-PAGE, the gel was incubated overnight in InstantBlue to stain protein. Red arrows highlight an enriched or depleted band compared to other lanes. P and S suffix denotes pellet or supernatant.

Figure 4.11 A clearly shows the reduction in protein that occurs as a result of F-PACS enrichment, with the samples that have undergone the entire process showing almost no recognisable bands, except a 50 kD band likely representing tubulin based on its size and abundance. The only other band noticeable is a 75 kD band that appears absent in the $CaCl_2$ lane. The whole cell lysate lane is comparable to the supernatant after the initial centrifugation step, indicating that the majority of protein is lost at this stage. Samples collected after the salt wash stage contain a comparatively small amount of protein, so differences between salt conditions cannot be assessed.

Figure 4.11 B shows the differences between different salt conditions more clearly. Based on the size and intensity of the bands, the KCl and NaCl pellets appear to be similar in composition. However, the $CaCl_2$ pellet shows several bands that are more intense, and one band that is absent or significantly diminished, compared to the other samples.

Though the presence of the flagellum was detected by microscopy in the final sample, the presence of other F-PACS was still yet to be confirmed. To determine this, samples were generated for western blotting using αBILBO1 and αMORN1 (Figure 4.12). BILBO1 is a major component of the flagellar pocket collar and MORN1 component of the hook complex, both these structures are linked to the MtQ. This is of interest because the FPC and hook complex are important for cell cycle regulation, with TbPLK localising to the FPC before duplication (Ikeda and de Graffenried, 2012), and Smee1 (a component of the hook complex) is a substrate of TbPLK (Perry et al., 2017). Eukaryotic elongation factor-1 (EF1) was used as a load control, this is

because in *T. brucei* it shows a dispersed cytosolic distribution (Dean et al., 2017). The presence of EF1 in the sample would indicate that not all cytosolic proteins are removed by the enrichment process.

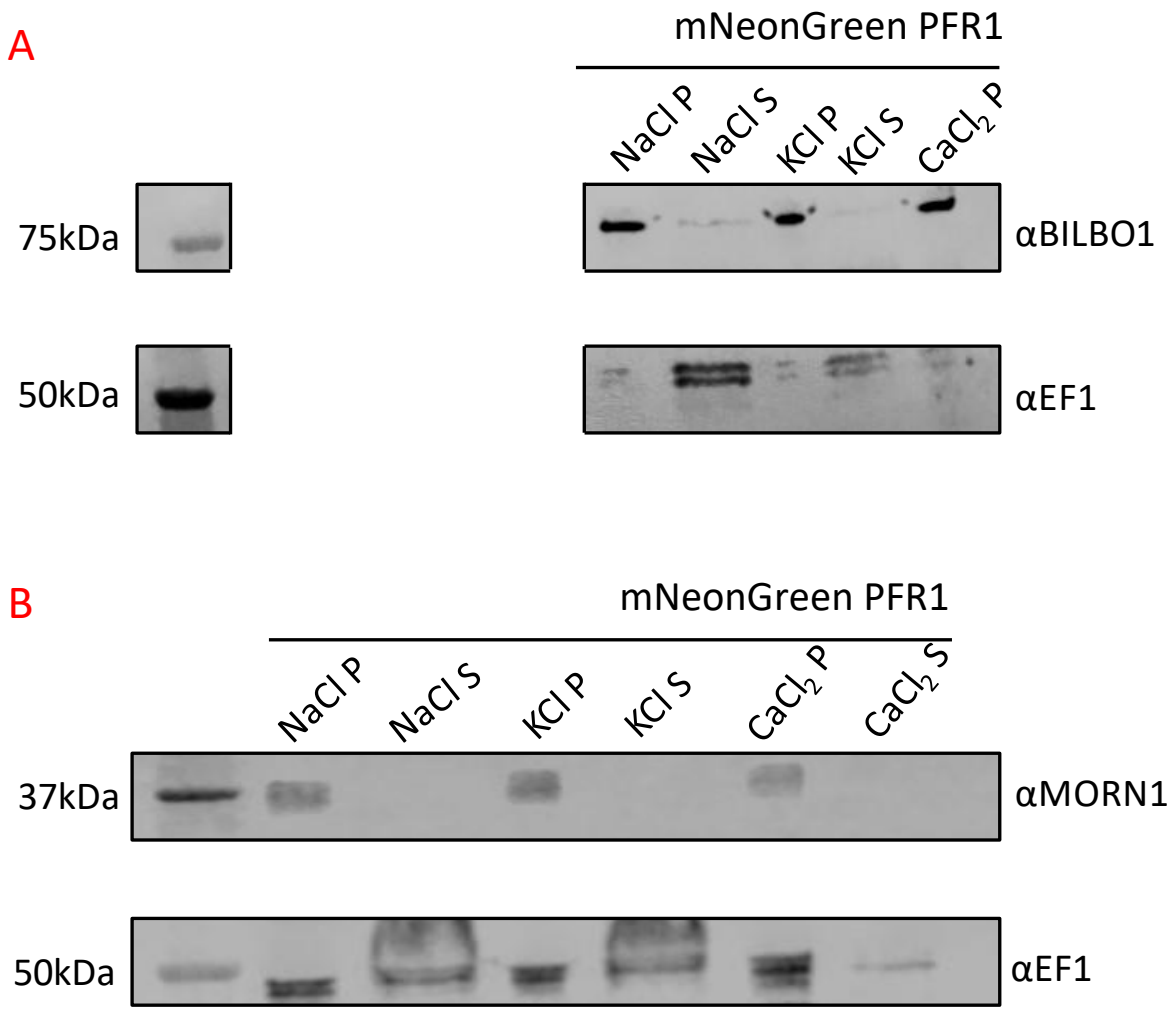

Figure 4.12 Western blot detecting key F-PACS proteins in F-PACS enrichment samples. Cells were lysed with H_2O and protease inhibitors to prevent degradation of proteins. (A) Western blot using αBILBO1, 15 µl were loaded in each lane and the antibody was diluted 1/500, EF1 was used as a load control. (B) Western blot using αMORN1, 15 µl were loaded in each lane and the antibody was diluted 1/500, EF1 was used as a load control. In each case, the size of the band matched the size of the target protein.

The results show the presence of MORN1 and BILBO1 in the generated samples, which suggests that the flagellar pocket collar and hook complex are maintained along with the flagellum. Figure 4.12 A Shows the presence of BILBO1 in the pellets of all 3 samples, indicating that the salt buffer does not affect the pulldown of the flagellar pocket. The width of the bands varies, with the supernatant bands being wider than the pellets. This may have been a result of the buffers used in the F-PACS enrichment protocol. Figure 1.12 B shows that all pellets show the presence of MORN1, which indicates the presence of the hook complex in the final samples. Again, the concentration of MORN1 appears equal between the different pellets. The width of the bands appears consistent in this western, likely due to performing an ethanol-chloroform extraction on the samples before denaturing them and loading on an SDS-PAGE. EF1 appears in both the supernatant and pellet, this may indicate that not all cytosolic proteins are removed by the enrichment process.

(4.2.4) Generation of samples for proteomic analysis

After proving the presence of key proteins of interest, samples were generated for proteomic analysis. Two sets of samples were generated, the first set was generated from cells that had been synchronised by CCE. Asynchronous procyclic cells were eluted at flow speeds of 20 and 22 ml/min, which correspond to mid and late G1 cells respectively. The F20 samples immediately underwent F-PACS enrichment. The F22 sample was returned to culture and incubated for 4.5 hours. This was selected based on (Lozano-Núñez et al., 2013), which showed that 5.5 hours into the cell cycle, TbPLK inhibition did not result in a cytokinesis defect until the following cell cycle. As

F22 represents late G1, these cells are likely at least 5.5 hours into the cell cycle. The F-PACS samples would be enriched for phosphopeptides before proteomic analysis, enabling comparison of phosphpeptides between G1 cells and cells that have undergone at least 1 important regulatory phosphorylation event. Before F-PACS enrichment, samples were taken for flow cytometry to prove the initial synchronisation and growth (Figure 4.13). Both the F20 and F22 fractions were split into 3, with each using one of the 3 salt buffers (NaCl, KCl, $CaCl_2$), showing which phosphoproteins are preserved in each method.

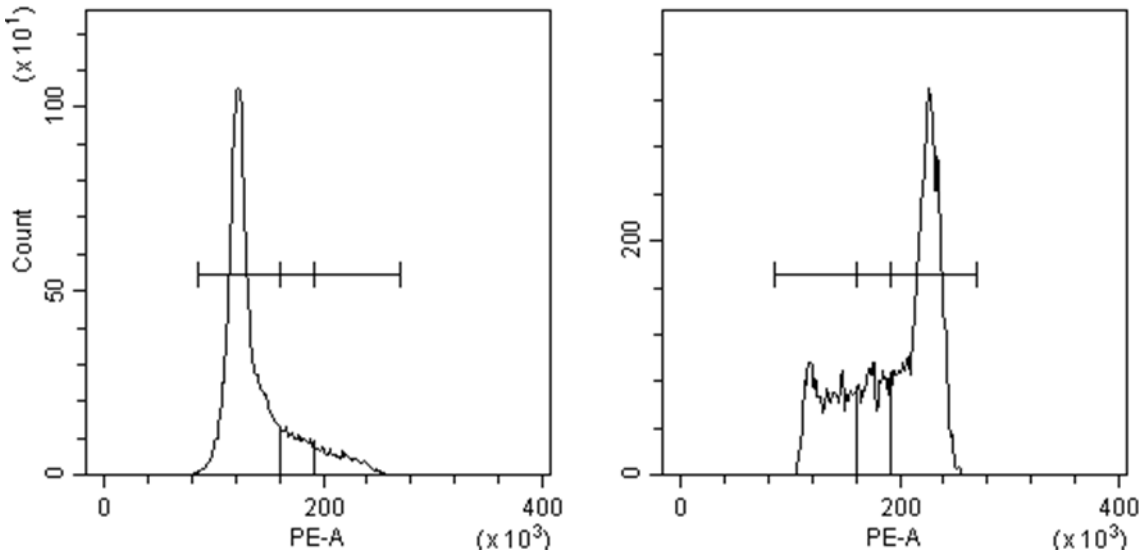

Figure 4.13 Flow cytometry histograms of fractions synchronised by CCE at flow speeds of 20 and 22 ml/min. 1.25x10^9 PCF *T. brucei* cells were synchronised by CCE (A) Flow cytometry histogram of G1 enriched cells collected at 20 ml/min, this fraction contained 8.75x10^7 cells. (B) Flow cytometry histogram of G1 enriched cells collected at 22 ml/min that were left to grow for 4.5 hours, this fraction contained 6.25x10^7 cells.

The F20 fraction in figure 4.13 A appears to closely resemble the F20 fraction in figure 4.2 A. The F22 fraction in figure 4.13 B resembles the F22 T4 fraction in figure

4.3 A. This suggests that the collected fractions represent cells in the desired cell cycle stages.

The second set of samples was unsynchronised but had been SILAC labelled using lysine and arginine. Cells were grown in light, medium and heavy SILAC media for 3 days before samples were generated. An equal number of light, medium and heavy cells were processed separately, with each processed using a different salt buffer and then combined. This would enable the analysis of the proteins and protein abundance in each of the salt buffer conditions. Both sets of samples have been generated, but further processing of the samples will be completed by members of the MDU lab, before being sent for proteomic analysis.

(4.3) Molecular cloning and early optimisations for *T. congolense* study

(4.3.1) Aims

Knowledge regarding the cell biology of *T. congolense* remains incomplete when compared *to T. brucei*, with knowledge of the cell cycle being especially limited. To date, there are no publications investigating *T. congolense* that describe or utilise a cell cycle synchronisation protocol. This presents an opportunity to further cell cycle study of the species by attempting to optimise a synchronisation protocol – preferably one that has already been shown to be effective in *T. brucei*. One of the main reasons that *T. brucei* became the unanimous model organism for the trypanosome genus was due to the ease of genetic manipulation – which has greatly accelerated the characterisation of the *T. brucei* proteome. This has enabled the

characterisation of key cell cycle regulators as highlighted in chapter 2.3.2. This section represents an early, yet incomplete, attempt to both optimise a synchronisation technique and tag key cell cycle regulators in *T. congolense*, which highlights the issues encountered while working with this comparatively difficult organism.

(4.3.2) Cloning strategy

Proteins were selected for tagging based on two criteria, a known role in regulation of the cell cycle and a measurable change in abundance tied to the cell cycle in *T. brucei*. The change in abundance is particularly important, (Benz and Urbaniak, 2019) showed that amongst cell cycle regulated proteins, few change in abundance, with most changing only in phosphorylation status. PLK and PUF9 were highlighted as proteins which did change significantly in abundance and therefore provided suitable targets for tagging (Table 4.1). The function of these proteins has not experimentally been confirmed to be shared between the two species, but they share significant sequence homology (Figure 4.14).

Table 4.1 Targets for endogenous tagging in *T. brucei* and *T. congolense*.

Protein name	Tb Gene ID	Tco Gene ID	Protein sequence identity	Terminus tagged	Role in CCR
PLK	Tb927.7.6310	TcIL3000_7_5220	75.1%	N	Regulation of cytoskeletal duplication
PUF9	Tb927.1.2600	TcIL3000_1_1350	51.8%	N	Regulates expression of CCR proteins

Figure 4.14 BLASTP alignment of *T. brucei* and *T. congolense* PUF9 and PLK. (A) Alignment of Tb927.1.2600 (TbPUF9) and TcIIL3000_1_1350 (TclPUF9). (B) Tb927.7.6310 (TbPLK) and TclIL3000_7_5220 (TbPUF9).

TbPUF9 and TclPUF9 share some sequence homology, with the N-terminal region of the protein showing the least conservation. TbPLK and TclPLK have greater sequence homology, especially around the C and N terminus. The N-terminal end of the protein contains the kinase domain (~40-300), and the C-terminal end contains the POLO-box domains (~550-776). The TbPLK and TbPUF9 homologues and their predicted protein sequence in *T. congolense* were found using TriTrypDB (Aslett et al., 2010). To determine the location of the tag, TrypTag (Dean et al., 2017) was utilised, this database aims to determine the localisation of all proteins in PCF *T. brucei*. PUF9 has been successfully tagged on the N-terminus for the TrypTag project (Dean et al., 2017), and localisation of the tagged protein matches the localisation

shown by antibody staining (Archer et al., 2009). Attempts to tag PLK at either terminus for the TrypTag project resulted in failed transfections (Dean et al., 2017). However, PLK has been epitope-tagged on the N-terminus (Hammarton et al., 2007), so we decided to attempt a YFP tag at the same location.

The method for N-terminal endogenous tagging of PLK and PUF9 is highlighted in figure 4.15. First, primers were designed to amplify ~500 BP from both the start of the ORF and from the end of the 5' UTR. Sequence data to design these primers was taken from TriTrypDB (Aslett et al., 2010). For the *T. brucei* specific primers, Lister strain 927 was used as a template for the primers as this strain has both the ORF and the UTR sequenced and defined. 927 and 427 (which is the strain used in our laboratory) are similar, but some genes have differences in their sequence, as a result, any sequence data was compared to the 427, not 927, strain. No strains of *T. congolense* have annotated UTRs for the two target proteins, so a 500bp sequence at the 5' end of the gene in the TrypTag genome browser was used and assumed to be the 5' UTR (Aslett et al., 2010). Restriction enzyme target sequences were included in the primer, to enable the ligation of the sequence into the desired backbone. Both UTRs and ORFs are flanked by cut sites for restriction enzymes, as seen in figure 4.15. All UTRs possess a *NotI* cut site at one end, with either a *Bam*HI or *Xho*I cut site at the other. All ORFs have one *Xba*I cut site, and either a *Bam*HI or *Xho*I cut site at the other. Directly next to the B*am*HI/*Xho*I cut site is a *Not*I cut site, once the ORF is ligated into the final backbone, the UTR can be inserted by digesting both with NotI. The NotI site will then act as a linearisation site for the circular backbone.

After PCR using the designed primers (Appendix 1), the inserts were ligated into the bacterial plasmid pGEM-T Easy. After confirmation through sequencing, the ORFs were ligated into the backbone pEnNY0, followed by the UTR. *Not*I could then be used to linearise the constructs, followed by transfection into BSF trypanosomes which enables the construct to be recombined into the trypanosome genome, enabling both fluorescent tagging and drug resistance.

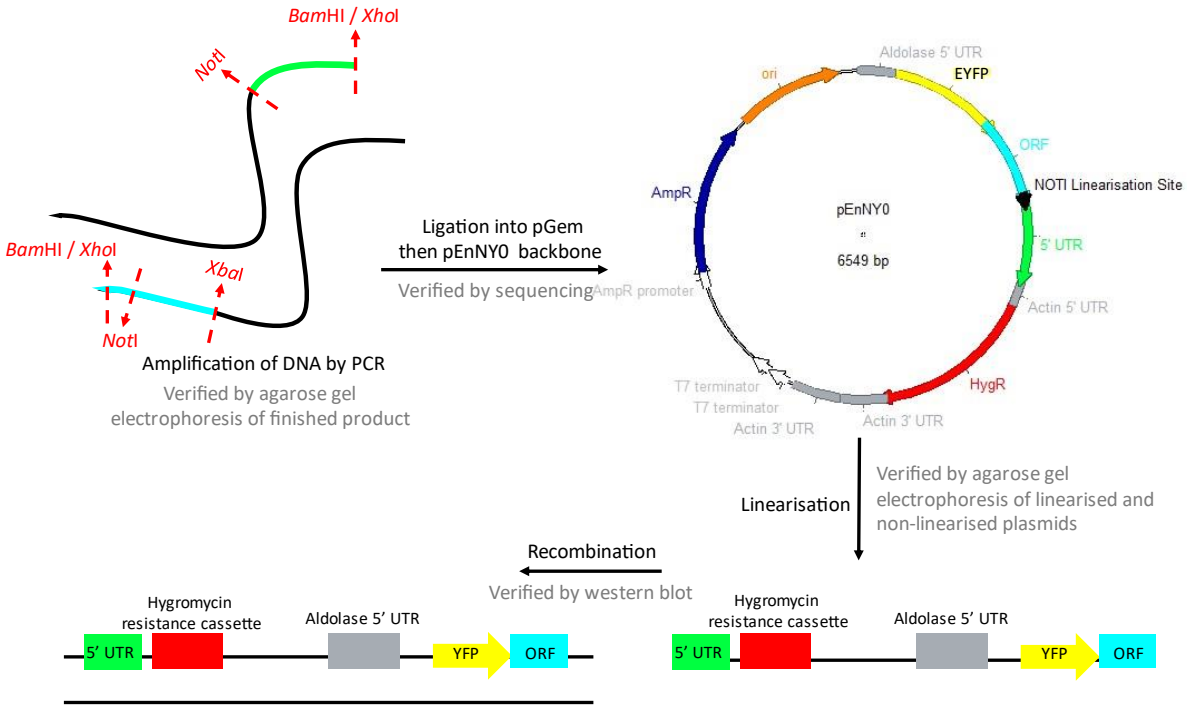

Figure 4.15 Overview of molecular cloning strategy. PCR products are ligated into pGEM-T Easy, then after sequence confirmation, into pEnNYO. The backbone can then be linearised by *Not*I and recombined into the trypanosome genome after transfection. The pEnNYO plasmid map was generated using A plasmid Editor (Davis and Jorgensen, 2022).

(4.3.3) Generating constructs

The aforementioned PCR primers flank and amplify a ~500bp region of extracted genomic DNA which encompasses a section of either the ORF or 5' UTR of the target protein. The resultant PCR products were then separated by gel electrophoresis, so the size of the PCR product could be compared to a DNA ladder. The agarose gels were then imaged, and the size of the observed bands was compared to the size of the flanked region, to check that the primers only bound to the desired sequence (Figure 4.16)

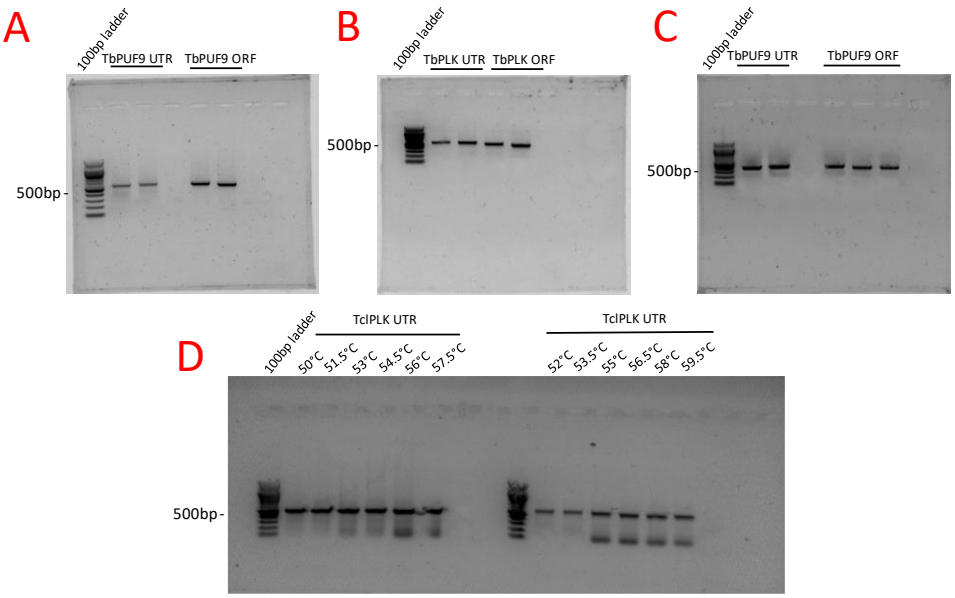

Figure 4.16 Agarose gel of PCR products. Primers were designed to flank a 500bp region of both the ORF and 5' UTR of PUF9 and PLK in both *T. brucei* and *T. congolense*. The TclPLK inserts (D) result from a temperature gradient PCR, with the temperature of the first lane being 50°C and 52°C respectively.

The expected size of all insert bands is 500 bp, which corresponds to the sizes of the bands seen in figure 4.16. In some cases, the predicted annealing temperature resulted in non-specific bands – indicating the primers can bind to an undesired genomic location and enable unwanted amplification, as seen in figure 4.16 D. In this

instance, a temperature gradient PCR was performed so that the annealing temperature was different in each lane. In TclPLK UTR and ORF non-specific bands do not appear at the lower temperatures (50°C and 52°C respectively), so the PCR reactions were repeated at these temperatures.

The generated inserts then needed to be ligated into the pGEM-T Easy backbone. After being separated by gel electrophoresis, the inserts were excised, and the gel extraction protocol was followed to isolate the insert DNA. The insert DNA was then ligated into pGEM-T Easy overnight, the following day the construct was transformed into competent bacterial cells. XGAL and IPTG were added to an agar plate before the transformed bacteria, enabling blue/white screening of colonies. White colonies were picked as this indicated successful ligation of the insert into the backbone. The LacZ gene present in pGEM-T Easy produces B-gal, which cleaves X-gal into a blue precipitate, this is only possible when IPTG (galactose analogue) inactivates the lac repressor. Colonies are picked and grown in LB broth overnight before the plasmid is purified by miniprep. The plasmid was then digested with the corresponding restriction enzymes, and the product was separated by gel electrophoresis (figure 4.17). This confirms the presence of the insert before the samples were sent off for sequencing.

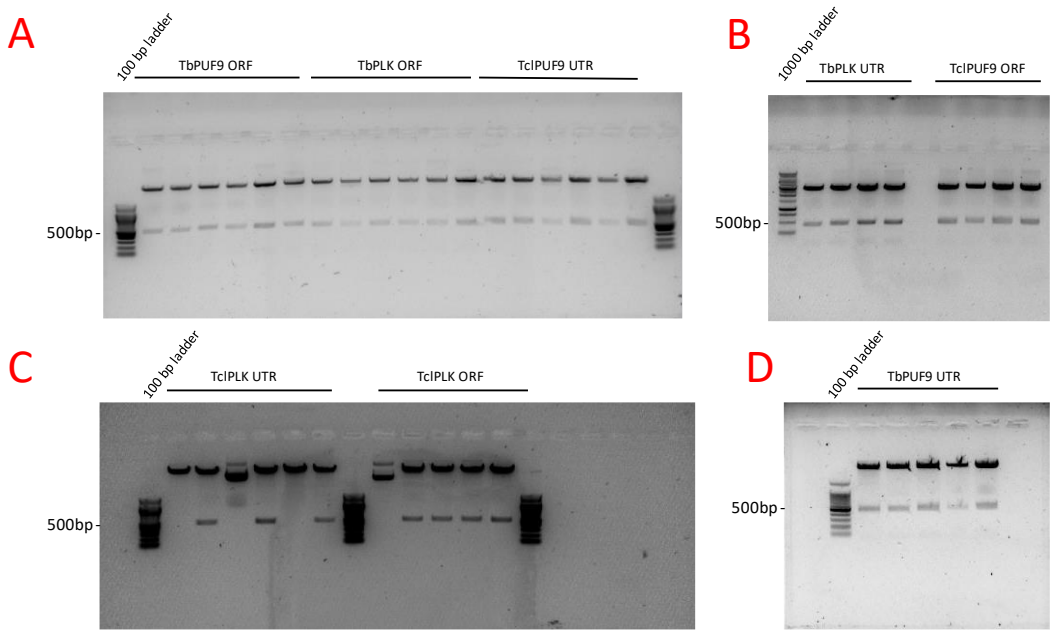

Figure 4.17 Agarose gel of restriction enzyme digests of constructs containing PLK and PUF9 sequences. Inserts are from *T. brucei* PUF9 ORF, *T. brucei* PLK ORF and *T. congolense* PUF9 UTR. (A) *T. brucei* PUF9 ORF, *T. brucei* PLK ORF and *T. congolense* PUF9 UTR; (B) *T. brucei* PLK UTR and *T. congolense* PUF9 ORF (C); *T. congolense* PLK UTR and ORF and (D) *T. brucei* PUF9 UTR. Plasmids were digested with restriction enzymes and separated by gel electrophoresis; the size of the bands was compared to the expected size to confirm the presence of the insert. All gels show >1 band at the correct size, with *T. congolense* PLK UTR and ORF showing some lanes without the correct bands.

Inserts isolated by restriction digest were separated by electrophoresis. If insert size corresponded to 500bp, as shown in figure 4.17, they were sequenced. The insert sequence was then aligned to the *T. brucei* 427 or *T. congolense* IL3000 sequence (Figure 4.18). The alignments were then deemed as suitable or not, for ORFs, only polymorphisms not resulting in an amino acid change would be tolerated as any changes could affect the functionality or localisation of the target protein. For UTRs, some small polymorphisms could be tolerated, but large changes in the sequence could result in an inability to recombine at the correct locus of the trypanosome genome.

Figure 4.18 Alignment of insert sequences to the desired sequences, either *T. brucei* 427 or *T. congolense* IL3000. (A) TbPLK UTR sequence (B) TclPLK UTR sequence (C) TclPUF9 UTR sequence. Sequences were amplified by PCR and ligated into the pGEM-T Easy backbone, then sequenced. The TbPLK insert was aligned with Tb427.07.6310-t26_1, TclPLK was aligned with TcIL3000_7_5220, and TclPUF9 was aligned with TcIL3000_1_1350. Inserts were sequenced from the T7 promoter found in the pGEM-T Easy backbone.

Though figure 4.18 does show some differences between the desired and returned sequences, overall, the returned sequences are very similar. The TriTrypDB sequence is assumed to be correct, but as strains naturally accumulate polymorphisms from extended time in culture, there may be some differences. As a result, when multiple samples of the same insert were sent for sequencing, if they all shared a specific

polymorphism it was assumed that this was a true part of the gDNA sequence, as the chance of different inserts sharing the same mutation is unlikely.

After the pGEM-T Easy sequences had been confirmed, the ORFs and pEnNY0 vector were digested with *Xba*I and *Bam*HI/*Xho*I. The products were separated by gel electrophoresis, with the insert and backbone bands being excised and isolated by gel extraction. The inserts, and backbone digested with the same restriction enzyme pair, were ligated, then transformed and plated onto agar plates. Colonies were selected and grown before the plasmids were purified using a miniprep kit. The resulting minipreps were digested and separated by gel electrophoresis to check for a 500bp band (Figure 4.19).

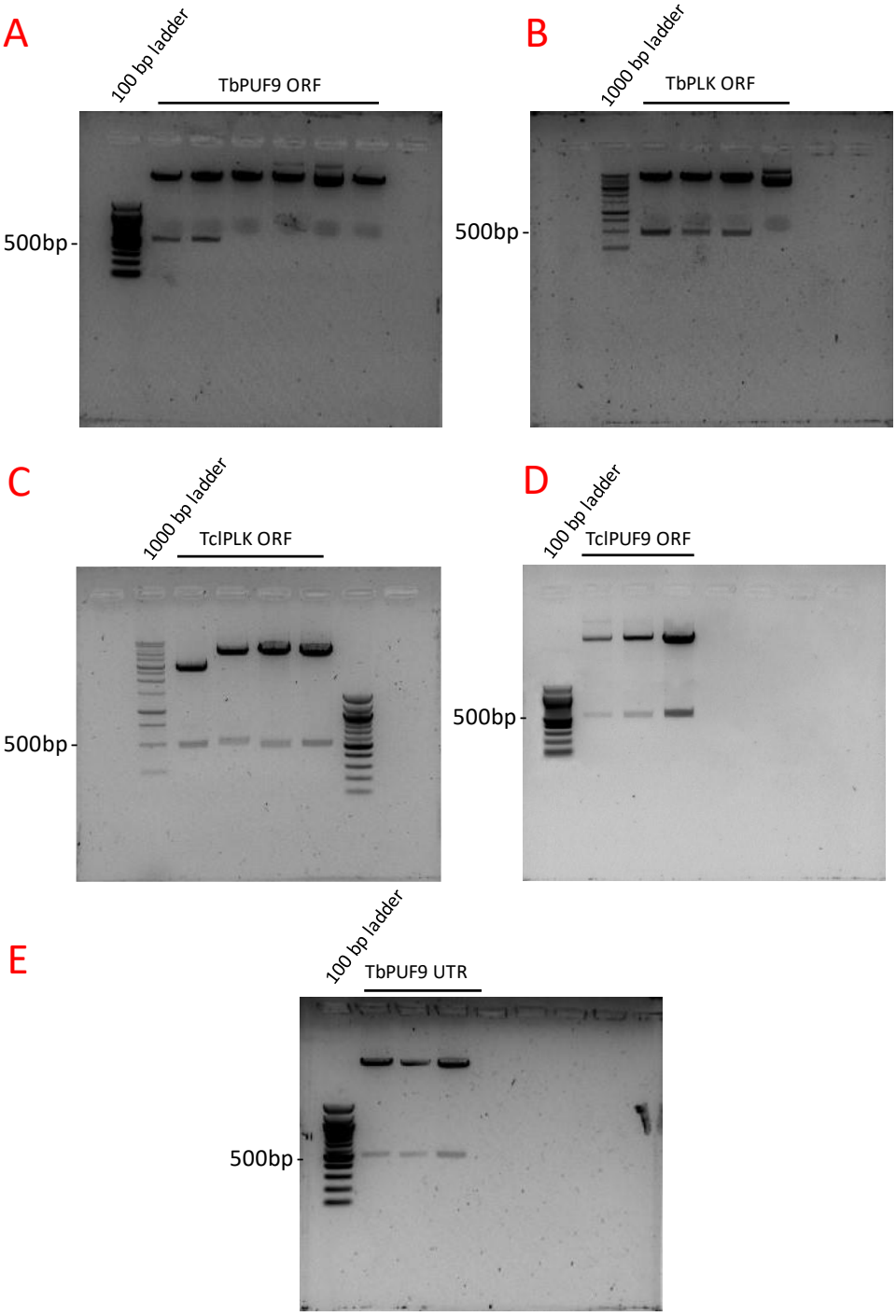

Figure 4.19 Agarose gel of restriction enzyme digests of constructs containing PLK and PUF9 sequences. (A) *T. brucei* PUF9 ORF digested (B) *T. brucei* PLK ORF (C) *T. congolense* PLK ORF (D) *T. congolense* PUF9 ORF (E) *T. brucei* PUF9 UTR. Plasmids were digested out of pEnNY0 with restriction enzymes and separated by gel electrophoresis; the size of the bands was compared to the expected size to confirm the presence of the insert. All gels show >1 band at the correct size.

Inserts of the correct size after restriction enzyme digests with *Xba*I and *Bam*HI/*Xho*I were then sent for sequencing (Figure 4.19 B-D). Figure 4.19 A and E represent the ORF and UTR of the same protein. To complete this construct, TbPUF9 UTR and TbPUF9 ORF-pEnNY0 were digested with *Not*I and *Bam*HI to generate matching sticky ends in the insert and backbone. These were then separated by electrophoresis and isolated using a gel extraction kit. After ligation, they were transformed into competent bacteria and grown. The UTR underwent a restriction digest with *Not*I and *Bam*HI and was then separated by gel electrophoresis (Figure 4.19 E) to confirm successful ligation. The completed construct was isolated using a miniprep kit, and all samples were sequenced (Figure 4.20).

Figure 4.20 Alignment of insert sequences to the desired sequences, either *T. brucei* 427 or *T. congolense* IL3000. (A) TbPLK ORF sequence (B) TclPUF9 ORF sequence (C) TclPLK ORF sequence (D) TbPUF9 UTR and ORF sequence. Inserts were digested out of the pGEM-T Easy backbone and ligated into the pEnNYO backbone, then sequenced. The TbPUF9 inserts were aligned with Tb427.01.2600-t26_1, TbPLK was aligned with Tb427.07.6310-t26_1, TclPLK was aligned with TcIL3000_7_5220, and TclPUF9 was aligned with TcIL3000_1_1350. (D) Represents a completed construct, with both the UTR, ORF and the Not1 linearisation site. Inserts were sequenced from the 3' EYFP site found in the pEnNY0 backbone.

Figure 4.20 (A, B, C) shows that the inserts match the reference sequence with no polymorphisms. The ORF of the completed TbPUF9 construct (Figure 4.20 D) is also identical to the reference sequence, however, the UTR has a 3 bp deletion and has been cut short. In order to be completed, the sequenced ORFs in pEnNY0 and UTRs in pGEM-T Easy would need to be digested with matching restriction enzymes and ligated.

(4.3.4) Analysis and synchronisation of *T. congolense*

Optimising a synchronisation method for use on *T. congolense* would provide a useful tool for studying the cell cycle. Both hydroxyurea and CCE were trialled on *T. congolense*, representing both a chemical and mechanical method of synchronisation. Synchronised populations were then analysed by flow cytometry, however, the preparation of samples for flow cytometry had to be assessed. Previous students had shown that the established method of sample preparation in *T. brucei* (3.4) when applied to *T. congolense*, had produced large quantities of lysed cells. This was avoided by initially fixing in 50% methanol, before increasing to 70% after 1 hour, rather than fixing in the final methanol concentration (70%) immediately (3.5). This was validated by generating samples for both *T. brucei* and *T. congolense* to compare the traces at different flow parameters (figure 4.21).

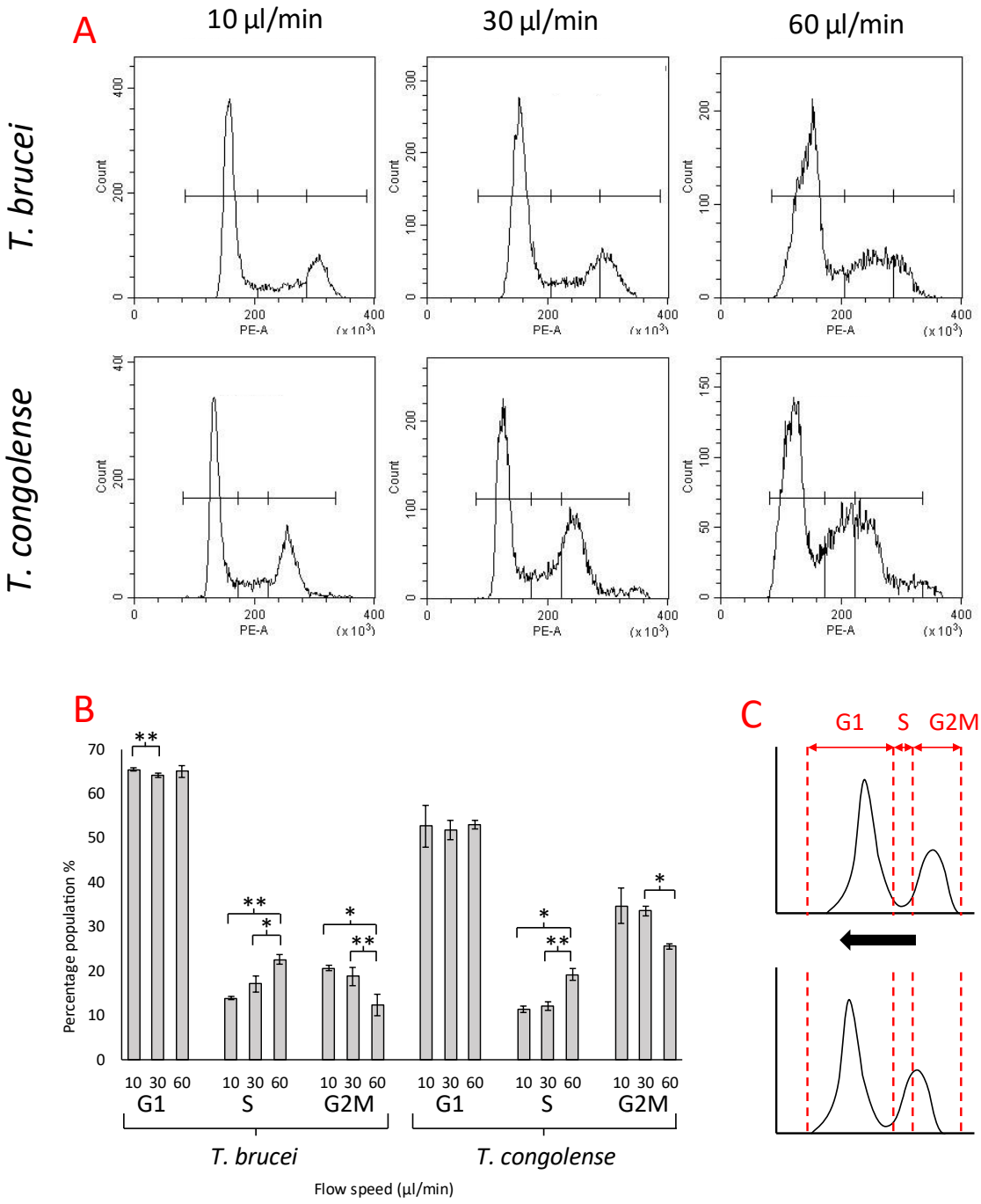

Figure 4.21 Flow cytometry of *T. brucei* and *T. congolense* at different flow speeds. (A) Flow cytometry histogram of *T. brucei* and *T. congolense* at increasing acquisition speeds. (B) Bar chart showing the percentage of cells in each cell cycle stage at different acquisition speeds, in *T. brucei* and *T. congolense*. (C) Graphic demonstrating how the leftward shift of the G1 and G2M peak seen in (A), results in the distribution changes in (B). Triplicate samples were generated, and a T-test was used to determine significant difference. * Represents ($p<0.05$), ** represents ($p<0.01$). Error bars represent standard deviation.

Flow cytometry of *T. congolense* using the modified protocol appears to produce similar results to *T. brucei* at 10 µl/min acquisition speed speeds. Both traces in figure 4.21 A show distinct, narrow, and symmetrical peaks that are similar in shape. This data also suggests that *T. congolense* has a proportionally short G1 phase compared to *T. brucei*. This is because in an asynchronous population, the percentage of cells in a cell cycle stage is proportional to the length of that stage. The data shows that on average ~65% of *T. brucei* cells are in G1, compared to ~52% in *T. congolense*. As the acquisition speed is increased, the traces show an increase in peak width and asymmetry in both species. Increase in the acquisition speed results in a significant increase in the proportion of S-phase cells, and a decrease in G2M cells, which occurs in both species (figure 4.21 B). The centre of the G1 and G2M peaks appears to move left as acquisition speed increases. If the boundaries marking cell cycle stage are kept consistent, the shift of the G2M peak into the S phase boundary results in the apparent increase in S phase cells and a decrease in G2M, this is shown in figure 4.21 C. This demonstrated that slower acquisition speeds are preferable, but more importantly all samples should be run the same acquisition speed to avoid potential experimental artefacts.

After confirmation that *T. congolense* cells could be analysed by flow cytometry, hydroxyurea synchronisation was then trialled. *T. congolense* cells were grown to mid-log before 10 µg/ml HU was added to the media. Cells were returned to culture for 6 hours, then the HU media was removed and replaced with fresh media. The cells were then grown for 12 hours, with samples taken for flow every hour for 12 hours – representing 1 cell cycle (Figure 4.22). As a direct comparison, the same was done for *T. brucei* (Forsythe et al., 2008).

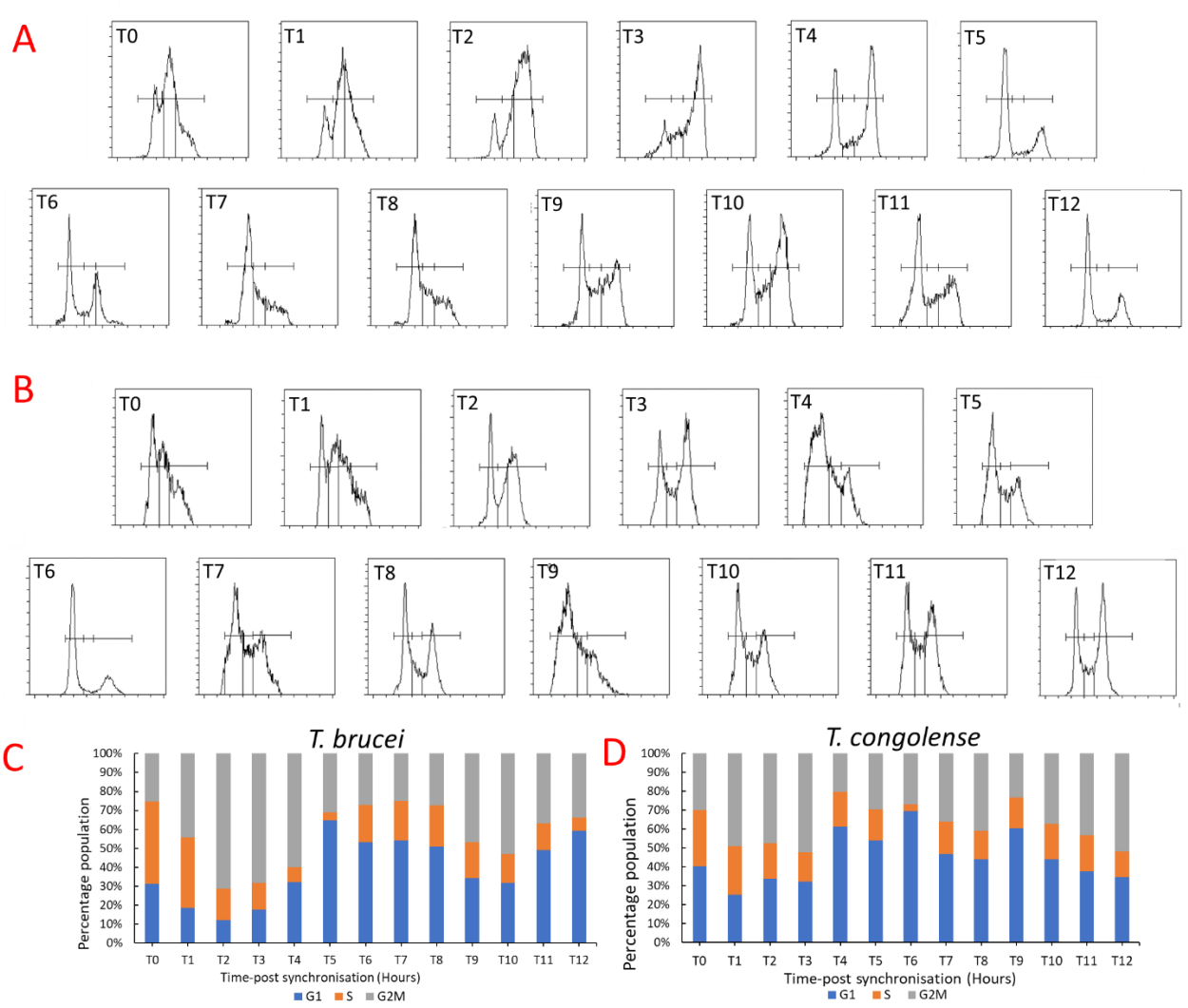

Figure 4.22 Growth and recovery of HU synchronised *T. brucei* and *T. congolense* cultures. Mid Log *T. brucei* and *T. congolense* cells were treated with 10 µg/ml HU and grown for 6 hours before removal. Cells were returned to culture and allowed to propagate; samples were collected for flow cytometry analysis every hour for 12 hours. (A) Flow cytometry histograms of HU synchronised *T. brucei* cells for 12 hours after HU removal. (B) Flow cytometry histograms of HU synchronised *T. congolense* cells for 12 hours after HU removal. (C) Bar chart showing the percentage of HU synchronised *T. brucei* cells in each cell cycle stage at each timepoint. (D) Bar chart showing the percentage of HU synchronised *T. congolense* cells in each cell cycle stage at each timepoint. Histograms show cell count (Y) against propidium iodide emission area (X).

Figure 4.22 A shows that initially after removal of HU, *T. brucei* cells appear enriched in S-phase, with 43% of cells present in S-phase at T0. There is also an increase in S-

phase population in *T. congolense*, representing 29.7% of the T0 population. In *T. brucei*, cells begin to progress through the cell cycle with G2M reaching a peak of 71% at T2. At this point, cells begin to divide and re-enter G1 until T7 when cells begin to enter G2M for a second time. This pattern, highlighted in Figure 4.22, fits roughly within the timescale of 2 BSF *T. brucei* cell cycles. The second cell cycle (from T7 onwards) appears to have reduced enrichment to S-phase, indicating that the cells are becoming less synchronised. This pattern is not seen in *T. congolense*, initially, cells begin to enter G2M, reaching a maximum of 51% at T3, and then the G1 population rapidly decreases. The changes in population composition appear to be relatively unpredictable, though there is an overall decrease in the G1 population. HU appears to have a less clear effect on *T. congolense* at this concentration. Though there is an initial enrichment to S-phase, it does not appear to be followed by synchronised progression through the cell cycle.

As an alternative to HU and chemical synchronisation, *T. congolense* cells were grown for synchronisation by CCE. Cells were grown to mid-log and loaded into the elutriator at 5 ml/min. Flow speed was increased and 150 ml fractions were collected at 7, 8, 9, 10, 11, 12, 14 and 16 ml/min. Flow cytometry samples were generated in each fraction for analysis (Figure 4.23).

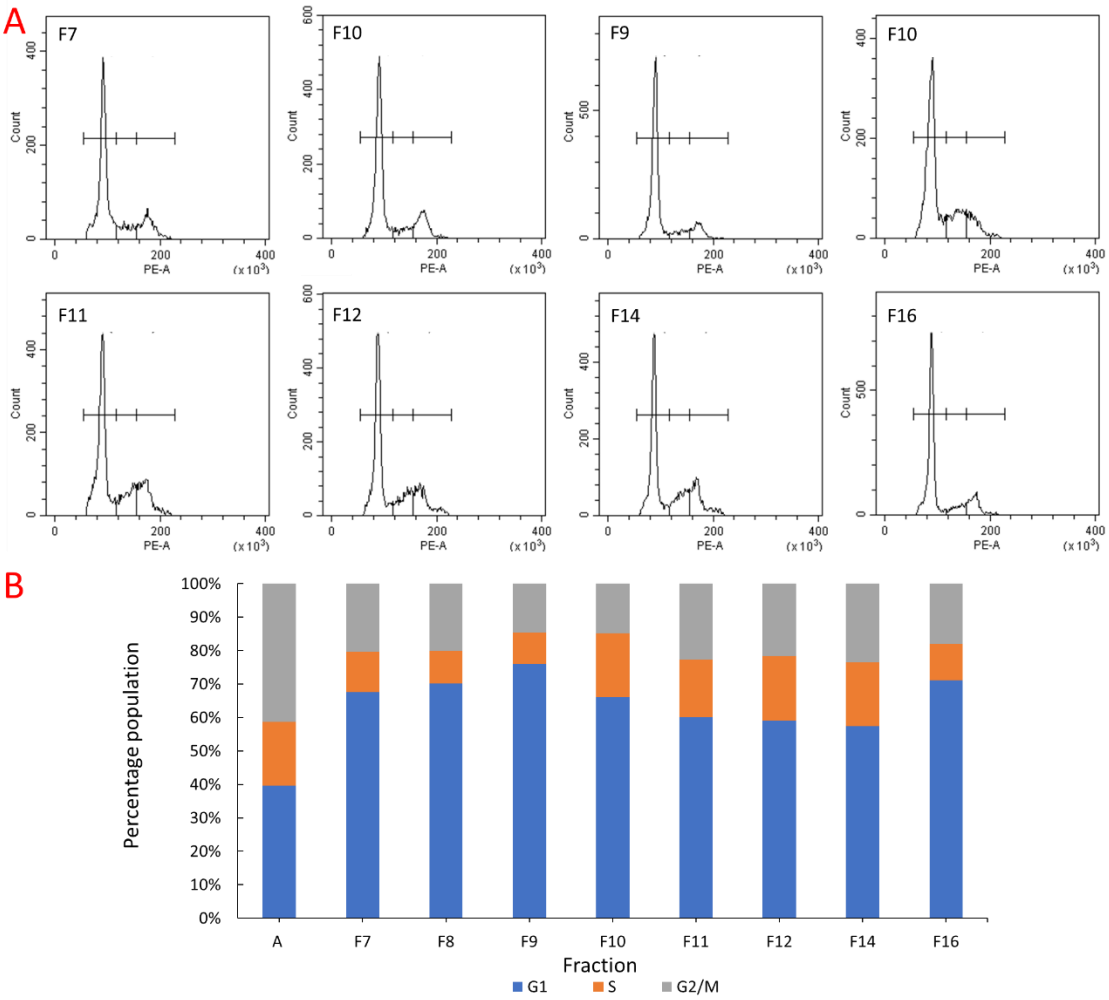

Figure 4.23 Characterisation of *T. congolense* elutriation fractions collected at a variety of flow speeds. 1x10^9 BSF *T. congolense* were loaded into an elutriating centrifuge, 150 ml fractions were collected at 15, 18, 20, 22, 28 and 35 ml/min. (A) Flow cytometry histograms of collected fractions, both F9 and F16 appear enriched in G1. (B) A bar chart showing the proportion of cells in each cell cycle stage and the cell count in each fraction, increasing flow rate does not result in a decrease in G1 cells. Asy represents asynchronous.

Figure 4.23 A shows that *T. congolense* can be enriched in G1 by CCE, though the extent of the enrichment is not as great as in *T. brucei*. The highest proportion of G1 cells is found in F9 at 76%, representing a ~1.9x enrichment. Though this is greater than the proportional G1 enrichment seen in *T. brucei*, the proportional enrichment is less valuable than the percentage of cells in G1. There are also no fractions that are

enriched in S-phase. All the collected fractions have reduced G2M population compared to the asynchronous, this indicates that most of the G2M cells were removed into waste after collecting the F16 fraction. However, this is unusual as based on the *T. brucei* data some of the later *T. congolense* fractions should have more G2M cells present. It is also unusual that increasing the flow rate does result in fewer G1 cells, with the most G1 enriched fraction occurring at the highest flow speed. This means that separation of cells cannot be based purely on sedimentation velocity of individual cells, as the data shows there is no clear correlation between the flow rate and amount of nucleic acid detected within the cell. In chapter 4.1.3, synchronisation of PCF *T. brucei* using a Sanderson chamber resulted in periodic breakdown of the visible cell boundary. This also occurred during the elutriation of *T. congolense* but with a slight difference, the cells seemed to congregate extremely far down the chamber away from the elution boundary. This was due to the low flow rate of 5 ml/min providing little resistance to the centrifugal force of the centrifuge. This low speed was chosen in turn, as any higher speeds resulted in complete loss of cells – which also indicates that the cells are smaller than *T. brucei*. Due to this, the entrance to the chamber would become periodically blocked, causing a steady increase in pressure that eventually resulted in the ejection of the cells into the chamber. As cells settled back into a boundary, pressure would build up again, as displayed on the pressure gauge.

Overall, this would suggest that CCE is an inappropriate method for synchronising *T. congolense* at this time. This is due to the inability to enrich G1 cells to the same degree as seen in *T. brucei*. It is also more inconsistent, with the distribution of cells collected in each fraction indicating that size difference is not the sole factor

determining the separation of cells. This may be due to their adhesive nature, with BSF *T. congolense* adhering to the bottom of a culture flask. This possibility and other discussion regarding *T. congolense* and its cell cycle will be discussed further in later chapters.

(5) Discussion

(5.1) Relevance and impact

Increasing the efficiency of cell cycle study in African trypanosomes would enable an increased understanding of how key cell cycle events are regulated. Cell cycle regulating proteins often provide targets for therapeutic drugs due to their necessity in maintaining cell viability. This is also known to be the case in trypanosomes, disruption of many identified cell cycle regulators results in failure of the cell to divide, as is seen when TbPLK is inhibited (Lozano-Núñez et al., 2013). Particularly important in *T. brucei* cell division is the flagellar pocket and its associated cytoskeletal structures. The cytoskeleton of mammalian cells in multiple different components, the actin cytoskeleton, intermediate network, and microtubules, it is also a highly dynamic structure which facilitates the wide range of functions it is involved with (Hohmann and Dehghani, 2019).

The cytoskeleton of trypanosomes contains the subpellicular array, a corset composed of microtubules that are maintained in a stable, helical conformation (Sun et al., 2018). The subpellicular array is responsible for determining cell shape and its flexible arrangement of equally spaced microtubules is required for cell motility (Sun et al., 2018). The cytoskeleton is also composed of a series of structures surrounding the flagellar pocket, including the flagellar pocket collar, hook complex and flagellum attachment zone (Lacomble et al., 2009). The coordinated duplication and movement of flagellar pocket associated cytoskeletal structures (F-PACS) is necessary for flagella inheritance and faithful cell division (Ikeda and de Graffenried, 2012).

However, the signalling pathway that regulates the assembly of F-PACS is not fully characterised.

Polo-like kinases are a group of serine/threonine kinases that have myriad functions in eukaryotes, including centrosome maturation, apoptosis, and cytokinesis (Lee et al., 2014). In *T. brucei*, PLK localises successively to the Basal body, flagellar pocket collar, hook complex and FAZ. Inhibition of TbPLK by RNAi in G1 results in cytokinesis defects, however, if you inhibit PLK at 5.5 hours into the cell cycle these defects only occur in the following cell cycle. This indicates that TbPLK phosphorylates F-PACS proteins at the start of the cell cycle, necessary later for cytokinesis, though the targets are currently unknown (Lozano-Núñez et al., 2013). (Benz and Urbaniak, 2019) Highlights the importance of dynamic phosphorylation events in regulating the *T. brucei* cell cycle, showing that, over the cell cycle, changes in phosphosite abundance is greater than changes in overall protein abundance. The proteins that most commonly increase in phosphorylation status are related to the mitotic cell cycle, chromosome segregation and cell division.

To attempt to further the knowledge regarding these important events, efficient protocols for studying the cell cycle must be used. Synchronisation methods enable global studies of cells at a particular stage of the cell cycle. Centrifugal counter-flow elutriation was used to synchronise both PCF and BSF *T. brucei* cells. A protocol for the enrichment of the *T. brucei* F-PACS was also optimised, and the two were combined to generate proteomic samples. The result of the proteomic analysis may reveal changes in phosphosites, though much more will be required to complete our understanding.

T. congolense is the major cause of AAT, and comparatively little is known about its cell biology when compared to *T. brucei* (Morrison et al., 2016). The cell is smaller overall, and the cell cycle is longer with a greater emphasis on G2M. Given the closeness of the evolutionary relationship, the regulation of key cytoskeletal events is likely also crucial to the progression of its cell cycle. However, no methods for synchronisation have been described in this species, and no definitive timing of cell cycle events has been published. Two different synchronisation methods were attempted on *T. congolense*, hydroxyurea and CCE, though neither seemed as effective when compared to *T. brucei*. Both the laboratory culture and genetic manipulation of *T. congolense* were established later than in *T. brucei*, and it is a comparatively difficult organism to culture. As a result, a complete understanding of the cell cycle of *T. congolense* is likely far away.

(5.2) Discussion of *T. brucei* elutriation results

(5.2.3) Summary of results

Centrifugal counter-flow elutriation of PCF *T. brucei* populations isolated fractions that were highly enriched in G1, with fractions collected at 18 ml/min possessing >97% of cells in G1. Once returned to culture, these fractions grew without noticeable delay in a synchronised fashion, enabling enrichment of population to S and G2M. The S-phase population reached a maximum of 37% and the G2M population reached a maximum of 80%. G1 enriched fractions were also collected at 18 and 22 ml/min – with 18, 20 and 22 ml/min fractions corresponding to early, mid, and late G1 populations. The different fractions all progress synchronously through

the cell cycle, however, the larger cells collected at a higher flow speed progress from a further starting point. This data supports the current literature, (Benz et al., 2017) saw similar G1 enrichment and maintenance of synchronisation after CCE of PCF *T. brucei*. They also measured the volume of collected fractions and showed that the later G1 fractions contained cells of a larger average volume. This is expected because CCE only separates cells based on their sedimentation velocity, not cell cycle stage, so separation of these fractions would only be possible if there was a difference in size or density.

CCE of BSF *T. brucei* had different results, though populations could still be enriched in G1. At 15 ml/min the collected fraction contained >98% of cells to G1, however, they did not progress as synchronously through the cell cycle as PCF cells. The minimum proportion of G1 cells seen in any BSF fraction is 31% compared to 9.3% in PCF. As a result of the G1 population not diminishing to the same extent as in PCF, it is impossible to enrich fractions to S or G2M stage to the same extent observable in PCF. The different G1 fractions collected also appear very similar, implying that early, mid and late G1 cells cannot be separated. This agrees with the existing literature, which also shows a subset of the population that remains in G1. However, the proportion of G1 cells that are 'stuck' is potentially smaller in (Benz et al., 2017). (Benz et al., 2017) also recorded the volume of G1 enriched cells as they were grown and noted that there was no significant increase in volume across the first 2 hours of G1 – explaining why early, mid and late G1 cells could not be separated in BSF.

The reason for the stalling of some cells in BSF and not PCF *T. brucei* is not definitively known, however, increasing the time spent in the elutriator results in

more BSF cells becoming stalled (Benz et al., 2017). Wt BSF *T. brucei* naturally regulate parasite density in the host through a quorum-sensing mediated pathway resulting in transformation into a non-proliferative stumpy form (Schuster et al., 2021). Though this does result in cells remaining in G0, it is caused by the accumulation of stumpy-inducible factor, which is released by BSF *T. brucei* at high density. This is unlikely to be the cause of the observed stalling, as cells in the elutriator are being washed at 15 – 19 ml/min, which would prevent the accumulation of any released signalling molecule (Schuster et al., 2021). The cause of stalling in *T. brucei* could be explored further through a variety of measures. Elutriated fractions could be stained with propidium iodide to estimate the proportion of viable cells. Limiting dilution could be used to add ~1 cell to a plate well, cells would then be grown and counted, and the number of cells could then be compared to the estimated cell number in a fully dividing population to reveal the proportion of non-dividing cells. Alternatively, BSF cells could be elutriated to separate the G1 population, then left to grow several hours, before undergoing separation to isolate G1 again. The remaining G1 isolated cells would represent the stalled cells, which could then be studied further.

(5.2.2) The Sanderson chamber

The Sanderson chamber is an alternative design to the standard chamber, designed to separate cells that are smaller or that have more consistent physical properties (Sanderson et al., 1976). However, for the purpose of separating PCF *T. brucei* cells, it is inadequate when compared to the standard chamber. The highest G1 enrichment

achieved was 79% compared to 97% using the standard chamber, this small enrichment makes it useless for synchronisation when the standard chamber is an option.

More interesting than the poor enrichment is the breakdown of the visible cell boundary, where the cells within the Sanderson chamber would become dispersed. When using a standard chamber, the cells remain visible throughout the entire process, with the maintenance of the visible cell boundary being a vital sign that the process is working as expected. A breakdown of the visible cell boundary means that in some way, the cells are not reaching an equilibrium in the chamber, indicating that the separation process cannot occur. In the normal chamber, the boundary appears as a relatively straight line parallel to the elution boundary, however, it does taper slightly to the left. The leftward taper appears similar to water climbing the edge of a glass due to surface tension. In the paper introducing the Sanderson chamber, (Sanderson et al., 1976) describes that other forces may result in fluid circulation in the chamber, mainly due to the Coriolis effect. This leftward taper matches the description of this force, but (Sanderson et al., 1976) argues that the forces would not impact separation as they are tangential to the centrifugal and fluid force. However, when using the Sanderson chamber, breakdown of the cell boundary was proceeded by an increase in the size of the lefthanded taper, appearing as if cells are being pulled in a clockwise spiral until all cells are dispersed. However, this is not the direction of fluid motion that the Coriolis effect should produce. The feature of the chamber's shape that produces the observed instability is unknown. One potential feature is the small size of the initial sorting section, this may result in molecular crowding as 1×10^9 cells are loaded into a 4 ml chamber. This is high compared to

the elutriation of mammalian cells, in which 1.5×10^8 cells are loaded into a 40 ml chamber (Liu et al., 2021). It is possible that the increase in sediment density provides an obstacle to fluid flow – resulting in the generation of eddies. In the elutriation of *T. congolense*, breakdown of the boundary in the standard chamber also occurred. However, this coincided with marked increases in pressure and may have been a result of the more adherent cells blocking the chamber entrance at low flow speeds. However, in the case of the Sanderson chamber, the breakdown only occurred at higher speeds – potentially as a result in more turbulent flow.

(5.2.3) Desirability of CCE

For the purposes of synchronising *T. brucei*, elutriation represents the most promising technique currently being utilised. Compared to chemical methods, the synchronisation achieved is far greater, and the potential for generating artefacts is much lower. Chemical methods have the advantage of being scalable, but this is not a problem for CCE as it has the capacity for sorting 1×10^9 cells, and that is while utilising the 4 ml chamber, rather than the larger 40 ml chamber. Chemical methods are also slower, with HU synchronisation requiring >6 hours (Forsythe et al., 2009) while generating a synchronised G1 fraction by elutriation takes <1 hour (Benz et al., 2017).

Compared to other mechanical methods it is also superior, with FACS based methods only synchronising 1×10^6 cells/hour (Morriswood and Engstler, 2016). More importantly, cells remain viable after CCE, and changes can be monitored over time. The largest drawbacks to CCE are simplicity and cost, with the latter arguably being

the main factor behind its relatively niche use. Though less simple than treating cells with HU or dye, the technique can be taught relatively quickly, and technical skill is not a huge barrier. However, it has a higher initial cost than chemical methods, requiring the elutriator rotor, compatible centrifuge, and pump system, though it is still cheaper than standard cell sorters. There is a risk in purchasing an elutriator for use on an organism that has not yet been synchronised through elutriation previously. However, if an elutriator is available, it should be the go-to method for synchronising *T. brucei* populations.

(5.3) Discussion of F-PACS enrichment results

(5.3.1) Summary of results

An F-PACS enrichment protocol was optimised for use on PCF *T. brucei* for the purpose of generating samples for proteomic analysis. Fluorescent microscopy images (Figure 4.9) show the gradual removal of DNA from the sample, as well as the isolation of the flagellum. The images appear comparable to existing literature, such as those shown in (Sunter et al., 2015). This study used a comparable method for flagella enrichment, using a $CaCl_2$ buffer rather than a KCl buffer used to generate figure 4.9. Some differences in the generated images include a more recognisable cell shape maintained further into the process and a lack of isolated flagella associating into concentrated areas. In figure 4.9, lysis of the cell results in a complete breakdown of the cell, looking at the polarised images it appears that lysis has resulted in the violent distribution of cell material throughout the sample, with only the flagellum being recognisable as a distinct structure. However, the protocol

in (Sunter et al., 2015) shows that after detergent extraction a clear trypanosome shape is still recognisable. The difference may be in the method for lysing the cell, our method combines two cell disruption techniques, hypotonic lysis and non-denaturing detergent solubilization. (Sunter et al., 2015) Utilises detergent solubilisation at the same concentration and incubation as in our protocol, rather than hypotonic lysis. This is an overall gentler treatment, and the hypotonic lysis method is likely the reason for the more severe lysis. However, hypotonic lysis is a suitable option for the purpose of F-PACS enrichment as it results in complete lysis, and maintaining the structure of the subpellicular array is not important for isolating F-PACS (Shehadul Islam et al., 2017).

The Bradford assay results provide an estimate of protein concentration at each stage of the sample. The largest issue is that the sum of the supernatant and pellet protein concentration at one stage exceeds the protein concentration of the pellet from the previous stage. This is likely due to flaws with the method, other alternative methods (BCA assay) were avoided due to the complete incompatibility with EGTA present in the buffers. The inherent flaw in the Bradford assay is the difference in binding affinity of the reagent to different amino acids or proteins. Many studies highlight the variability of the Bradford assay to a variety of hypothesised factors, but all agree that lysine and arginine are extremely reactive with the CB-dye (Sapan et al., 1999). This may explain why the standard curve is consistent and has small variability – as the curve was generated with one protein (bovine albumen). Samples that are deliberately different in protein composition are therefore particularly challenging to accurately estimate through this method. One other possibility is a difference in the solubility of the generated sample. Though only based on

observation – the pellet produced by $CaCl_2$ incubation appeared consistently more difficult to resuspend, and this may contribute to the low value of protein concentration in this sample. The evidence supporting this is seen in figure 4.11 B. The Bradford assay predicts that the KCl samples contain 7.6 × more protein than the $CaCl_2$ sample, but analysis of the Coomassie-stained SDS-PAGE (with the same number of loaded cells) does not show this change. An improvement would have been to utilise several techniques for estimating protein concentration.

Figure 4.11 shows a Coomassie stain of an SDS-PAGE with each lane representing samples at different stages in the F-PACS enrichment protocol. The supernatant of the WCL appears nearly identical to the entire WCL, with the pellet appearing very faint by comparison. This disagrees with the Bradford assay which suggests that the supernatant should only contain 1.4 × more protein than the pellet. Figure 4.11 B shows the final samples with greater clarity, with a 50 kD and 75 kD protein appearing as the most intense bands, indicating high abundance in the sample. There are some notable differences between the samples, although these are mainly differences between the $CaCl_2$ sample and both the KCl and NaCl samples. One such difference is the presence of 3-4 low molecular weight bands seen in the $CaCl_2$ sample not present in the other pellets, though 2-3 of these proteins can be seen at roughly the same concentration as the $CaCl_2$ pellet in the NaCl and KCl supernatants. The $CaCl_2$ also lacks a 37-50 kD band that is seen in both other treatments. There are arguably many more differences, but only clear differences between bands can be seen if the protein enriched is abundant in the sample. However, it does justify the optimisation of the salt buffer as there are clear differences in the proteins enriched.

MORN1 and BILBO1 were chosen as targets for western blot as they are key components of the hook complex and flagellar pocket collar respectively. Figure 4.12 shows that both these proteins are present in the sample. The presence of BIBLO1 shows the retainment of the flagellar pocket collar while the MORN1 shows that the hook complex is present. Both MORN1 and BIBLO1 appear to be present at the same concentration in each sample. This is a result of BILBO1 being a structural component of the flagellar pocket collar, which is rigidly defined (Vidilaseris et al., 2015). Each FPC should be the same size, and on average (accounting for dividing cells) should be present in the same number (1-2) in each cell. The visually identical concentrations of BILB01 could point to an all-or-nothing retention of the FPC. The role of MORN1 in the hook complex is less understood, but the same may apply to this protein and structure. Retainment of other F-PACS could be verified through utilising an antibody targeting a component of the structure and detecting its presence by western blot. For example, targeting TbCentrin4 would confirm the retainment of the centrin arm (Esson et al., 2012). The presence of the microtubule quartet in the F-PACS samples is likely as it connects to both the FPC and hook complex. Similarly, the basal body also wasn't detected; however, it connects to the flagella which may indicate that it too is present. The basal body could also be detected by utilising antibodies, however, the results of the proteomic analysis may also validate the presence of these structures.

The presence of the cytosolic protein EF1 in the F-PACS extracted fractions indicates that some cytosolic proteins are not removed during the enrichment process. αEF1 bands can be seen in both the pellet and supernatant of extracted F-PACS, this may be the result of incomplete lysis. Alternatively, EF1 has been shown to associate with

polysomes in *T. brucei* (Klein et al., 2015), and it may be that polysomes are retained in the final fraction, leading to EF1 detection. Analysis of the proteomic sample will determine the extent of cytosolic protein retention in the F-PACS enriched fractions.

(5.3.2) Proteomic samples

Samples were generated for proteomic analysis, as seen in chapter 4.2.4. SILAC labelled samples were generated to compare differences between the KCl, NaCl and $CaCl_2$ buffers in retaining F-PACS proteins. SILAC labelling enables comparison between the ratio of light, medium and heavy isotope-labelled proteins which can be distinguished by mass spectrometry analysis. This enables quantification of the amount of the present protein, which can then be compared between samples. Once collected, this information can inform future experiments aiming to elucidate the function of an F-PACS protein, as the salt buffer that enriches for the target protein most can be used.

The second sample is not SILAC labelled, instead, it compares synchronised cells at different points in the cell cycle. The first is early G1, soon after cytokinesis has occurred, and the second occurs >5.5 hours into the cell cycle – which is after TbPLK has phosphorylated its target and enabled correct cytokinesis. The protein samples will first be enriched for phosphopeptides before proteomic analysis. This may reveal proteins differentially phosphorylated between the samples, which could, with further investigation, reveal the targets for key cell cycle regulated protein kinases including PLK.

Unfortunately, due to limitations (discussed in a later chapter), the proteomic data acquisition could not be completed within the timeframe of this Masters. However, optimisation of the enrichment protocol and subsequent generation proteomic samples may help in defining the regulation of F-PACS events in the cell cycle of *T. brucei*.

(5.4) Discussion of *T. congolense* results

(5.4.1) Summary of hydroxyurea synchronisation results

A 6-hour incubation of BSF *T. brucei* with 10 µg/ml hydroxyurea results in the enrichment of S-phase, with 43% of cells in S-phase immediately after removal. Figure 4.22 A shows the growth and recovery of the population after enrichment. The flow cytometry histogram at T0 shows a large S-phase peak and a smaller G1 peak. This peak is broad and 57% of cells are in other cell cycle stages, unlike samples synchronised by CCE. Cells progress through the cell cycle without obvious delay and remain partially synchronised. By T3 the G1 peak has almost completely diminished and the greatest G2M enrichment is achieved, representing ~70% of the population. Cells then begin to re-enter the cell cycle and repopulate G1. At T5 G1 cells represent ~64% of the population, from here the cells undergo a second cell cycle, less synchronised than the first. The lower synchronisation can be seen in figure 4.22 C, with T0-T6 showing greater enrichment of G1 and G2M when compared to T6-T12. This enrichment is similar to existing literature, (Forsythe et al., 2009) carried out a near-identical experiment and the resulting flow cytometry histograms are highly similar. Unfortunately, they did not continue to take timepoints further than 6 hours,

but it also likely would have shown a reduction in synchronisation. The slight G1 peak is not seen in (Forsythe et al., 2009), but was seen every time HU synchronisation was attempted on *T. brucei* (data not shown). This may be a result of cells stalling, as is seen in CCE of BSF *T. brucei*, However, a smaller proportion of cells appear stuck from HU synchronisation.

The results of HU synchronisation of *T. congolense* are less clear, with no examples in the literature for comparison. It is clear from figure 4.22 B that HU results in a population different from a standard asynchronous population. The T0 histogram is similar to the corresponding time-point in *T. brucei* but shows a larger G1 peak. This timepoint is also the most enriched in S-phase, at 29.7% of the population. The population does show progression through the cell cycle, with the most G2M enriched population occurring at T3 (47%), however, T1, T2 and T3 are all very similar. The G1 population then increases, suggesting re-entrance into the cell cycle, the G1 population reaches a maximum of 68.9% at T6. From T7 to T12 the G1 population decreases, except for T9.

HU synchronisation works because it inhibits the enzyme ribonucleotide reductase, preventing cells from replicating DNA, which mainly affects cells in S-phase (Koç et al., 2004). This leads to activation of the S-phase checkpoint, preventing cells from progressing into G2M. The difference between *T. brucei* and *T. congolense* response to HU is likely not based on differences between the replication or licensing machinery given the close evolutionary relationship. The increased G1 peak and debatable synchronisation may be a result of differences in sensitivity to HU, as the same concentration was used to synchronise both species. Alternatively, the *T.*

congolense cell cycle is 12 hours, with data from figure 4.21 A indicating that 90% (or 10.8 hours) of time is spent in G2M or G1. This means that a cell just entering G2 at the time of HU induction would be part way through G1 after 6 hours, preventing accumulation in S-phase and leading to a greater G1 peak. Regardless, HU incubation has a clear and reversible effect on the *T. congolense* cell cycle, which has the potential for synchronisation if the concentration and timing of HU addition is optimised further.

(5.4.2) Discussion of CCE synchronisation

CCE of *T. congolense* produces enriched G1 fractions as seen in figure 4.23 A. The highest G1 enrichment achieved was 76%, this occurred at a flow speed of 9 ml/min. The G1 population appears to decrease slightly from here as flow speed increases, until F16 which is also highly G1 enriched. Due to the comparatively shorter length of time spent in G1 compared to *T. brucei*, this enrichment is proportionally greater than can be achieved by CCE of *T. brucei*. It is also greater than the enrichment seen by HU synchronisation of *T. congolense*. Despite this, the proportional enrichment is less important than the overall percentage of cells in G1, and so overall *T. brucei* synchronisation by CCE is more successful. *T. congolense* does grow once returned to culture, but samples were not taken to analyse this so the synchronicity of the population during growth is unknown.

This data raises many questions, as increasing flow rate should correspond to increasing cell sizes eluted, which in turn should correspond to cell cycle stage. However, all fractions retrieved are G1 enriched, and there is no clear correlation

between flow speed and cell-cycle stage observable. Furthermore, loading *T. congolense* cells into the elutriator at F12 (as for BSF *T. brucei*) results in loss of cells and no visible cell boundary forming. This led to loading *T. congolense* at the low speed 5 ml/min, cells can then be collected at 7 ml/min – the ability to collect cells at this speed suggests that these cells are much smaller than *T. brucei*, which is confirmed by light microscopy. Despite this, the first G2M enriched fraction was collected at 27 ml/min (data not shown), which is higher than the first G2M BSF *T. brucei* fraction collected at 25 ml/min. Together, this implies that *T. congolense* varies more in hydrodynamic volume over the cell cycle. Alternatively, a factor other than hydrodynamic volume may be influencing separation.

One possible factor is the adherent properties of BSF *T. congolense*, which have specialised flagella for adhering to the vasculature of the mammalian host (Hemphill and Ross, 1995) and, In vitro, to culture flasks (Thonnus et al., 2017). From visual inspection of culture flasks during routine culture, they also appear to adhere to each other when not adhering to the flask. In culture, *T. congolense* appear to maintain a uniform and maximum density on the flask surface, exceeding this density appears to increase the number of adhered cells in suspension. Before elutriation, it was a concern that cells may adhere to the tubing, however, this does not present a problem when cells are analysed by flow cytometry, and in culture suspended cells may take hours to re-attach. Cell-cell connections could interfere with separation, so long as cells did not remain attached after elutriation – as these doublets would be excluded during flow cytometry analysis. Another possibility is that the view of sedimentation velocity is limited, as density and size are the factors affecting a particle assuming it is a rigid sphere. Like *T. brucei*, *T. congolense* is a non-rigid, non-

spherical cell, other factors such as cell shape, surface coat and motility could affect sedimentation velocity. As an example, *T. brucei* has evolved for motility in a viscous fluid environment whereas *T. congolense* adheres to surfaces, perhaps *T. brucei* aligns head-on against the flow whereas *T. congolense* rotates in the chamber. It is known that *T. brucei* are faster and more directional swimmers, owing to a more flexible and hydrodynamic cell body, while *T. congolense* are poor swimmers that constantly rotate and change direction (Bargul et al., 2016). This is an example explanation, as there is insufficient data to draw conclusions.

Other factors worth considering include the rate of volume increase over the cell cycle, PCF *T. brucei* grows uniformly while BSF does not grow during G1. The rate of *T. congolense* growth is currently unknown, so which cell cycle stages can be separated cannot be determined. The final factor to consider is the health of the cells before elutriation. This is because the culture of BSF *T. congolense* can be somewhat difficult, with population crashes occurring approximately once a month. Assuming that the culture conditions are not perfectly optimal for *T. congolense* (chapter 5.5.1), elutriation may result in stress that impacts synchronisation.

Overall, CCE of *T. congolense* does produce G1 enriched fractions that grow when returned to culture and represents a better option for synchronisation than hydroxyurea. However, further optimisation will be required to improve the enrichment, and analysis of fractions after synchronisation will be required before the protocol is adopted.

(5.4.3) Summary of cloning results

Overall, 1 complete construct was generated representing an eYFP tag of TbPUF9. However, the transfection of this construct failed, either due to the 5' UTR deletion (Figure 4.20 B) or due to the late application of selection drugs. This means for all constructs, the correctly sequenced ORF is in the final pEnNYO vector, requiring the addition of unmutated 5' UTRs all present in pGEM-T Easy.

Table 5.1 Progress of eYFP tagged constructs

Protein	**In pGEM-T Easy**	**In pEnNYO**	**Cell line**
TbPUF9	5' UTR	ORF	Generated (failed)
TbPLK	5' UTR	ORF	No
TclPUF9	5' UTR	ORF	No
TclPLK	5' UTR	ORF	No

Due to time constraints, the constructs could not be completed. In the future, these should be complete and transfected into *T. brucei* and *T. congolense*. After verification, the abundance and localisation of these proteins across the cell cycle should be analysed in synchronised *T. congolense* by western blot and immunofluorescence microscopy. These results should then be compared to the tagged *T. brucei* cell lines.

(5.5) Limitations

(5.5.1) Study and culture of *T. congolense*

The culture of *T. congolense* IL3000 strain has proved routinely challenging over the course of this Masters project. The culture of *T. congolense* utilising the media recipe from (Coustou et al., 2010) was usually stable. However, cultures crashed semi-frequently, usually preceded by a reduction in growth and an accumulation of cells on the bottom of the flask. These dead cells can be differentiated from live attached cells, of which only the flagellum contacts the flask, as the dead cells appear opaque. These crashes may have been the result of an expirable factor in the media, as they could occur while utilising the same batch of media.

Longer periods without *T. congolense* also occurred because of MEM supply delays. The media recipe from (Coustou et al., 2010) required Thermo Fisher powdered MEM, when there was a 2-month delay in MEM shipment I spent significant effort attempting to find an alternative recipe. To do this, I attempted to optimise media using both Thermo Fisher liquid MEM and two alternative brands powdered of MEM. The potential issue with optimising the liquid MEM is that 1 L has the same contents as 10 g of MEM powder resuspended in 1 L, but it can be resuspended in ddH_2O + serum + pen/strep and L-glutamine. 1 L of liquid MEM lacks these essential components, and reducing the amount of liquid MEM reduces the concentration of its components. The powdered alternatives also did not produce viable media, despite having a nearly identical composition – with the only differences being in non-essential components such as phenol-red. This may mean there is another factor in the manufacturing (e.g., processing, quality control, ingredient supplier) of the

MEM necessary for *T. congolense* survival. Culture continued only when the original MEM was supplied, however, despite the failure to find an alternative media, a lot was learnt regarding *T. congolense* and making/controlling quality of the media. One of the first observations was the increase in pH that occurred after addition of goat sera, which is usually added to the media ahead of filtration. Instead, media is now filtered, then the pH is measured a second time and adjusted, before refiltration. Since starting this practice culture of *T. congolense* has been routine. Another correction was to reduce the pen-strep concentration by half, following advice from the Steketee group (Personal communication).

Another recurring issue was contamination of the goat sera. Even following filtration, goat sera from all trialled manufacturers have differing levels of fungal contamination. Though the current manufacturer shows the least, this contamination did appear at least once while culturing *T. congolense*. To combat this, goat sera was only added to the current bottle in use, not the entire batch, to limit the time a potential contaminant has to establish. After the 2-month loss of *T. congolense* culture, this changed to only making 50 ml of complete media at a time with each lab member being responsible for their own media. This further reduced the likelihood of contamination while ensuring that any media issues only affected one lab member.

There are also potential issues with the *T. congolense* lab strain IL3000. This was the first *T. congolense* strain to be continually cultured in an axenic environment, and genetic drift may have resulted in differences between it and the wild type (Chantal et al., 2021). This can be seen by the varying culture conditions of the strain seen in

different laboratories, with some able to culture IL3000 at 37 °C with goat sera, or at 34 °C using FBS, somewhat representing the host conditions. However, some lab groups, including MDU, can only grow IL3000 at 34 °C using goat sera, which does not reflect the conditions of the host in nature.

Overall, the various issues have impacted aims specifically looking at *T. congolense*, which led to the optimisation of *T. congolense* CCE being left incomplete. Unfortunately, the 2-month culture gap occurred after the 4th time elutriating *T. congolense*, so the planned optimisations of culture conditions, elution buffer conditions and potential changes never came to fruition. In the future, as understanding of *T. congolense* biology improves, culture and study of the organism may become more fruitful. Current work on the species has highlighted key areas differing between it and *T. brucei* (Awuah-Mensah et al., 2021). There are also groups working to improve culture media, with long-chain fatty acids seeming to be more important for growth than in *T. brucei*.

Overall, *T. congolense* represents a challenging yet intriguing organism to study. Though not much is known about its biology, significant effort is being made to improve culture conditions and enable more efficient study of the parasite.

(5.5.2) Global vs reductionist approach to cell cycle study

There is much debate surrounding the philosophical approaches to the study of complex systems, with molecular biologists utilising ever more advanced holistic and reductionist techniques. Though the two approaches are not directly opposed, both

present advantages while being subject to limitations. In this project, both reductionist and global techniques have been utilised, and the optimisation of CCE facilitates the use of both approaches.

The reductionist approach is characterised by splitting complex phenomena into their smallest constituents, with the hope that understanding the constituents will lead to understanding the whole. The success of the reductionist approach in molecular biology is undeniable. Without isolating DNA from its bacterial context, it would be impossible to prove it to be the transforming factor (Avery et al., 1944). This approach has also been a mainstay in the study of trypanosome biology, such as in the discovery that tRNA can be imported from the cytosol to the mitochondrial matrix, discovered after failing to hybridize tRNA-specific probes to an isolated kinetoplast (Mottram et al., 1991). A key methodology in the reductionist scientist's toolkit is RNAi, the discovery of which revolutionised the way protein function is experimentally determined (Fire et al., 1998). However, RNAi is not without flaws, off-target effects can occur due to either hybridisation with non-target RNA sequences or downregulation of the target resulting in downregulation of other genes through a regulatory cascade (Seinen et al., 2011). Other methods have also been established for studying individual protein function, including targeted degradation (Röth et al., 2019) and small molecule inhibition (Lopez et al., 2014). These methods are more time and resource-intensive but are more specific and provide faster-acting inhibition that does not rely on protein turnover. The cloning aspect of this project is an example of the reductionist approach, by attempting to tag PLK in *T. congolense* to monitor it is localisation and understand more about cell cycle regulation as a whole.

The global approach is based on the belief that the whole is greater than the sum of its parts. It emphasises understanding complex networks and pathways on the principle that complex systems may display emergent behaviours unpredictable from analysis of their constituents. An example of this in molecular biology is the rise in genomics, transcriptomics and proteomics which provide a top-down approach for exploring cellular phenomena. These techniques can generate large quantities of data, with the ability to generate large databases such as TriTrypDB which integrates genomic datasets to provide a useful tool for the scientific community (Aslett et al., 2010). Proteomic studies of *T. brucei* have provided invaluable insight into the regulation of the cell cycle by phosphorylation of cell cycle regulators and RNA binding proteins (Benz and Urbaniak, 2019). There have been many advancements in global methodologies, such as single-cell transcriptomics which was used to identify differences in gene expression between *T. brucei* at different locations within the tsetse fly vector (Howick et al., 2022). The generation of F-PACS enrichment samples for proteomics is an example of the global approach in this project.

Reductionism may result in missing important connections between components in a system or provide results that are not seen in a natural context. Global studies, however, may provide so much data that important results are drowned out, and there is a risk of providing more data than can reasonably be analysed. Overall, a combination of both principles will yield the best results, as the two are interconnected. Analysis of global datasets may rely on knowledge from reductionist studies, while targets for further reductionist study may be highlighted from global datasets. Optimisation of CCE for *T. congolense* provides an opportunity for both reductionist and global approaches to understanding its biology.

(5.5.3) Other limitations

There were several other limitations encountered during the project worth noting. The first was the disruption caused by lab renovations that resulted in all lab groups migrating to a shared lab space. Though the time spent aiding the move was minimal, it caused a slight reduction in overall productivity as the availability of equipment varied. This also meant that use of the elutriator had to be much more carefully orchestrated. Another technical limitation was that phosphoproteomic enrichment could not be carried out in-house due to technical issues with the HPLC. This unfortunately delayed further processing of F-PACS enriched samples, meaning the data could not be generated and analysed in time for inclusion in this thesis.

(5.6) Future work

The results and analysis generated from this Masters project reveal avenues for future work.

- F-PACS enrichment samples should be sent off for proteomic analysis. This will reveal the optimal F-PACS enrichment conditions for analysis of desired target proteins.
- Work on *T. congolense* should continue, firstly by validating the remaining constructs and comparing the localisation of the tagged proteins between the species in a synchronised population. Differences in the localisation of PLK, for example, would imply large differences in regulation of the cell cycle.
- Synchronization methods for *T. congolense* should continue to be optimised.

- For hydroxyurea synchronisation, the effect of duration and concentration of HU addition should be fully characterised to attempt to enable reliable S-phase enrichment.
- For CCE, significantly lowering the density of cultured cells, trialling methods for removing doublets through filtration, or optimising the elution buffer conditions may provide useful starting points for continued optimisation.

(5.7) Conclusions

In conclusion, continued review and improvement of the methods used to explore cellular interactions and processes will lead to a continuous increase in our understanding. As demonstrated, centrifugal counter-flow elutriation represents the best method currently available for the study of the *T. brucei* cell cycle, and where possible should replace other less desirable techniques. F-PACS enrichment provides a tool for overcoming the shortcomings of mass-spectrometry dynamic range. When combined with CCE, it can be used to generate proteomic datasets that may reveal the targets of protein kinases involved in cell cycle regulation, such as TbPLK. Finally, the study of other trypanosome species will become increasingly relevant as AAT overtakes HAT as a priority for elimination. We demonstrate that *T. congolense* can be enriched to G1 through CCE and to S-phase by hydroxyurea, though further optimisation of these techniques is required.

(6) Acknowledgments

I would like to acknowledge my supervisors Professor Mick Urbaniak and Professor Christopher L de Graffenried for the guidance they have given me over the course of this project. I would also like to thank Dr Caroline Dewar and Dr Harsh Pawar for their support and patience. Without this support and guidance, the completion of the research and writing for this project would not have been possible.

(7) References

Albisetti, A., Florimod, C., Sahin, A., Eggenspiler, M., Cingal, O., Robinson, D., Bonhiver, M. 2015. FPC4: a new cytoskeletal component in *T. brucei*. Cilia, 4, P45.

Abbas, A. H., Silva Pereira, S., D'archivio, S., Wickstead, B., Morrison, L. J., Hall, N., Hertz-Fowler, C., Darby, A. C. & Jackson, A. P. 2018. The Structure of a Conserved Telomeric Region Associated with Variant Antigen Loci in the Blood Parasite *Trypanosoma congolense*. Genome Biol Evol, 10, 2458-2473.

Abro, Z., Kassie, M., Muriithi, B., Okal, M., Masiga, D., Wanda, G., Gisèle, O., Samuel, A., Nguertoum, E., Nina, R. A., Mansinsa, P., Adam, Y., Camara, M., Olet, P., Boucader, D., Jamal, S., Garba, A. R. I., Ajakaiye, J. J., Kinani, J. F., Hassan, M. A., Nonga, H., Daffa, J., Gidudu, A. & Chilongo, K. 2021. The potential economic benefits of controlling trypanosomiasis using waterbuck repellent blend in sub-Saharan Africa. PLoS One, 16, e0254558.

Adung'a, V. O., Gadelha, C. & Field, M. C. 2013. Proteomic analysis of clathrin interactions in trypanosomes reveals dynamic evolution of endocytosis. Traffic, 14, 440-57.

Aksoy, S., Buscher, P., Lehane, M., Solano, P. & Van Den Abbeele, J. 2017. Human African trypanosomiasis control: Achievements and challenges. PLoS Negl Trop Dis, 11, e0005454.

Albisetti, A., Florimond, C., Landrein, N., Vidilaseris, K., Eggenspieler, M., Lesigang, J., Dong, G., Robinson, D. R. & Bonhivers, M. 2017. Interaction between the flagellar

pocket collar and the hook complex via a novel microtubule-binding protein in *Trypanosoma brucei*. PLoS Pathog, 13, e1006710.

Alencar, M., Ramos, E., Silber, A., Zikova, A. & Oliveira, M. 2022. The extraordinary energy metabolism of the bloodstream *Trypanosoma brucei* forms: a critical review and a hypothesis.

Alizadehrad, D., Krüger, T., Engstler, M. & Stark, H. 2015. Simulating the complex cell design of *Trypanosoma brucei* and its motility. PLoS Comput Biol, 11, e1003967.

Álvarez-Rodríguez, A., Jin, B. K., Radwanska, M. & Magez, S. 2022. Recent progress in diagnosis and treatment of Human African Trypanosomiasis has made the elimination of this disease a realistic target by 2030. Front Med (Lausanne), 9, 1037094.

Archer, S. K., Luu, V. D., De Queiroz, R. A., Brems, S. & Clayton, C. 2009. *Trypanosoma brucei* PUF9 regulates mRNAs for proteins involved in replicative processes over the cell cycle. PLoS Pathog, 5, e1000565.

Aslett, M., Aurrecoechea, C., Berriman, M., Brestelli, J., Brunk, B. P., Carrington, M., Depledge, D. P., Fischer, S., Gajria, B., Gao, X., Gardner, M. J., Gingle, A., Grant, G., Harb, O. S., Heiges, M., Hertz-Fowler, C., Houston, R., Innamorato, F., Iodice, J., et al., 2010. TriTrypDB: a functional genomic resource for the *Trypanosomatidae*. Nucleic Acids Res, 38, D457-62.

Avery, O. T., Macleod, C. M. & McCarty, M. 1944. STUDIES ON THE CHEMICAL NATURE OF THE SUBSTANCE INDUCING TRANSFORMATION OF PNEUMOCOCCAL

TYPES : INDUCTION OF TRANSFORMATION BY A DESOXYRIBONUCLEIC ACID FRACTION ISOLATED FROM PNEUMOCOCCUS TYPE III. J Exp Med, 79, 137-58.

Awuah-Mensah, G., McDonald, J., Steketee, P. C., Autheman, D., Whipple, S., D'archivio, S., Brandt, C., Clare, S., Harcourt, K., Wright, G. J., Morrison, L. J., Gadelha, C. & Wickstead, B. 2021. Reliable, scalable functional genetics in bloodstream-form *Trypanosoma congolense* in vitro and in vivo. PLoS Pathog, 17, e1009224.

Baker, N., De Koning, H. P., Mäser, P. & Horn, D. 2013. Drug resistance in African trypanosomiasis: the melarsoprol and pentamidine story. Trends Parasitol, 29, 110-8.

Bargul, J. L., Jung, J., McOdimba, F. A., Omogo, C. O., Adung'a, V. O., Krüger, T., Masiga, D. K. & Engstler, M. 2016. Species-Specific Adaptations of Trypanosome Morphology and Motility to the Mammalian Host. PLoS Pathog, 12, e1005448.

Bart, J. M., Cordon-Obras, C., Vidal, I., Reed, J., Perez-Pastrana, E., Cuevas, L., Field, M. C., Carrington, M. & Navarro, M. 2015. Localization of serum resistance-associated protein in *Trypanosoma brucei rhodesiense* and transgenic *Trypanosoma brucei brucei*. Cell Microbiol, 17, 1523-35.

Beckman Coulter. 2020. JE-5.0 Elutriation System [Online]. Available at: www.beckmancoulter.com/wsrportal/techdocs?docname=JE5-IM-13. [Accessed 07/09/2023].

Bengaly, Z., Sidibe, I., Ganaba, R., Desquesnes, M., Boly, H. & Sawadogo, L. 2002. Comparative pathogenicity of three genetically distinct types of *Trypanosoma congolense* in cattle: clinical observations and haematological changes. Vet Parasitol, 108, 1-19.

Bengaly, Z., Vitouley, S. H., Somda, M. B., Zongo, A., Têko-Agbo, A., Cecchi, G., Adam, Y., Sidibé, I., Bayala, B., Belem, A. M. G., Van Den Abbeele, J. & Delespaux, V. 2018. Drug quality analysis of isometamidium chloride hydrochloride and diminazene diaceturate used for the treatment of African animal trypanosomosis in West Africa. BMC Veterinary Research, 14, 361.

Benz, C., Dondelinger, F., McKean, P. G. & Urbaniak, M. D. 2017. Cell cycle synchronisation of *Trypanosoma brucei* by centrifugal counter-flow elutriation reveals the timing of nuclear and kinetoplast DNA replication. Sci Rep, 7, 17599.

Benz, C. & Urbaniak, M. D. 2019. Organising the cell cycle in the absence of transcriptional control: Dynamic phosphorylation co-ordinates the T*rypanosoma brucei* cell cycle post-transcriptionally. PLoS Pathog, 15, e1008129.

Bernhard, S., Kaiser, M., Burri, C. & Mäser, P. 2022. Fexinidazole for Human African Trypanosomiasis, the Fruit of a Successful Public-Private Partnership. Diseases, 10.

Bessat, M. & Ersfeld, K. 2009. Functional characterization of cohesin SMC3 and separase and their roles in the segregation of large and minichromosomes in *Trypanosoma brucei*. Mol Microbiol, 71, 1371-85.

Bessat, M., Knudsen, G., Burlingame, A. L. & Wang, C. C. 2013. A minimal anaphase promoting complex/cyclosome (APC/C) in *Trypanosoma brucei*. PLoS One, 8, e59258.

Bílý, T., Sheikh, S., Mallet, A., Bastin, P., Pérez-Morga, D., Lukeš, J. & Hashimi, H. 2021. Ultrastructural Changes of the Mitochondrion During the Life Cycle of *Trypanosoma brucei*. J Eukaryot Microbiol, 68, e12846.

Bleichert, F., Botchan, M. R. & Berger, J. M. 2015. Crystal structure of the eukaryotic origin recognition complex. Nature, 519, 321-6.

Breidbach, T., Ngazoa, E. & Steverding, D. 2002. *Trypanosoma brucei*: in vitro slender-to-stumpy differentiation of culture-adapted, monomorphic bloodstream forms. Exp Parasitol, 101, 223-30.

Briggs, L. J., McKean, P. G., Baines, A., Moreira-Leite, F., Davidge, J., Vaughan, S. & Gull, K. 2004. The flagella connector of *Trypanosoma brucei*: an unusual mobile transmembrane junction. J Cell Sci, 117, 1641-51.

Broster Reix, C. E., Florimond, C., Cayrel, A., Mailhé, A., Agnero-Rigot, C., Landrein, N., Dacheux, D., Havlicek, K., Bonhivers, M., Morriswood, B. & Robinson, D. R. 2021. Bhalin, an Essential Cytoskeleton-Associated Protein of *Trypanosoma brucei* Linking TbBILBO1 of the Flagellar pocket Collar with the Hook Complex. Microorganisms, 9.

Brown, S. V., Hosking, P., Li, J. & Williams, N. 2006. ATP synthase is responsible for maintaining mitochondrial membrane potential in bloodstream form *Trypanosoma brucei*. Eukaryot Cell, 5, 45-53.

Chantal, I., Minet, C. & Berthier, D. 2021. In vitro cultivation of *Trypanosoma congolense* bloodstream forms: State of the art and advances. Vet Parasitol, 299, 109567.

Chitanga, S., Marcotty, T., Namangala, B., Van Den Bossche, P., Van Den Abbeele, J. & Delespaux, V. 2011. High prevalence of drug resistance in animal trypanosomes without a history of drug exposure. PLoS Negl Trop Dis, 5, e1454.

Choi, S., Kelber, J., Jiang, X., Strnadel, J., Fujimura, K., Pasillas, M., Coppinger, J. & Klemke, R. 2014. Procedures for the biochemical enrichment and proteomic analysis of the cytoskeletome. Anal Biochem, 446, 102-7.

Clayton, C. 2013. The regulation of trypanosome gene expression by RNA-binding proteins. PLoS Pathog, 9, e1003680.

Clayton, C. 2019. Regulation of gene expression in trypanosomatids: living with polycistronic transcription. Open Biol, 9, 190072.

Cooper, S., Wadsworth, E. S., Ochsenreiter, T., Ivens, A., Savill, N. J. & Schnaufer, A. 2019. Assembly and annotation of the mitochondrial minicircle genome of a differentiation-competent strain of *Trypanosoma brucei*. Nucleic Acids Res, 47, 11304-11325.

Cooper, S., Wadsworth, E. S., Schnaufer, A. & Savill, N. J. 2022. Organization of minicircle cassettes and guide RNA genes in *Trypanosoma brucei*. Rna, 28, 972-992.

Courtin, F., Camara, M., Rayaisse, J. B., Kagbadouno, M., Dama, E., Camara, O., Traoré, I. S., Rouamba, J., Peylhard, M., Somda, M. B., Leno, M., Lehane, M. J., Torr, S. J., Solano, P., Jamonneau, V. & Bucheton, B. 2015. Reducing Human-Tsetse Contact Significantly Enhances the Efficacy of Sleeping Sickness Active Screening Campaigns: A Promising Result in the Context of Elimination. PLoS Negl Trop Dis, 9, e0003727.

Coustou, V., Guegan, F., Plazolles, N. & Baltz, T. 2010. Complete in vitro life cycle of *Trypanosoma congolense*: development of genetic tools. PLoS Negl Trop Dis, 4, e618.

Cunningham, I. 1977. New culture medium for maintenance of tsetse tissues and growth of trypanosomatids. J Protozool, 24, 325-9.

Da Silva, M. S., Pavani, R. S., Damasceno, J. D., Marques, C. A., McCulloch, R., Tosi, L. R. O. & Elias, M. C. 2017. Nuclear DNA Replication in Trypanosomatids: There Are No Easy Methods for Solving Difficult Problems. Trends Parasitol, 33, 858-874.

Dang, H. Q. & Li, Z. 2011. The Cdc45·Mcm2-7·GINS protein complex in trypanosomes regulates DNA replication and interacts with two Orc1-like proteins in the origin recognition complex. J Biol Chem, 286, 32424-35.

Daniels, J. P., Gull, K. & Wickstead, B. 2010. Cell biology of the trypanosome genome. Microbiol Mol Biol Rev, 74, 552-69.

Das, A. M., Chitnis, N., Burri, C., Paris, D. H., Patel, S., Spencer, S. E. F., Miaka, E. M. & Castaño, M. S. 2021. Modelling the impact of fexinidazole use on human African trypanosomiasis (HAT) transmission in the Democratic Republic of the Congo. PLoS Negl Trop Dis, 15, e0009992.

Davis, M. W. & Jorgensen, E. M. 2022. ApE, A Plasmid Editor: A Freely Available DNA Manipulation and Visualization Program. Front Bioinform, 2, 818619.

Dean, S., Sunter, J. D. & Wheeler, R. J. 2017. TrypTag.org: A Trypanosome Genome-wide Protein Localisation Resource. Trends Parasitol, 33, 80-82.

Delespaux, V., Geerts, S., Brandt, J., Elyn, R. & Eisler, M. C. 2002. Monitoring the correct use of isometamidium by farmers and veterinary assistants in Eastern Province of Zambia using the isometamidium-ELISA. Vet Parasitol, 110, 117-22.

Demmel, L., Schmidt, K., Lucast, L., Havlicek, K., Zankel, A., Koestler, T., Reithofer, V., De Camilli, P. & Warren, G. 2014. The endocytic activity of the flagellar pocket in

Trypanosoma brucei is regulated by an adjacent phosphatidylinositol phosphate kinase. J Cell Sci, 127, 2351-64.

Dolan, M. T., Reid, C. G. & Voorheis, H. P. 1986. Calcium ions initiate the selective depolymerization of the pellicular microtubules in bloodstream forms of Trypanosoma brucei. J Cell Sci, 80, 123-40.

Engstler, M., Thilo, L., Weise, F., Grünfelder, C. G., Schwarz, H., Boshart, M. & Overath, P. 2004. Kinetics of endocytosis and recycling of the GPI-anchored variant surface glycoprotein in *Trypanosoma brucei*. J Cell Sci, 117, 1105-15.

Esson, H. J., Morriswood, B., Yavuz, S., Vidilaseris, K., Dong, G. & Warren, G. 2012. Morphology of the trypanosome bilobe, a novel cytoskeletal structure. Eukaryot Cell, 11, 761-72.

Fairlamb, A. H. & Horn, D. 2018. Melarsoprol Resistance in African Trypanosomiasis. Trends Parasitol, 34, 481-492.

Fervers, P., Fervers, F., Makałowski, W. & Jąkalski, M. 2018. Life cycle adapted upstream open reading frames (uORFs) in *Trypanosoma congolense*: A post-transcriptional approach to accurate gene regulation. PLoS One, 13, e0201461.

Fire, A., Xu, S., Montgomery, M. K., Kostas, S. A., Driver, S. E. & Mello, C. C. 1998. Potent and specific genetic interference by double-stranded RNA in Caenorhabditis elegans. Nature, 391, 806-11.

Forsythe, G. R., McCulloch, R. & Hammarton, T. C. 2009. Hydroxyurea-induced synchronisation of bloodstream stage *Trypanosoma brucei*. Mol Biochem Parasitol, 164, 131-6.

Franco, J. R., Cecchi, G., Paone, M., Diarra, A., Grout, L., Kadima Ebeja, A., Simarro, P. P., Zhao, W. & Argaw, D. 2022. The elimination of human African trypanosomiasis: Achievements in relation to WHO road map targets for 2020. PLoS Negl Trop Dis, 16, e0010047.

Gadelha, C., Rothery, S., Morphew, M., McIntosh, J. R., Severs, N. J. & Gull, K. 2009. Membrane domains and flagellar pocket boundaries are influenced by the cytoskeleton in African trypanosomes. Proc Natl Acad Sci U S A, 106, 17425-30.

Gale, M., Jr., Carter, V. & Parsons, M. 1994. Cell cycle-specific induction of an 89 kDa serine/threonine protein kinase activity in *Trypanosoma brucei*. J Cell Sci, 107 (Pt 7), 1825-32.

Gluenz, E., Povelones, M. L., Englund, P. T. & Gull, K. 2011. The kinetoplast duplication cycle in *Trypanosoma brucei* is orchestrated by cytoskeleton-mediated cell morphogenesis. Mol Cell Biol, 31, 1012-21.

Gourguechon, S., Savich, J. M. & Wang, C. C. 2007. The multiple roles of cyclin E1 in controlling cell cycle progression and cellular morphology of *Trypanosoma brucei*. J Mol Biol, 368, 939-50.

Halliday, C., Billington, K., Wang, Z., Madden, R., Dean, S., Sunter, J. D. & Wheeler, R. J. 2019. Cellular landmarks of *Trypanosoma brucei* and *Leishmania mexicana*. Mol Biochem Parasitol, 230, 24-36.

Halliday, C., De Castro-Neto, A., Alcantara, C. L., Cunha, E. S. N. L., Vaughan, S. & Sunter, J. D. 2021. Trypanosomatid Flagellar pocket from Structure to Function. Trends Parasitol, 37, 317-329.

Hammarton, T. C., Kramer, S., Tetley, L., Boshart, M. & Mottram, J. C. 2007. Trypanosoma brucei Polo-like kinase is essential for basal body duplication, kDNA segregation and cytokinesis. Mol Microbiol, 65, 1229-48.

Hammarton, T. C., Monnerat, S. & Mottram, J. C. 2007. Cytokinesis in trypanosomatids. Curr Opin Microbiol, 10, 520-7.

He, C. Y., Pypaert, M. & Warren, G. 2005. Golgi duplication in *Trypanosoma brucei* requires Centrin2. Science, 310, 1196-8.

Hemphill, A., Lawson, D. & Seebeck, T. 1991. The Cytoskeletal Architecture of *Trypanosoma brucei*. The Journal of Parasitology, 77, 603-612.

Hemphill, A. & Ross, C. A. 1995. Flagellum-mediated adhesion of *Trypanosoma congolense* to bovine aorta endothelial cells. Parasitol Res, 81, 412-20.

Hirumi, H. & Hirumi, K. 1989. Continuous cultivation of *Trypanosoma brucei* blood stream forms in a medium containing a low concentration of serum protein without feeder cell layers. J Parasitol, 75, 985-9.

Hoffmann, A., Käser, S., Jakob, M., Amodeo, S., Peitsch, C., Týč, J., Vaughan, S., Zuber, B., Schneider, A. & Ochsenreiter, T. 2018. Molecular model of the mitochondrial genome segregation machinery in Trypanosoma brucei. Proc Natl Acad Sci U S A, 115, E1809-e1818.

Hohmann, T. & Dehghani, F. 2019. The Cytoskeleton-A Complex Interacting Meshwork. Cells, 8, 362.

Howick, V. M., Peacock, L., Kay, C., Collett, C., Gibson, W. & Lawniczak, M. K. N. 2022. Single-cell transcriptomics reveals expression profiles of *Trypanosoma brucei* sexual stages. PLoS Pathog, 18, e1010346.

Ikeda, K. N. & De Graffenried, C. L. 2012. Polo-like kinase is necessary for flagellum inheritance in *Trypanosoma brucei*. J Cell Sci, 125, 3173-84.

Isch, C., Majneri, P., Landrein, N., Pivovarova, Y., Lesigang, J., Lauruol, F., Robinson, D. R., Dong, G. & Bonhivers, M. 2021. Structural and functional studies of the first tripartite protein complex at the *Trypanosoma brucei* flagellar pocket collar. PLoS Pathog, 17, e1009329.

Jackson, A. P., Berry, A., Aslett, M., Allison, H. C., Burton, P., Vavrova-Anderson, J., Brown, R., Browne, H., Corton, N., Hauser, H., Gamble, J., Gilderthorp, R., Marcello, L., McQuillan, J., Otto, T. D., Quail, M. A., Sanders, M. J., Van Tonder, A., Ginger, M. L., Field, M. C., Barry, J. D., Hertz-Fowler, C. & Berriman, M. 2012. Antigenic diversity is generated by distinct evolutionary mechanisms in African trypanosome species. Proc Natl Acad Sci U S A, 109, 3416-21.

Jensen, R. E. & Englund, P. T. 2012. Network news: the replication of kinetoplast DNA. Annu Rev Microbiol, 66, 473-91.

Kabani, S., Waterfall, M. & Matthews, K. R. 2010. Cell-cycle synchronisation of bloodstream forms of *Trypanosoma brucei* using Vybrant DyeCycle Violet-based sorting. Mol Biochem Parasitol, 169, 59-62.

Kabayo, J. P. 2002. Aiming to eliminate tsetse from Africa. Trends Parasitol, 18, 473-5.

Kariuki, C. K., Stijlemans, B. & Magez, S. 2019. The Trypanosomal Transferrin Receptor of *Trypanosoma Brucei*-A Review. Trop Med Infect Dis, 4.

Kasozi, K. I., Macleod, E. T., Ntulume, I. & Welburn, S. C. 2022. An Update on African Trypanocide Pharmaceutics and Resistance. Front Vet Sci, 9, 828111.

Kasozi, K. I., Zirintunda, G., Ssempijja, F., Buyinza, B., Alzahrani, K. J., Matama, K., Nakimbugwe, H. N., Alkazmi, L., Onanyang, D., Bogere, P., Ochieng, J. J., Islam, S., Matovu, W., Nalumenya, D. P., Batiha, G. E., Osuwat, L. O., Abdelhamid, M., Shen, T., Omadang, L. & Welburn, S. C. 2021. Epidemiology of Trypanosomiasis in Wildlife-Implications for Humans at the Wildlife Interface in Africa. Front Vet Sci, 8, 621699.

Katabazi, A., Aliero, A. A., Witto, S. G., Odoki, M. & Musinguzi, S. P. 2021. Prevalence of *Trypanosoma congolense* and *Trypanosoma vivax* in Lira District, Uganda. Biomed Res Int, 2021, 7284042.

Kennedy, P. G. E. & Rodgers, J. 2019. Clinical and Neuropathogenetic Aspects of Human African Trypanosomiasis. Front Immunol, 10, 39.

Klein, C., Terrao, M., Inchaustegui Gil, D. & Clayton, C. 2015. Polysomes of Trypanosoma brucei: Association with Initiation Factors and RNA-Binding Proteins. PLoS One, 10, e0135973.

Koç, A., Wheeler, L. J., Mathews, C. K. & Merrill, G. F. 2004. Hydroxyurea arrests DNA replication by a mechanism that preserves basal dNTP pools. J Biol Chem, 279, 223-30.

Kohl, L., Robinson, D. & Bastin, P. 2003. Novel roles for the flagellum in cell morphogenesis and cytokinesis of trypanosomes. The EMBO Journal, 22, 5336-46.

Koyfman, A. Y., Schmid, M. F., Gheiratmand, L., FU, C. J., Khant, H. A., Huang, D., He, C. Y. & Chiu, W. 2011. Structure of Trypanosoma brucei flagellum accounts for its bihelical motion. Proc Natl Acad Sci U S A, 108, 11105-8.

Kues, W. A., Anger, M., Carnwath, J. W., Paul, D., Motlik, J. & Niemann, H. 2000. Cell cycle synchronization of porcine fetal fibroblasts: effects of serum deprivation and reversible cell cycle inhibitors. Biol Reprod, 62, 412-9.

Lacomble, S., Vaughan, S., Gadelha, C., Morphew, M. K., Shaw, M. K., McIntosh, J. R. & Gull, K. 2009. Three-dimensional cellular architecture of the flagellar pocket and associated cytoskeleton in trypanosomes revealed by electron microscope tomography. J Cell Sci, 122, 1081-90.

Lacomble, S., Vaughan, S., Gadelha, C., Morphew, M. K., Shaw, M. K., McIntosh, J. R. & Gull, K. 2010. Basal body movements orchestrate membrane organelle division and cell morphogenesis in *Trypanosoma brucei*. J Cell Sci, 123, 2884-91.

Langousis, G. & Hill, K. L. 2014. Motility and more: the flagellum of *Trypanosoma brucei*. Nat Rev Microbiol, 12, 505-18.

Lee, S. Y., Jang, C. & Lee, K. A. 2014. Polo-like kinases (plks), a key regulator of cell cycle and new potential target for cancer therapy. Dev Reprod, 18, 65-71.

Li, Z. 2012. Regulation of the cell division cycle in *Trypanosoma brucei*. Eukaryot Cell, 11, 1180-90.

Li, Z., Gourguechon, S. & Wang, C. C. 2007. Tousled-like kinase in a microbial eukaryote regulates spindle assembly and S-phase progression by interacting with Aurora kinase and chromatin assembly factors. J Cell Sci, 120, 3883-94.

Li, Z., Lee, J. H., Chu, F., Burlingame, A. L., Günzl, A. & Wang, C. C. 2008. Identification of a novel chromosomal passenger complex and its unique localization during cytokinesis in *Trypanosoma brucei*. PLoS One, 3, e2354.

Liebenehm, S., Affognon, H. & Waibel, H. 2011. Collective livestock research for sustainable disease management in Mali and Burkina Faso. International Journal of Agricultural Sustainability, 9, 212-221.

Ligasová, A. & Koberna, K. 2021. Strengths and Weaknesses of Cell Synchronization Protocols Based on Inhibition of DNA Synthesis. Int J Mol Sci, 22.

Link, F., Borges, A. R., Jones, N. G. & Engstler, M. 2021. To the Surface and Back: Exo- and Endocytic Pathways in *Trypanosoma brucei*. Front Cell Dev Biol, 9, 720521.

Liu, B., Wang, J., Yaffe, N., Lindsay, M. E., Zhao, Z., Zick, A., Shlomai, J. & Englund, P. T. 2009. Trypanosomes have six mitochondrial DNA helicases with one controlling kinetoplast maxicircle replication. Mol Cell, 35, 490-501.

Liu, Y., Nan, B., Niu, J., Kapler, G. M. & Gao, S. 2021. An Optimized and Versatile Counter-Flow Centrifugal Elutriation Workflow to Obtain Synchronized Eukaryotic Cells. Front Cell Dev Biol, 9, 664418.

Llauró, A., Hayashi, H., Bailey, M. E., Wilson, A., Ludzia, P., Asbury, C. L. & Akiyoshi, B. 2018. The kinetoplastid kinetochore protein KKT4 is an unconventional microtubule tip-coupling protein. J Cell Biol, 217, 3886-3900.

Lopez, M. S., Kliegman, J. I. & Shokat, K. M. 2014. The logic and design of analog-sensitive kinases and their small molecule inhibitors. Methods Enzymol, 548, 189-213.

Lozano-Núñez, A., Ikeda, K. N., Sauer, T. & De Graffenried, C. L. 2013. An analogue-sensitive approach identifies basal body rotation and flagellum attachment zone elongation as key functions of PLK in *Trypanosoma brucei*. Mol Biol Cell, 24, 1321-33.

Lutje, V., Seixas, J. & Kennedy, A. 2013. Chemotherapy for second-stage human African trypanosomiasis. Cochrane Database Syst Rev, 2013, Cd006201.

Machila, N., Wanyangu, S. W., McDermott, J., Welburn, S. C., Maudlin, I. & Eisler, M. C. 2003. Cattle owners' perceptions of African bovine trypanosomiasis and its control in Busia and Kwale Districts of Kenya. Acta Trop, 86, 25-34.

Malvy, D. & Chappuis, F. 2011. Sleeping sickness. Clin Microbiol Infect, 17, 986-95.

Manful, T., Fadda, A. & Clayton, C. 2011. The role of the 5'-3' exoribonuclease XRNA in transcriptome-wide mRNA degradation. RNA, 17, 2039-47.

Maree, J. P. & Patterton, H. G. 2014. The epigenome of *Trypanosoma brucei*: a regulatory interface to an unconventional transcriptional machine. Biochim Biophys Acta, 1839, 743-50.

Marques, C. A., Tiengwe, C., Lemgruber, L., Damasceno, J. D., Scott, A., Paape, D., Marcello, L. & McCulloch, R. 2016. Diverged composition and regulation of the *Trypanosoma brucei* origin recognition complex that mediates DNA replication initiation. Nucleic Acids Res, 44, 4763-84.

Matthews, K. R. 2005. The developmental cell biology of *Trypanosoma brucei*. J Cell Sci, 118, 283-90.

Maxfield, L. & Bermudez, R. 2023. Trypanosomiasis. StatPearls. Treasure Island (FL): StatPearls Publishing Copyright © 2023, StatPearls Publishing LLC. Available from: https://www.ncbi.nlm.nih.gov/books/NBK535413/

Mekonnen, G., Mohammed, E. F., Kidane, W., Nesibu, A., Yohannes, H., Van Reet, N., Büscher, P. & Birhanu, H. 2018. Isometamidium chloride and homidium chloride fail to cure mice infected with Ethiopian *Trypanosoma evansi* type A and B. PLoS Negl Trop Dis, 12, e0006790.

Morrison, L. J., Steketee, P. C., Tettey, M. D. & Matthews, K. R. 2022. Pathogenicity and virulence of African trypanosomes: from laboratory models to clinically relevant hosts. Virulence, 14, 2150445.

Morriswood, B. & Engstler, M. 2018. Let's get fISSical: fast in silico synchronization as a new tool for cell division cycle analysis. Parasitology, 145, 196-209.

Morriswood, B., He, C. Y., Sealey-Cardona, M., Yelinek, J., Pypaert, M. & Warren, G. 2009. The bilobe structure of *Trypanosoma brucei* contains a MORN-repeat protein. Mol Biochem Parasitol, 167, 95-103.

Morriswood, B. & Schmidt, K. 2015. A MORN Repeat Protein Facilitates Protein Entry into the Flagellar pocket of *Trypanosoma brucei*. Eukaryot Cell, 14, 1081-93.

Moti, Y., De Deken, R., Thys, E., Van Den Abbeele, J., Duchateau, L. & Delespaux, V. 2015. PCR and microsatellite analysis of diminazene aceturate resistance of bovine trypanosomes correlated to knowledge, attitude and practice of livestock keepers in South-Western Ethiopia. Acta Trop, 146, 45-52.

Mottram, J. C., Bell, S. D., Nelson, R. G. & Barry, J. D. 1991. tRNAs of *Trypanosoma brucei*. Unusual gene organization and mitochondrial importation. J Biol Chem, 266, 18313-7.

Munday, J. C., Rojas López, K. E., Eze, A. A., Delespaux, V., Van Den Abbeele, J., Rowan, T., Barrett, M. P., Morrison, L. J. & De Koning, H. P. 2013. Functional expression of TcoAT1 reveals it to be a P1-type nucleoside transporter with no capacity for diminazene uptake. Int J Parasitol Drugs Drug Resist, 3, 69-76.

Musiałek, M. W. & Rybaczek, D. 2021. Hydroxyurea-The Good, the Bad and the Ugly. Genes (Basel), 12, 1096.

Ogbadoyi, E., Ersfeld, K., Robinson, D., Sherwin, T. & Gull, K. 2000. Architecture of the *Trypanosoma brucei* nucleus during interphase and mitosis. Chromosoma, 108, 501-13.

Ogbadoyi, E. O., Robinson, D. R. & Gull, K. 2003. A high-order trans-membrane structural linkage is responsible for mitochondrial genome positioning and segregation by flagella basal bodies in trypanosomes. Mol Biol Cell, 14, 1769-79.

Ozioko, K. U., Okoye, C. I., Obiezue, R. N., Idika, I. K., Awudu, R. A., Ezewudo, B. I. & Ezea, C. O. 2020. Accelerating towards human African trypanosomiasis elimination: Issues and opportunities. J Vector Borne Dis, 57, 105-113.

Pays, E. & Vanhollebeke, B. 2009. Human innate immunity against African trypanosomes. Curr Opin Immunol, 21, 493-8.

Peacock, L., Cook, S., Ferris, V., Bailey, M. & Gibson, W. 2012. The life cycle of *Trypanosoma (Nannomonas) congolense* in the tsetse fly. Parasit Vectors, 5, 109.

Peña-Diaz, P., Vancová, M., Resl, C., Field, M. C. & Lukeš, J. 2017. A leucine aminopeptidase is involved in kinetoplast DNA segregation in *Trypanosoma brucei*. PLoS Pathog, 13, e1006310.

Perdomo, D., Bonhivers, M. & Robinson, D. R. 2016. The Trypanosome Flagellar pocket Collar and Its Ring Forming Protein-TbBILBO1. Cells, 5, 9.

Perry, J. A., Sinclair-Davis, A. N., McAllaster, M. R. & De Graffenried, C. L. 2018. TbSmee1 regulates hook complex morphology and the rate of flagellar pocket uptake in *Trypanosoma brucei*. Mol Microbiol, 107, 344-362.

Povelones, M. L., Tiengwe, C., Gluenz, E., Gull, K., Englund, P. T. & Jensen, R. E. 2013. Mitochondrial shape and function in trypanosomes requires the outer membrane protein, TbLOK1. Mol Microbiol, 87, 713-29.

Read, L. K., Lukeš, J. & Hashimi, H. 2016. Trypanosome RNA editing: the complexity of getting U in and taking U out. Wiley Interdiscip Rev RNA, 7, 33-51.

Richards, S., Morrison, L. J., Torr, S. J., Barrett, M. P., Manangwa, O., Mramba, F. & Auty, H. 2021. Pharma to farmer: field challenges of optimizing trypanocide use in African animal trypanosomiasis. Trends Parasitol, 37, 831-843.

Robinson, D. R. & Gull, K. 1991. Basal body movements as a mechanism for mitochondrial genome segregation in the trypanosome cell cycle. Nature, 352, 731-3.

Rodríguez, J. A., Lopez, M. A., Thayer, M. C., Zhao, Y., Oberholzer, M., Chang, D. D., Kisalu, N. K., Penichet, M. L., Helguera, G., Bruinsma, R., Hill, K. L. & Miao, J. 2009. Propulsion of African trypanosomes is driven by bihelical waves with alternating chirality separated by kinks. Proc Natl Acad Sci U S A, 106, 19322-7.

Rose, C., Casas-Sánchez, A., Dyer, N. A., Solórzano, C., Beckett, A. J., Middlehurst, B., Marcello, M., Haines, L. R., Lisack, J., Engstler, M., Lehane, M. J., Prior, I. A. & Acosta-Serrano, Á. 2020. *Trypanosoma brucei* colonizes the tsetse gut via an immature peritrophic matrix in the proventriculus. Nat Microbiol, 5, 909-916.

Röth, S., Fulcher, L. J. & Sapkota, G. P. 2019. Advances in targeted degradation of endogenous proteins. Cell Mol Life Sci, 76, 2761-2777.

Sanderson, R. J., Bird, K. E., Palmer, N. F. & Brenman, J. 1976. Design principles for a counterflow centrifugation cell separation chamber. Anal Biochem, 71, 615-22.

Sapan, C. V., Lundblad, R. L. & Price, N. C. 1999. Colorimetric protein assay techniques. Biotechnol Appl Biochem, 29, 99-108.

Schuster, S., Lisack, J., Subota, I., Zimmermann, H., Reuter, C., Mueller, T., Morriswood, B. & Engstler, M. 2021. Unexpected plasticity in the life cycle of *Trypanosoma brucei*. Elife, 10, e66028.

Seinen, E., Burgerhof, J. G., Jansen, R. C. & Sibon, O. C. 2011. RNAi-induced off-target effects in *Drosophila melanogaster*: frequencies and solutions. Brief Funct Genomics, 10, 206-14.

Sharma, R., Peacock, L., Gluenz, E., Gull, K., Gibson, W. & Carrington, M. 2008. Asymmetric cell division as a route to reduction in cell length and change in cell morphology in trypanosomes. Protist, 159, 137-51.

Shehadul Islam, M., Aryasomayajula, A. & Selvaganapathy, P. R. 2017. A Review on Macroscale and Microscale Cell Lysis Methods. Micromachines (Basel), 8.

Sheriff, O., Lim, L. F. & He, C. Y. 2014. Tracking the biogenesis and inheritance of subpellicular microtubule in *Trypanosoma brucei* with inducible YFP-α-tubulin. Biomed Res Int, 2014, 893272.

Sherwin, T. & Gull, K. 1989. The cell division cycle of *Trypanosoma brucei* brucei: timing of event markers and cytoskeletal modulations. Philos Trans R Soc Lond B Biol Sci, 323, 573-88.

Siegel, T. N., Hekstra, D. R. & Cross, G. A. 2008. Analysis of the *Trypanosoma brucei* cell cycle by quantitative DAPI imaging. Mol Biochem Parasitol, 160, 171-4.

Siegel, T. N., Hekstra, D. R., Kemp, L. E., Figueiredo, L. M., Lowell, J. E., Fenyo, D., Wang, X., Dewell, S. & Cross, G. A. 2009. Four histone variants mark the boundaries of polycistronic transcription units in *Trypanosoma brucei*. Genes Dev, 23, 1063-76.

Silva Pereira, S., Trindade, S., De Niz, M. & Figueiredo, L. M. 2019. Tissue tropism in parasitic diseases. Open Biol, 9, 190036.

Silvester, E., Ivens, A. & Matthews, K. R. 2018. A gene expression comparison of *Trypanosoma brucei* and *Trypanosoma congolense* in the bloodstream of the mammalian host reveals species-specific adaptations to density-dependent development. PLoS Negl Trop Dis, 12, e0006863.

Simarro, P. P., Cecchi, G., Franco, J. R., Paone, M., Diarra, A., Ruiz-Postigo, J. A., Fèvre, E. M., Mattioli, R. C. & Jannin, J. G. 2012. Estimating and mapping the population at risk of sleeping sickness. PLoS Negl Trop Dis, 6, e1859.

Sinclair, A. N. & De Graffenried, C. L. 2019. More than Microtubules: The Structure and Function of the Subpellicular Array in Trypanosomatids. Trends Parasitol, 35, 760-777.

Sinclair, A. N., Huynh, C. T., Sladewski, T. E., Zuromski, J. L., Ruiz, A. E. & De Graffenried, C. L. 2021. The *Trypanosoma brucei* subpellicular microtubule array is organized into functionally discrete subdomains defined by microtubule associated proteins. PLoS Pathog, 17, e1009588.

Smithson, L., Ihuoma Akazue, P., Findlater, L., Gwira, T. M., Vaughan, S. & Sunter, J. D. 2022. Diversity in new flagellum tip attachment in bloodstream form African trypanosomes. Mol Microbiol, 118, 510-525.

Stephens, N. A. & Hajduk, S. L. 2011. Endosomal localization of the serum resistance-associated protein in African trypanosomes confers human infectivity. Eukaryot Cell, 10, 1023-33.

Sun, S. Y., Kaelber, J. T., Chen, M., Dong, X., Nematbakhsh, Y., Shi, J., Dougherty, M., Lim, C. T., Schmid, M. F., Chiu, W. & He, C. Y. 2018. Flagellum couples cell shape to motility in *Trypanosoma brucei*. Proc Natl Acad Sci U S A, 115, E5916-e5925.

Sunter, J. D. & Gull, K. 2016. The Flagellum Attachment Zone: 'The Cellular Ruler' of Trypanosome Morphology. Trends Parasitol, 32, 309-324.

Sunter, J. D., Varga, V., Dean, S. & Gull, K. 2015. A dynamic coordination of flagellum and cytoplasmic cytoskeleton assembly specifies cell morphogenesis in trypanosomes. J Cell Sci, 128, 1580-94.

Tchamdja, E., Kulo, A. E., Vitouley, H. S., Batawui, K., Bankolé, A. A., Adomefa, K., Cecchi, G., Hoppenheit, A., Clausen, P. H., De Deken, R., Van Den Abbeele, J., Marcotty, T. & Delespaux, V. 2017. Cattle breeding, trypanosomosis prevalence and drug resistance in Northern Togo. Vet Parasitol, 236, 86-92.

Thomas, J. A., Baker, N., Hutchinson, S., Dominicus, C., Trenaman, A., Glover, L., Alsford, S. & Horn, D. 2018. Insights into antitrypanosomal drug mode-of-action from cytology-based profiling. PLoS Negl Trop Dis, 12, e0006980.

Thonnus, M., Guérin, A. & Rivière, L. 2017. A multigene family encoding surface glycoproteins in *Trypanosoma congolense*. Microb Cell, 4, 90-97.

Torii, S., Yamamoto, T., Tsuchiya, Y. & Nishida, E. 2006. ERK MAP kinase in G cell cycle progression and cancer. Cancer Sci, 97, 697-702.

Trindade, S., Rijo-Ferreira, F., Carvalho, T., Pinto-Neves, D., Guegan, F., Aresta-Branco, F., Bento, F., Young, S. A., Pinto, A., Van Den Abbeele, J., Ribeiro, R. M., Dias, S., Smith, T. K. & Figueiredo, L. M. 2016. *Trypanosoma brucei* Parasites Occupy and Functionally Adapt to the Adipose Tissue in Mice. Cell Host Microbe, 19, 837-48.

Utz, S., Roditi, I., Kunz Renggli, C., Almeida, I. C., Acosta-Serrano, A. & Bütikofer, P. 2006. *Trypanosoma congolense* procyclins: unmasking cryptic major surface glycoproteins in procyclic forms. Eukaryot Cell, 5, 1430-40.

Van Reet, N., Patient Pyana, P., Dehou, S., Bebronne, N., Deborggraeve, S. & Büscher, P. 2021. Single nucleotide polymorphisms and copy-number variations in the *Trypanosoma brucei* repeat (TBR) sequence can be used to enhance amplification and genotyping of Trypanozoon strains. PLoS One, 16, e0258711.

Vaughan, S. & Gull, K. 2015. Basal body structure and cell cycle-dependent biogenesis in *Trypanosoma brucei*. Cilia, 5, 5.

Vaughan, S., Kohl, L., Ngai, I., Wheeler, R. J. & Gull, K. 2008. A repetitive protein essential for the flagellum attachment zone filament structure and function in *Trypanosoma brucei*. Protist, 159, 127-36.

Venturelli, A., Tagliazucchi, L., Lima, C., Venuti, F., Malpezzi, G., Magoulas, G. E., Santarem, N., Calogeropoulou, T., Cordeiro-Da-Silva, A. & Costi, M. P. 2022. Current Treatments to Control African Trypanosomiasis and One Health Perspective. Microorganisms, 10, 1298.

Vickerman, K. & Preston, T. M. 1970. Spindle microtubules in the dividing nuclei of trypanosomes. J Cell Sci, 6, 365-83.

Vidilaseris, K., Lesigang, J., Morriswood, B. & Dong, G. 2015. Assembly mechanism of *Trypanosoma brucei* BILBO1 at the flagellar pocket collar. Commun Integr Biol, 8, e992739.

Wamwiri, F. N. & Changasi, R. E. 2016. Tsetse Flies (Glossina) as Vectors of Human African Trypanosomiasis: A Review. Biomed Res Int, 2016, 6201350.

Wang, M., Gheiratmand, L. & He, C. Y. 2012. An interplay between Centrin2 and Centrin4 on the bi-lobed structure in *Trypanosoma brucei*. Mol Microbiol, 83, 1153-61.

Wheeler, R. J., Gull, K. & Sunter, J. D. 2019. Coordination of the Cell Cycle in Trypanosomes. Annu Rev Microbiol, 73, 133-154.

Wheeler, R. J., Scheumann, N., Wickstead, B., Gull, K. & Vaughan, S. 2013. Cytokinesis in *Trypanosoma brucei* differs between bloodstream and tsetse trypomastigote forms: implications for microtubule-based morphogenesis and mutant analysis. Mol Microbiol, 90, 1339-55.

WHO. 2022. Elimination of human African trypanosomiasis as a public health problem validated in Equatorial Guinea. Available at: https://tinyurl.com/274n4mx5. [Accessed: 25/07/2023].

WHO. 2019. WHO interim guidelines for the treatment of gambiense human African Trypanosomiasis. Available at: https://www.who.int/publications/i/item/9789241550567. [Accessed: 24/07/2023]

Yaro, M., Munyard, K. A., Stear, M. J. & Groth, D. M. 2016. Combatting African Animal Trypanosomiasis (AAT) in livestock: The potential role of trypanotolerance. Vet Parasitol, 225, 43-52.

Yun, O., Priotto, G., Tong, J., Flevaud, L. & Chappuis, F. 2010. NECT is next: implementing the new drug combination therapy for *Trypanosoma brucei gambiense* sleeping sickness. PLoS Negl Trop Dis, 4, e720.

(8) Appendix

Appendix 1 List of all primers and PCR conditions. Restriction sites are underlined.

Primer	Sequence	Direction	Target protein	Annealing temp	Product size (bp)	Enzymes
MP1	ACATTAGCGGCCGCAAAT	F	Tb927.1.2600	50	508	*Not*I

	ATAAGACTC ACTCACGCA ATCCAT		5'UTR			
MP2	CGTATTGGA TCCAATGAC TGGTGACGG AGGCT	R	Tb927.1.2 600 5' UTR	50	508	*Bam*HI
MP3	ACATTATCT AGAATGGAA GTACGCGAT GTGAA	F	Tb927.1.2 600 ORF	55	508	*Xba*I
MP4	CGTATTGGA TCCGCGGCC GCGGGCGG GTCGCGAGA G	R	Tb927.1.2 600 ORF	55	508	*Not*I + *Bam*HI
MP5	ACATTAGCG GCCGCAAGG AAACGAAG GGGCGACC	F	Tb927.7.6 310 5'UTR	52	500	*Not*I
MP6	CGTATTGGA TCCTCTTTTT TTTTTTTACC CCCCCCC	R	Tb927.7.6 310 5'UTR	52	500	*Bam*HI
MP7	ACATTATCT AGAATGCAC GCAACCGCT GAGAC	F	Tb927.7.6 310 ORF	53	500	*Xba*I
MP8	CGTATTGGA TCCGCGGCC GCAGTTTCA GGTCACGAT GAATAACAC ATTG	R	Tb927.7.6 310 ORF	53	500	*Not*I + *Bam*HI
MP9	ACATTAGCG GCCGCTTTG	F	TcIL3000_ 7_5220 5' UTR	50	500	*Not*I

	ATCCGCTCT CATCGCC					
MP10	CGTATTGGA TCCTTTGTTA CGCAGCAAC TCAATTG	R	TcIL3000_ 7_5220 5'UTR	50	500	*Bam*H1
MP11	ACATTATCT AGAATGCAT CCAGTGATT GATACGCAC	F	TcIL3000_ 7_5220 ORF	52	500	*Xba*I
MP12	CGTATTGGA TCCGCGGCC GCTGAATGG CGGAAAGTG ACTG	R	TcIL3000_ 7_5220 ORF	52	500	*Not*I + *Bam*HI
MP13	ACATTAGCG GCCGCAAAA GAGCATATC ACAGGAAA GG	F	TcIL3000_ 1_1350 5' UTR	49	500	*Not*I
MP14	CGTATTCTC GAGGATGA GCAGCTTAG AAATGGTCT	R	TcIL3000_ 1_1350 5' UTR	49	500	*Xho*I
MP15	ACATTATCT AGAATGGA GATACGCGA CGTTAA	F	TcIL3000_ 1_1350 ORF	49	500	*Xba*I
MP16	CGTATTCTC GAGGCGGC CGCGGCTGG TGCTGAATA ACATG	R	TcIL3000_ 1_1350 ORF	49	500	*Not*I + *Xho*I